

Corrosion Testing

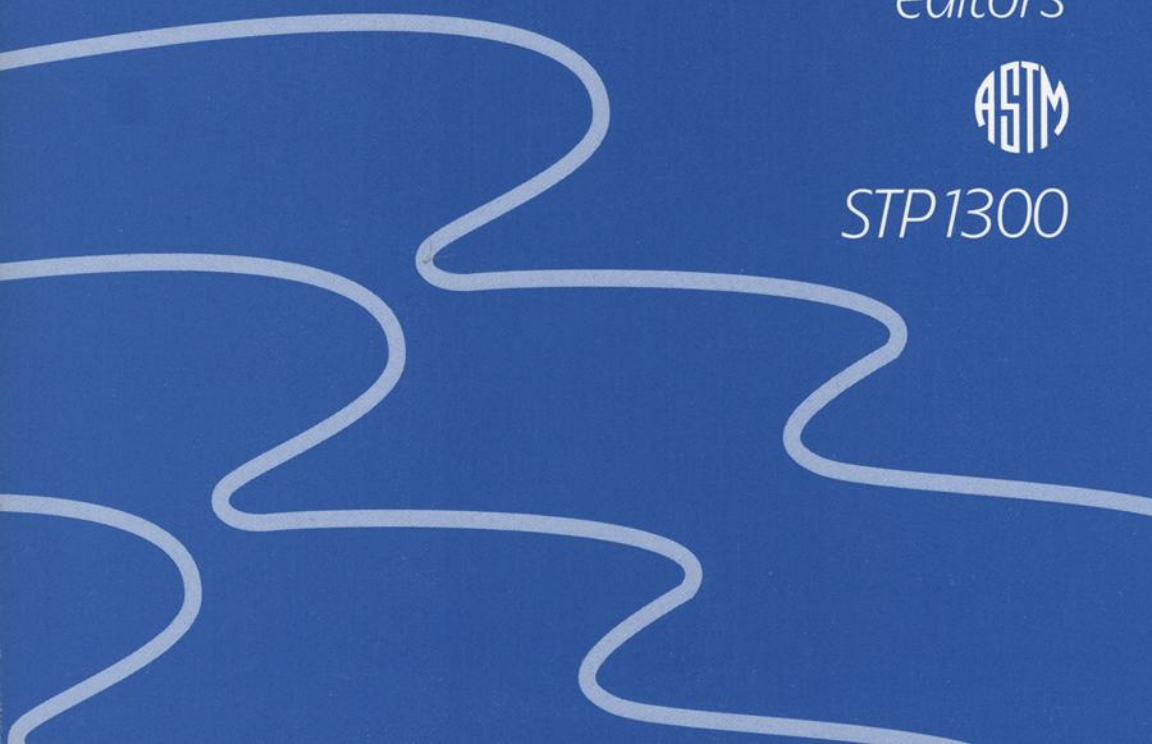
in Natural Waters

Second Volume

Robert M. Kain and Walter T. Young
editors



STP1300



STP 1300

Corrosion Testing in Natural Waters: Second Volume

Robert M. Kain and Walter T. Young, Editors

ASTM Publication Code Number (PCN):
04-013000-27



ASTM
100 Barr Harbor Drive
West Conshohocken, PA 19428-2959
Printed in the U.S.A.

Library of Congress

ISBN: 0-8031-2025-7

ASTM Publication Code Number (PCN): 04-013000-27

Copyright © 1997 AMERICAN SOCIETY FOR TESTING AND MATERIALS, West Conshohocken, PA. All rights reserved. This material may not be reproduced or copied, in whole or in part, in any printed, mechanical, electronic, film, or other distribution and storage media, without the written consent of the publisher.

Photocopy Rights

Authorization to photocopy items for internal, personal, or educational classroom use, or the internal, personal, or educational classroom use of specific clients, is granted by the American Society for Testing and Materials (ASTM) provided that the appropriate fee is paid to the Copyright Clearance Center, 222 Rosewood Drive, Danvers, MA 01923, Tel: 508-750-8400; online: <http://www.copyright.com/>.

Peer Review Policy

Each paper published in this volume was evaluated by two peer reviewers and at least one editor. The authors addressed all of the reviewers' comments to the satisfaction of both the technical editor(s) and the ASTM Committee on Publications.

To make technical information available as quickly as possible, the peer-reviewed papers in this publication were prepared "camera-ready" as submitted by the authors.

The quality of the papers in this publication reflects not only the obvious efforts of the authors and the technical editor(s), but also the work of these peer reviewers. The ASTM Committee on Publications acknowledges with appreciation their dedication and contribution of time and effort on behalf of ASTM.

Foreword

This publication, *Corrosion Testing in Natural Waters: Second Volume*, contains papers presented at the Second Symposium on Corrosion Testing in Natural Waters held 7 November 1995 in Norfolk, VA. This symposium was held in conjunction with the standards development meetings of Committee G1 on Corrosion of Metals, the symposium sponsor. Robert M. Kain, LaQue Center for Corrosion Technology, Inc., and Walter T. Young, Corpro Companies, Inc., served as co-chairmen of the symposium and editors of the resulting publication.

Contents

Overview	vii
Monitoring Biofilm Formation in Power Plant Environments —GEORGE J. LICINA AND GEORGE NEKOKSA	1
Modeling of Marine Corrosion of Steel Specimens —ROBERT E. MELCHERS	20
Seawater Corrosivity Around the World: Results from Five Years of Testing —BOPINDER S. PHULL, STANLEY J. PIKUL, AND ROBERT M. KAIN	34
Twenty Year Field Study of the Performance of Coatings in Seawater —ASHOK KUMAR, VICKI L. VAN BLARICUM, ALFRED BEITELMAN, AND JEFFREY H. BOY	74
Crevice Corrosion Testing of Austenitic, Superaustenitic, Superferritic, and Superduplex Stainless Type Alloys in Seawater —ALBERT W. ZEUTHEN AND ROBERT M. KAIN	91
Statistical Analysis of Pitting Corrosion in Condenser Tubes —J. PETER AULT AND GEORGE A. GEHRING, JR.	109
Corrosion Coupon Testing in Natural Waters: A Case History Dealing with Reverse Osmosis Desalination of Seawater —ROBERT M. KAIN, WAYNE L. ADAMSON, AND BRIAN WEBER	122
Comparison of Current Reversal Chronopotentiometry (CRC) and Small Amplitude Cyclic Voltammetry (SACV) Method to Determine the Long-Term Corrosion Tendency of Copper-Nickel Alloys in Polluted and Unpolluted Seawater Under Jet-Impingement Conditions —MAHMOUD R. REDA AND JAMAL N. ALHAJJI	143

Overview

This is the second STP of the same title. The first volume, STP 1086, was published in 1990 and contained papers on seawater corrosivity, crevice corrosion resistance of stainless steels, corrosion fatigue testing, and corrosion in potable water. Since then, final results have become available from the worldwide study on corrosion behavior of metals in seawater, and additional studies have been performed that should be brought to the attention of the corrosion engineering community. The eight papers presented in this volume were presented at the ASTM symposium in Norfolk, Virginia on 7 November 1995. A brief description of each paper follows.

Monitoring Biofilm Formation in Power Plant Environments

Power plants experience severe general corrosion, pitting, underdeposit corrosion, and microbiologically influenced corrosion in cooling water systems. Corrosion results in significant reductions in plant operating efficiency and high costs of operation and maintenance. Microbiological corrosion (MIC) is a particularly difficult problem since alloys that should be corrosion resistant in the general environment often fail in a short period of time when microbiological mechanisms are also active.

This paper discusses a test procedure that can be used to monitor biological activity. The procedure is based on an electrochemical probe that can be placed on-line to provide early warning of biological activity so that early action can be taken.

Modeling of Marine Corrosion of Steel Specimens

A mathematical model would prove to be quite useful in predicting the corrosion performance of steel and other metals in seawater where detailed exposure data are not available. This paper considers the variables of temperature, marine growth, wave action, pollutants, dissolved oxygen, and salinity on the long-term general corrosion rate of steel. A conceptual mathematical model dealing with immersion corrosion, tidal corrosion, and atmospheric corrosion is presented in the first part of the paper. The model is applied to data in the literature for longer-term corrosion. The model is found to be incompatible with the standard non-linear model for atmospheric corrosion. The paper discusses the uncertainties of dealing with literature data.

Seawater Corrosivity Around the World: Results from Five Years of Testing

In 1980, ASTM Task Group G1.09.02.03 established a test program aimed at assessing seawater corrosivity worldwide. Fourteen locations in eight countries, where capabilities were available for testing in general compliance with ASTM Standard G52, "Recommended Practice of Conducting Surface Seawater Exposure Tests on Metals and Alloys," were selected. The task group also selected three baseline test materials to assess corrosivities at the designated test sites. The materials were aluminum alloys A95036, copper-nickel alloy C71500, and carbon steel alloy K01501.

The present report summarizes the five-year corrosivity results. It was concluded that experiments that rank or characterize test sites can be significantly affected by many variables. The paper reviews the variables that influenced the test results.

Twenty-Year Field Study of the Performance of Coatings in Seawater

The primary means of corrosion protection for steel immersed in seawater is the use of barrier coatings with or without cathodic protection. This paper presents the results of a study by the U.S. Army Construction Engineering Research Laboratories where steel H-piles were coated with various coatings and exposed to natural seawater in Cape Cod and LaCosta Island, Florida. The pilings were coated with epoxy, glass flake polyester, polyurethane, flame-sprayed zinc, and flame-sprayed aluminum coatings. Cathodic protection using sacrificial anodes was used on some of the uncoated and coated pilings. Evaluation was performed using electrochemical polarization and polarization decay techniques. Some of the piles were removed for measurement of corrosion.

Crevice Corrosion Testing of Austenitic, Superaustenitic, Superferritic, and Superduplex Stainless Steel Type Alloys in Seawater

In industry, many problems from corrosion occurring in crevices have been experienced and reported. These include the refining industry, offshore drilling platforms, nuclear power plants, chemical plants, and public utilities. The services are highly variable. Corrosion mechanisms and the results experienced are influenced by severe environments that can not always be avoided.

This paper provides the results of a series of crevice corrosion tests on a number of ferritic, austenitic, super austenitic, and duplex alloys in seawater. The test results are considered useful not in comparing materials, but also in selecting materials for design. The ultimate goal is to use materials that are superior to those currently in use. This will result in fewer outages, reduce repairs, and significantly lower costs.

Statistical Analysis of Pitting Corrosion in Condenser Tubes

Condenser tube failure by means of wall penetration allows cooling water to contaminate the working fluid (steam). Contamination, especially from brackish or seawater, lowers steam quality, and thus lowers overall plant efficiency. Because of the importance of minimizing leaks, power plant engineers are primarily concerned with the maximum localized corrosion in a unit rather than average corrosion values or rates. Extreme value statistical analysis is a useful tool for evaluating the chances of maximum corrosion rates based on relatively small data sizes. Extreme value statistical techniques allow the prediction of the most probable deepest pit in a given surface area based on data acquired from a smaller surface area. This paper describes the use of extreme value statistical methods as applied to pit depth analysis and presents examples of how it can be used.

Corrosion Coupon Testing in Natural Waters: A Case History Dealing with Reverse Osmosis Desalination of Seawater

Corrosion testing is generally intended to assess either the corrosion resistance of a material in a given environment and/or characterizing environmental corrosivity. This paper describes the tests conducted to evaluate the corrosivity of the environment and possible materials for use in a reverse osmosis plant to convert natural seawater to fresh water. The

tests were conducted according to ASTM Standard G4, "Standard Guide for Conducting Corrosion Coupon Tests in Field Applications," and ASTM Standard G78, "Standard Guide for Crevice Corrosion Testing of Iron-Base and Nickel-Base Stainless Alloys in Seawater and Other Chloride-Containing Waters." The paper focuses heavily on the experimental design of the program as it related to ASTM Standards G4 and G78.

Comparison of Current Reversal Chronopotentiometry (CRC) and Small Amplitude Cyclic Voltammetry (SACV) Method to Determine the Long-Term Corrosion Tendency of Copper-Nickel Alloys in Polluted and Unpolluted Seawater Under Jet-Impingement Conditions

This paper reports on tests using the technique of cyclic current reversal chronopotentiometry to measure the corrosion tendency of two copper-nickel alloys in sulfide polluted seawater. The results are compared to the polarization resistance method.

The symposium committee gratefully acknowledges the efforts of the authors and ASTM personnel that have made this publication possible.

Walter T. Young

Corpro Companies, Inc.
West Chester, PA;
Symposium co-chairman and editor.

Robert M. Kain

LaQue Corrosion Services
Wrightsville Beach, NC;
Symposium co-chairman and editor.

George J. Licina¹, George Nekoksa²

MONITORING BIOFILM FORMATION IN POWER PLANT ENVIRONMENTS

REFERENCE: Licina, G. J., Nekoksa, G., “**Monitoring Biofilm Formation in Power Plant Environments,**” *Corrosion Testing in Natural Waters: Second Volume, ASTM STP 1300*, Robert M. Kain, Walter T. Young, Eds., American Society for Testing and Materials, 1997.

ABSTRACT: Power plants have experienced severe general corrosion, pitting, under deposit corrosion, and microbiologically influenced corrosion (MIC) in cooling water systems, resulting in decreased plant availability and significantly increased operations and maintenance costs. MIC has been a particularly difficult problem since corrosion resistant alloys in relatively benign environments have failed as a result of microbiological influences in short times. Copper base alloys, carbon steels and stainless steels have all been susceptible. In a number of instances, replacement of piping and heat exchangers has been required to alleviate corrosion-related problems.

Monitoring is a key element to improved corrosion control in cooling water systems. On-line methods provide evaluations of corrosion rates in real time and are sensitive to localized corrosion. Electrochemical methods of corrosion measurement are readily automated, both for acquisition of corrosion data and for process control. An electrochemical probe for on-line monitoring of biofilm activity has been shown to provide an early warning of biofilm formation and incipient MIC in fresh and saline waters.

KEYWORDS: monitoring, biofilm activity, microbiologically influenced corrosion, electrochemical methods

¹ Associate, Structural Integrity Associates, 3315 Almaden Expressway, Suite 24, San Jose, California 95118

² President, Corrosion Failure Analysis and Control, 209 Gaucho Court, San Ramon, California 94583

BACKGROUND

Many industries, including nuclear and fossil-fueled power plants, oil and gas production, chemical processing, pulp and paper, transportation, and water distribution networks have experienced damage due to corrosion in natural waters. This damage results in increased downtime of equipment, increased operating costs, and can jeopardize the safe operation of plant equipment. These industries have recognized the importance of corrosion control on continued reliability and economic operation of their plants. In most circumstances, general corrosion has been adequately controlled or addressed during design. Localized corrosion due to pitting, crevice corrosion, underdeposit corrosion, or microbiologically influenced corrosion (MIC) has, of necessity, received greater attention during the 1980s and 1990s. Methods for control of localized attack require a greater understanding of the types of local environments that can exist in power plant equipment. The power generation industry has devoted increasing attention to corrosion monitoring in cooling water environments. These environments range from "soft", fairly low conductivity fresh waters to scale-forming freshwater to brackish waters and seawater. Monitoring tools for a power plant must address the corrosion concerns associated with that plant's cooling water, including both the seasonal fluctuations that may be expected and the creation of local environments due to corrosion products, deposits, and microbiological growth.

On-line monitors must be:

- **Simple to use.** Installation and routine maintenance of the monitor(s) should not impact power plant operations.
- **Simple to interpret.** Results should be readily interpreted by operations personnel. Corrosion specialists should not need to be consulted routinely. Outputs should be amenable to automation (alarms, etc.).
- **Rugged.** The probes and equipment must be sufficiently rugged that frequent, unscheduled maintenance is avoided. Sensitivity to external noise (e.g., welding, the plant's turbine-generators) is unacceptable.
- **Sensitive.** Detectable electrochemical effects should appear on the probe before thick biofilms are established on plant components.
- **Accurate.** A monitoring device must provide reliable detection of biofilm activity with a minimum of false calls.
- **Economical.** Cost for installation, maintenance, and operation must be cost effective, as reflected by potential savings realized as a result of the improved monitoring capabilities.

The influence of MIC in power plant cooling waters has been a major source of problems as noted in a number of publications [1-4]. In many cases, corrosion resistant alloys have experienced rapid, through-wall penetration when exposed to potable waters from rivers, lakes, estuaries, and ponds; environments that would normally be considered benign. The influence of biofilms in establishing corrosion initiation sites and in providing conditions for the propagation of pits has been clearly demonstrated. Power plants have been required to modify, repair, or replace such lines in their entirety. A number of large, nuclear units have replaced their service water systems, at costs of the order of \$30,000,000 per plant.

Experience has shown that monitoring of corrosion and biofilm formation is best achieved in the plant's cooling water environment. The following discussion will describe the approach used for monitoring biofilm activity in several power plant and test installations using fresh and saline surface waters.

APPROACH

The BI^oGEORGE³ probe (Figure 1) consists of two identical electrodes (where each electrode is made up of a stack of identical stainless steel discs), mounted on a threaded stainless steel body, and a simple control and data acquisition system. The electrode stacks are electrically isolated from each other and from the probe body. An epoxy resin fills the spaces between the electrode discs to provide a probe that is a smooth, rigid, circular cylinder. One set of discs is polarized relative to the other for a short time (one hour) each day. Polarity always remains the same. During the remaining 23 hours of the day, the electrodes are connected through a precision resistor. Currents (measured as the potential drop across the resistor) and potentials are monitored continuously.

The basis for the probe as an MIC monitor is that microbiologically influenced corrosion will not occur without a biofilm. If biofilm is controlled, MIC will be controlled. Interaction between the biofilm and metallic surfaces, which may also be affected by temperature and flow conditions must be understood and factored into plant control schemes.

The low level of polarization also simulates conditions conducive to microbial colonization such as those resulting from local anodic sites like inclusions or weldments.

³ BI^oGEORGE is a trademark of Structural Integrity Associates, Inc., San Jose, California

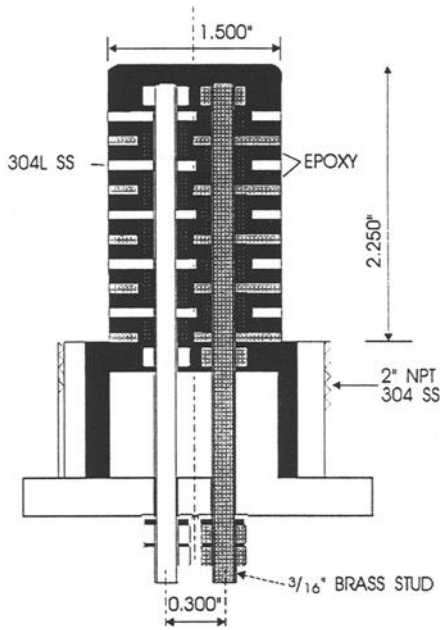


FIG. 1 -- Electrochemical Biofilm Probe

The “gentle” cathodic polarization can also encourage microbial colonization, similar to that observed on cathodically protected structures in biologically active environments as reported by Nekoxsa and by Guezenec [5, 6] (Figure 2). Short polarization times also avoid shifting of the natural potential of the electrodes.

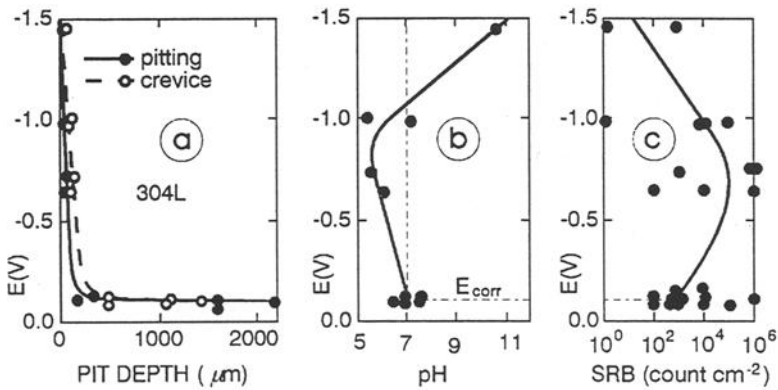


FIG. 2 -- Cathodic Protection Potential on Type 304L Stainless Steel versus (a) corrosion, (b) pH on the sample and (c) SRB count. E = potential (SCE); PD = pit depth (max.); CP = corrosion potential (From Reference 13)

The probe provides two methods for reliably monitoring biofilm activity on line. The **applied current**, the current required to achieve the pre-set potential applied between the two electrodes, remains fairly constant until a depolarizing influence, such as biofilm formation, occurs. Deposits such as biofilms produce a distinct increase in the applied current, consistent with a decrease in the polarization resistance. Generally, the applied current remains at an elevated level until the biofilm is removed or rendered inactive. For example, biofilms that catalyze the reduction of oxygen in aerated environments or which produce alternative cathodic reactions (e.g., the result of sulfate reducing bacteria or acid producing bacteria) are readily detectable, simply by observing changes in the current during the polarization cycle.

The **generated current**, the current that flows between the two nominally identical electrodes when no external potential is applied, provides an additional, usually more sensitive, indicator of biofilm activity. The generated current is determined by monitoring the potential drop across a precision resistor that connects the probe's positive and negative electrodes. Prior to formation of a biofilm, the generated current would be expected to be essentially zero; a reasonable assumption for two nominally identical electrodes exposed to the same environment. However, as a biofilm forms and the local environments on the discs of different polarity are changed, some current flow would be expected between the electrodes, even when no external potential is applied.

The probe was originally designed to monitor biofilm formation in fresh water cooled power plants, particularly in untreated waters. The early success in those environments prompted investigations into biofilm monitoring in saline waters. The primary concern with such waters was the potential for pitting or crevice corrosion of the stainless steel electrodes. Design modifications included the use of electrode materials that are commonly used in saline water service, such as commercially pure titanium and copper alloys (e.g., aluminum brass, 90-10 copper-nickel). Modified polarization schedules were also investigated to achieve the required levels of sensitivity and probe life.

The sensors described in this paper were installed in three different nuclear plants (Plants #1 thru 3), a large (>2000 MWe) fossil-fired station (Plant #4), and in a U.S. Navy test flume exposed to seawater from the Atlantic Ocean. Two of the three nuclear units are cooled by, "soft", scale-dissolving waters from a river or reservoir while the other nuclear facility uses a spray pond containing a scale-forming water. Exposure locations included a high pressure fire protection system line that served as the make-up source for the service water system and a treated essential equipment cooling water system line at Plant #1, a sidestream taken from the once-through service water system of another nuclear plant (Plant #2), an intermittent flow test stand exposed to the plant's emergency service water system spray pond (Plant #3), brackish water from the discharge canal at Plant #4, and the test flume. In addition to the site-to site variations, all of these installations also experience seasonal variability in water chemistry, influenced by seasonal differences in temperature and precipitation from year to year. The nature of the dissolved

and suspended solids and the microbiological character of the plants' cooling waters vary dramatically.

All of these plants have experienced general and localized corrosion of carbon steel piping, pitting of stainless steel components, or localized attack of heat exchanger tubes, including aluminum brass, admiralty, and copper-nickel alloys, due to localized corrosion. Many of the heat exchanger tube failures have been attributed to inlet end erosion, pitting, crevice corrosion, and MIC. The relative importance of MIC to the overall failure picture was not clear, however, all of the facilities were known to be in biologically active environments that had produced significant fouling of heat exchangers and offered the potential for MIC of structural materials. The probes were installed to evaluate their applicability as biofilm activity monitors for the particular water chemistry and operational philosophy and to assess the suitability of the probes for in-plant use.

In all of the exposures, the probes were exposed to the variations in flow rate, temperature, water chemistry, etc. inherent in the system. No attempts were made to control those parameters. Data collection was performed automatically using a data logger or chart recorder. In some installations, the probe was also interfaced to a personal computer. In all cases, analysis of the data was performed off-line.

Probes with stainless steel electrodes have been shown to be effective in monitoring biofilm activity in fresh water cooling systems [7-11]. Both stainless steel and titanium have been demonstrated to be compatible as biofilm monitoring electrodes in seawater [12]. For saline water exposures, probes with three different types of electrode materials were used. The standard probe with stainless steel electrodes (Type 304 and 304L in fresh waters; Type 316 in seawater) was polarized to 100 mV or 200 mV in all the fresh water installations and to 25 to 100 mV in saline waters. Copper base alloy electrodes, aluminum brass or 90-10 copper-nickel, were polarized to 60 or 200 mV in saline water environments. In order to optimize the signals from probes built with commercially pure titanium electrodes, a larger potential, 400 mV, was applied between the electrodes. Data were collected on a data logger or hybrid chart recorder. Plots were created from those data off-line using QuattroPro™ spreadsheet software.

RESULTS

Plant #1

The first probe was installed in the high pressure fire protection system in 1991. This plant had experienced significant corrosion of carbon steel piping and a build up of corrosion products on the pipe wall that effectively reduced the system's flow capacity. Attack beneath these deposits had been observed. The microbiological influences had not

been well characterized. The probe was installed directly into the flow stream. Normal fluid velocities past the probe were approximately 1.5 m/s.

The results from that probe are shown in Figure 3. Both the applied and generated currents exhibited a definite increase approximately 50 days into the exposure (December, 1991). In the Spring of 1992, the applied current increased to a value of more than 60 μA . At about the same time, the generated current actually changed sign, reaching levels of nearly $-40\mu\text{A}$ in the Summer of 1992. A very definite generated current of negative sign was maintained until the probe was replaced in October, 1993. Post-test examination of the probe revealed that the stainless steel electrodes were covered with a thick but patchy film consisting primarily of iron oxide. Microbiological characterization of the films, done at the site using MICKits™ and from microscopic analyses performed by Bioindustrial Technologies, showed that the films contained both aerobic and anaerobic bacteria, acid producing bacteria (APB), and iron oxidizing bacteria only on the negative electrode. No sulfate reducing bacteria (SRB) were detected nor was any corrosion of the electrodes detected. Probably of greatest significance, the pH at the positive electrode was 4.9 vs. 8.3 at the negative electrode.

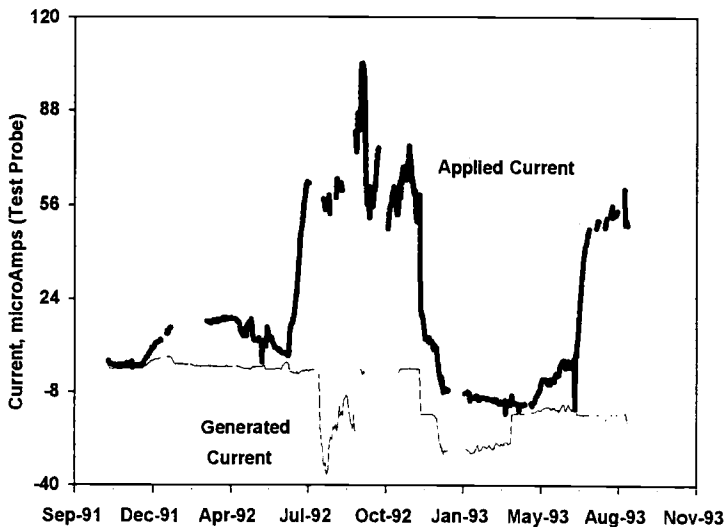


FIG. 3 -- Results from Plant #1 Fire Protection System

When the probe in the fire protection system was replaced in October, 1993, an additional probe was installed in the essential equipment cooling water (EECW) system. That probe gave no indication of any biofilm activity for the first ninety days of exposure (Figure 4). After about ninety days, a very definite generated current, with a negative sense, was observed. Since the generated current influenced the magnitude of the applied current, the arithmetic difference between the two currents (i.e., applied - generated) was used as the indicator of biofilm activity. That difference value reached a level of approximately 10 μA in April, 1994, then abruptly decreased to the baseline level of about 1.5 μA . The time that the abrupt decrease in the indicator variable occurred approximately two days after the plant's spring chlorination treatment, done to control Asiatic clams. The applied and generated currents (and their difference) began to increase again about one month later. In June, 1994, another abrupt decrease, again corresponding to a system chlorination, was observed. This cycle of indications of microbiological activity and destruction was repeated again. All probe tracking activities were turned over to the site in August, 1994.

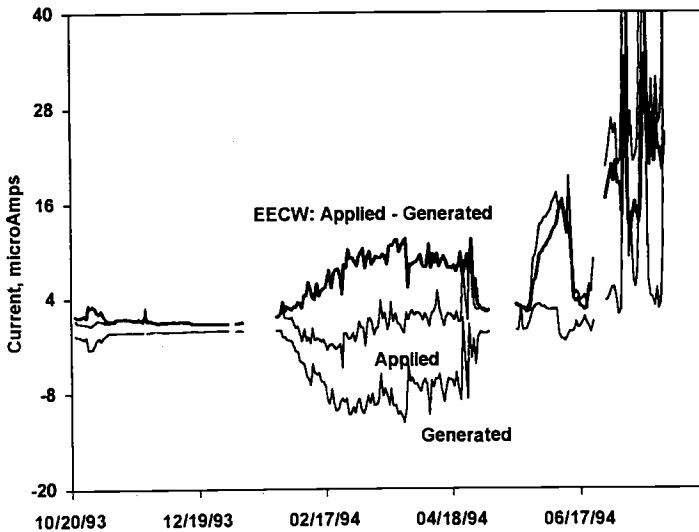


FIG. 4 -- Results from Plant #1 EECW

Plant #2

A probe was installed into a portable sidestream used to monitor fouling and the performance of biocides and other treatments in the once-through service water system of another large nuclear plant. The system was located immediately downstream of components that were known to be subject to fouling and corrosion. As shown in Figure 5, the probe fouled very rapidly, was effectively returned to the clean condition by chlorination, then fouled again. The applied current never responded to the chlorination (the abrupt decrease in applied current was the result of a mechanical cleaning of the probe), however, the generated current slowly decreased during and after the second chlorination. No post-test examination of the probe was performed.

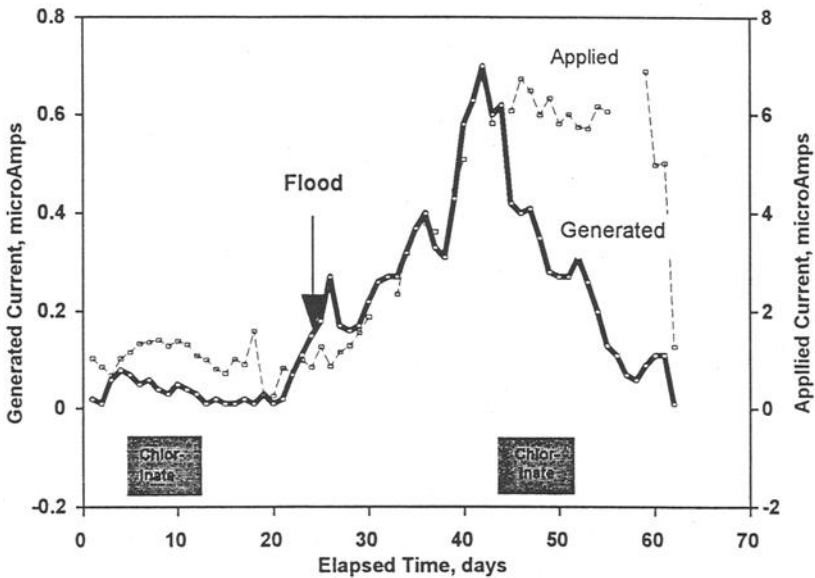


FIG. 5 -- Results from Plant #2

Plant #3

This probe formed a part of a test stand to investigate the attack of Type 321 stainless steel flex hoses that were used to connect the carbon steel service water system piping and stainless steel heat exchanger bodies. The pitting of the first few convolutions of the flex hose has been described by Morgan and Willertz [13]. As shown in Figure 6, only minor indications of any microbiological activity were observed in the first six months of exposure. Characterization of the films on the probe in March, 1995, revealed no microbiological activity. The probe was wiped clean, rinsed with system water, and returned to the test stand. In late April, 1995, a small but definite generated current (negative sense) was observed. The indications coincided with warmer waters ($\geq 20^{\circ}\text{C}$). At about the same time, the applied current began to exhibit large deviations from one day to the next. This system flows for two or three hours each day and remains stagnant the remainder of the time, a factor which account for the differences in the daily values for the applied current.

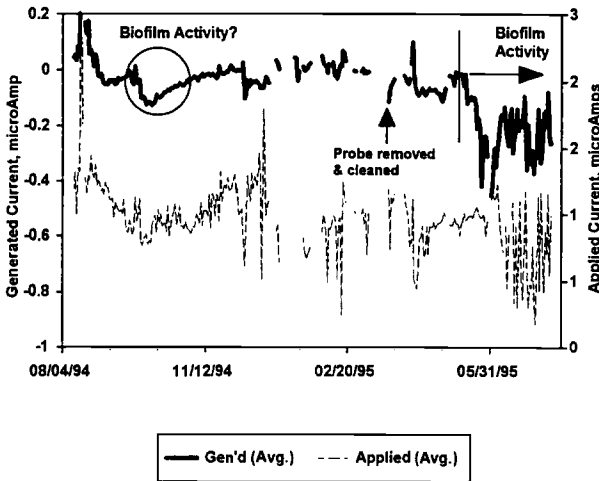


FIG. 6 -- Results from Plant #3

Plant #4

Three probes were installed into a small flow loop that took suction from the brackish water cooled plant's discharge canal. This plant has experienced localized corrosion in carbon steel, stainless steel, and, especially, in aluminum brass and 90-10 copper-nickel heat exchanger tubes. Results from the probes are shown in Figures 7 and 8.

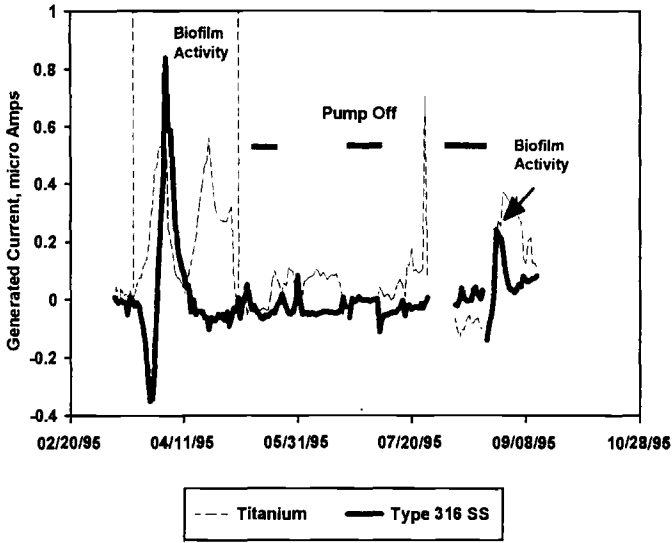


FIG. 7 -- Results from Plant #4 (Stainless Steel and Titanium)

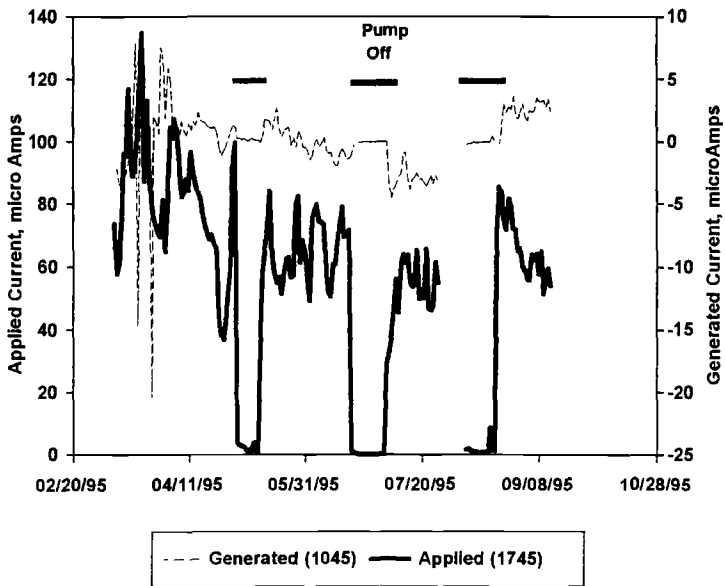


FIG. 8 -- Results from Plant #4 (Aluminum Brass)

The stainless steel probe appeared to provide a useful indicator of biofilm activity. The generated current was again the most useful parameter. Indications of biofilm activity were observed within the first ten days of the exposure, signaled by a deviation of the generated current from the zero level that would be expected for unfouled electrodes. As has been observed in a number of other exposures, the initial generated current had a negative sense, that is, opposite to the direction of current flow when an external potential was applied. The generated current rapidly changed sign after another ten days or so, peaked at (a positive value of) about $0.8 \mu\text{A}$ on about April 10, then decayed to lower levels. The generated current indicated only minimal activity thereafter. The generated and applied currents were generally not affected by disturbances to flow. There was some indication of a small increase in activity following the two week period of stagnation that occurred in late June.

The performance of the titanium probe was similar to that of the stainless steel probe. The generated current also provided the most useful indicator. Like the stainless steel probe, the titanium probe indicated that biofilm activity initiated within the first ten days of exposure. Unlike the stainless steel probe, the generated currents on the titanium probe were positive. The generated current reached a peak of about $0.7 \mu\text{A}$ that persisted for a day or two, dropped to near zero, then peaked again with evidence of activity persisting for almost a month. Some smaller indications followed in the ensuing weeks. A stagnation period during June produced some activity, however, the activity was small or non-existent after another pump failure in August.

The aluminum brass probe provided no useful information, similar to what has been observed in seawater exposures [12]. The probe exhibited very high applied currents ($\sim 70 \mu\text{A}$) for most of the exposure. These applied currents dropped to zero when the flow was off, suggesting that the outlet end of the test vessel where these probes were located may have drained to the point where the probe was not immersed. The generated currents exhibited some noise, especially early in the exposure, however, the probe provided no definitive indications of biofilm formation.

Seawater Test Flume

These results were similar to those from the brackish water exposure [12]. Exposure of stainless steel, titanium, and 90-10 copper-nickel probes (Figure 9) to static seawater, inoculated with a biologically active soil revealed the characteristic increase in generated current (difference between applied and generated currents for the stainless steel) early in the test, a persistent biofilm activity, then a rapid decrease to the baseline level following the addition of biocide. As noted in [12], the copper-nickel probe showed no indications of biofilm activity. Post-exposure investigation confirmed that those probes had no biofilm growth.

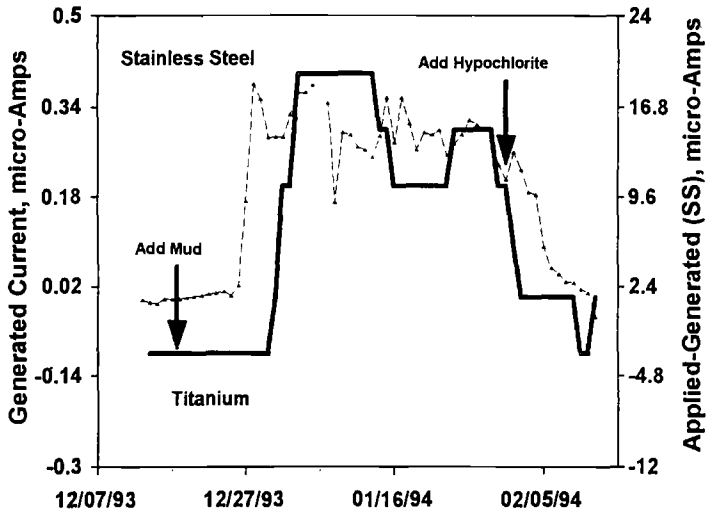


FIG. 9 -- Results from Static Seawater Exposure (Stainless Steel and Titanium)

DISCUSSION

Biological consortia on metallic surfaces can affect the electrochemical nature of the surface by influencing the rates and nature of such reactions, particularly, the cathodic half-reaction. For example, stainless steels in aerated seawater undergo a noble shift in the open circuit potential (OCP) as a result of such effects [14-19]. Similar effects have been observed in fresh waters as well [19-20]. Experience with cathodically protected structures also suggests that microbiological growth can be stimulated by cathodic protection [5-6]. The design and operation of the two-electrode probe incorporates these effects to provide a simple and reliable method for encouraging microbiological colonization on normally passive electrode materials. The microbiological activity on the electrodes should be accelerated relative to that on plant structures, thus providing a means for monitoring that settlement.

Biofilms produce crevices, "living crevices", that can and often do produce localized attack in alloys that exhibit excellent corrosion resistance in the same water, without the influence of the microorganisms. Microbes can influence corrosion by producing aggressive metabolites (e.g., mineral or organic acids, sulfides, ammonia), by increasing the rate of key reactions (e.g., the rate of oxygen reduction in aerated waters) or permitting alternate half-reactions (e.g., the influence of SRB in soils or waters), by shifting the electrochemical potential to higher levels, or, simply, by creating a more effective crevice such that "normal" crevice corrosion can occur. Alerting a system operator of the existence of a biofilm on metallic surfaces and providing some indication

of its activity permits him to take an action, well before a thick biofilm is formed, and prevent corrosive conditions from becoming established. Such early actions are also more likely to be effective.

The polarization of the probe is intended to encourage microbiological settlement on the probe discs so that an active biofilm will form on the probe before it forms on piping or heat exchange surfaces. An active biofilm, which increases the rate of one or more operative half-reactions (e.g., oxidation reduction at the cathode) or which permits more rapid, alternative half-reactions to occur will cause the applied current to increase. Most inorganic films would be expected to have only minimal effect on the applied current as they typically present an impediment to such reactions. Calcareous deposits dramatically reduce the current required to maintain a cathodic protection potential.

The presence of thick films or films that short the probe electrodes necessitate cleaning of the probe surfaces. The presence of an active biofilm produces differences in the local environments on the electrodes that provide the probe's indicators, the applied and generated currents. As the films grow and trap debris (e.g., corrosion products from upstream locations) or as a continuous or semi-continuous calcareous deposit forms across electrodes, the electrical performance of the probe will degrade. Such degradation mechanisms define the probe's maintenance interval. Maintenance typically consists of gentle cleaning that will range from rinsing in clean water to mechanical cleaning with a wet paper towel or a fingernail, depending upon the nature of the film that must be removed. Thick calcareous deposits are the most difficult to remove. Biofilms that have trapped corrosion products, silt, etc. are readily removed by rinsing or very light mechanical cleaning. Long term exposure in fresh water laden with corrosion products has shown that minor maintenance every eighteen to twenty-four months is probably sufficient [10].

Copper base alloy probes failed to provide any indication of biofilm activity in either seawater or brackish water. Post-test examination of the 90-10 copper-nickel probe from the seawater exposure revealed no viable biofilm on the probe. This effect is probably due to the polarization schedule. One of the probe electrodes is polarized by tens or even hundreds of millivolts relative to the other daily. During that polarization cycle, some dissolution of copper occurs. Copper ions are toxic to many life forms, including microbes. This daily dose of copper is probably sufficient to discourage microbial settlement of the probe surfaces.

In the intermittent flow facility at Plant #3, the biofilm probes provided an interesting demonstration of the effects of intermittent flow on stainless steels, an effect that may best illustrate the interaction between biofilm activity and oxygen. Before the probe provided any indication of biofilm, from changes in either the applied or generated current, the initiation of flow each day was essentially invisible. As shown in Figure 10, the current trace remained at a constant level both before, during, and after the several

hour period of flow. However, once the probe had provided a fairly definite indication of biofilm activity, the change in the current signal from the probe, resulting from the initiation of flow, was actually larger than the applied current (Figure 11).

An interesting effect noted in the brackish water exposure was that both the stainless steel and titanium probes indicated the formation of biofilm on the probe surfaces at essentially the same time, early in the exposure. The current on the titanium probe exhibited the same sign as that of the applied current. The stainless steel probe first exhibited a "negative" current that rapidly changed sign to reach a "positive" peak, then changed sign again, providing a fairly steady but small negative current. Since the probes were not removed from the system, the nature of the films at each time were not characterized, hence, this difference and the shift remain unexplained. The effect, that is, differences and changes in sign of generated currents, have been observed before in cooling waters. The effect appears to be related to differences in the types of microbiological species that dominate the biofilm on the surfaces as a function of time.

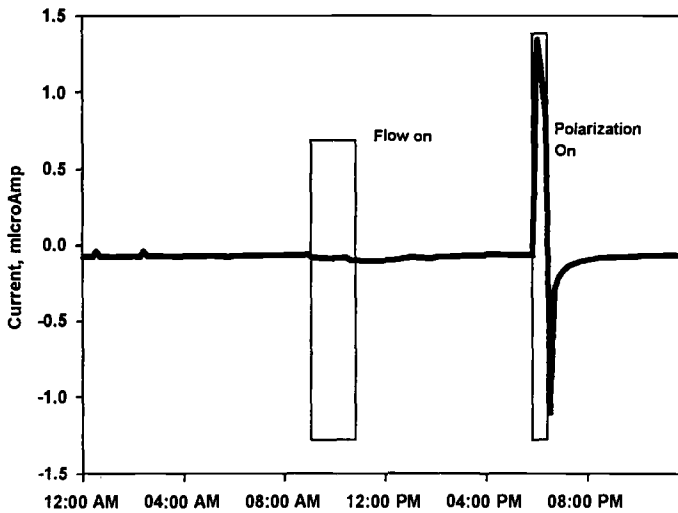


FIG. 10 -- Daily Current Trace, Plant #3 (April 13, 1995; No Biofilm)

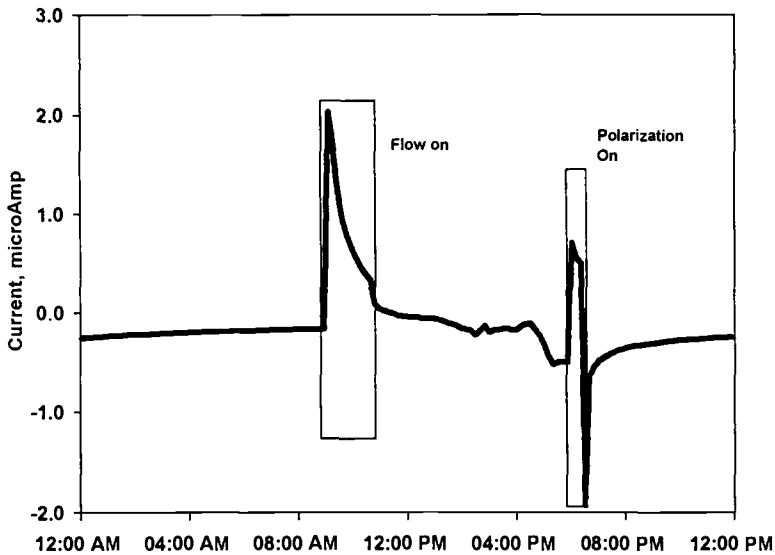


FIG. 11 -- Daily Current Trace, Plant #3 (June 22, 1995; With Biofilm)

CONCLUSIONS

The multiple disc electrodes and intermittent cathodic polarization schedule used for the electrochemical biofilm probe provide local environments that are amenable to micro-biological colonization. By tracking changes in the applied current and generated current, biofilm activity can be monitored on line.

Probes with Types 304, 304L, and 316 stainless steel, titanium, and copper base alloys (90-10 copper-nickel and aluminum brass) have been exposed in power plant cooling waters (fresh waters, brackish water, and seawater). Probes built with stainless steel or titanium electrodes have all provided a rapid and definitive indication of biofilm activity. Copper base alloys do not appear to be useful for probe electrodes because of the daily polarization and the release of copper ions.

The influence of a biofilm on the electrochemical response of stainless steel was demonstrated under the intermittent flow conditions at Plant #3. Prior to biofilm formation, flow had no effect on the measured currents between the electrodes. Once a biofilm had become established, the introduction of flowing, aerated fresh water produced a very large current; larger than that from an external potential of 200 mV.

Similar effects were observed in brackish water and seawater. Biofilms grew rapidly and the electrochemical influence of the biofilms was similar to the effect observed in fresh waters.

The addition of biocide produced a definite response in the probes. Probe indications did not always return to the base line level nor were responses immediate. Biofilms appeared to re-form very rapidly after biocide additions.

Post-test examinations revealed that probe responses corresponded to the presence of an active biofilm. Different microbial populations were observed on electrodes of different polarities in most cases.

The electrochemical biofilm probe worked well in an unattended mode and provided an early warning of conditions that would produce MIC.

ACKNOWLEDGMENTS

The work described in this paper was sponsored by the Tennessee Valley Authority (Mr. R. E. Taylor, Mr. R. L. Howard), Alabama Power Company (Mr. W. E. Garrett), the Naval Surface Warfare Center (Dr. Marianne Walch), Pennsylvania Power & Light Company (Mr. D. J. Morgan and Dr. L. E. Willertz), and the Electric Power Research Institute (Mr. Ramtin Mahini).

REFERENCES

1. *A Practical Manual on Microbiologically Influenced Corrosion*, G. Kobrin, ed., NACE-International, Houston, TX, 1993.
2. Pope, D.H., "Microbial Corrosion in Fossil-Fired Power Plants - a Study of Microbiologically Influenced Corrosion and a Practical Guide for Its Treatment and Prevention", EPRI CS-5495, Electric Power Research Institute, Palo Alto, CA, 1987.
3. Licina, G. J., "Sourcebook for Microbiologically Influenced Corrosion in Nuclear Power Plants", EPRI NP-5580, Electric Power Research Institute, Palo Alto, CA, 1988.
4. Borenstein, S.W., *Microbiologically Influenced Corrosion Handbook*, Woodhead Publishing, Ltd., Industrial Press, 1994.

5. Nekoksa, G. and Gutherman, B., "Cathodic Protection Criteria for Controlling Microbially Influenced Corrosion in Power Plants", EPRI NP-7312, Electric Power Research Institute, Palo Alto, CA.
6. Guezennec, J., et. al., "Cathodic Protection in Marine Sediments and the Aerated Seawater Column", *Microbially Influenced Corrosion and Biodeterioration*, ed. by N.J. Dowling, M.W. Mittleman, and J.C. Danko, University of Tennessee, 1991.
7. Licina, G. J., Nekoksa, G., Howard, R. L., "An Electrochemical Method for On-Line Monitoring of Biofilm Activity in Cooling Water Using the BIOGEORGE™ Probe", *Microbiologically Influenced Corrosion Testing, ASTM STP 1232*, Jeffrey R. Kearns and Brenda J. Little, Eds., American Society for Testing and Materials, Philadelphia, 1994, pp. 118-127.
8. Licina, G. J., Nekoksa, G., "An Electrochemical Method for On-Line Monitoring of Biofilm Activity", *CORROSION/93*, Paper No. 403, NACE-International, Houston, TX, 1993.
9. Licina, G. J., Nekoksa, G., "Experience with On-Line Monitoring of Biofilm Activity in Power Plant Environments", *CORROSION/94*, Paper No. 257, NACE-International, Houston, TX, 1994.
10. Licina, G. J., Nekoksa, G., "The Influence of Water Chemistry and Biocide Additions on the Response of an On-Line Biofilm Monitor", *CORROSION/95*, Paper No. 527, NACE-International, Houston, TX, 1995.
11. Garrett, Jr., W.E., Licina, G.J., "Monitoring Microfouling in a Once-Through Service Water System", 8th EPRI Service Water System Reliability Improvement Seminar, Electric Power Research Institute, Charlotte, NC, 1995.
12. Licina, G.J., Nekoksa, G., "An Innovative Method for Rapid Detection of Microbiologically Influenced Corrosion", Tri-Service Corrosion Conference, June, 1994, Orlando, FL.
13. Morgan, D.J., Willertz, L.E., "Pitting of Stainless Steel in an Emergency Service Water System", *Heat Exchanger Technologies for the Global Environment*, PWR-Vol. 25, ed. by J.R. Maurer, American Society of Mechanical Engineers, New York, 1994.
14. Mollica, A., Traverso, E., Ventura, G., "Electrochemical Monitoring of the Biofilm Growth on Active-Passive Alloy Tubes of Heat Exchanger Using Seawater as Cooling Medium", *Proceedings 11th International Corrosion Congress*, Florence, Italy, April, 1990, Associazione Italiana di Metallurgia.

15. Dexter, S. C. and Gao, G. Y., "Effect of Seawater Biofilms on Corrosion Potential and Oxygen Reduction of Stainless Steel", CORROSION/87, Paper No. 377, National Association of Corrosion Engineers, Houston, TX, 1987.
16. Gundersen, G., Johansen, B., Gartland, P.O., Vintermyr, I., Tunold, R., and Hagen, G., "The Effect of Sodium Hypochlorite on the Electrochemical Properties of Stainless Steel and on Bacterial Activity in Seawater", CORROSION/89, Paper No. 108, National Association of Corrosion Engineers, Houston, TX, 1989.
17. Scotto, V., "Electrochemical Studies of Biocorrosion of Stainless Steel in Seawater", 1988 Proceedings of EPRI Microbial Corrosion Workshop, ed. by G. J. Licina, EPRI ER-6345, Electric Power Research Institute, Palo Alto, CA, 1989.
18. Holthe, R., Bardal, E., Gartland, P. O., "The Time Dependence of Cathodic Properties of Stainless Steels, Titanium, Platinum and 90-10 CuNi in Seawater", CORROSION/89, Paper No. 393, National Association of Corrosion Engineers, Houston, TX, 1989.
19. Dexter, S.C., Zhang, H.-J., "Effect of Biofilms, Sunlight, and Salinity on Corrosion Potential and Corrosion Initiation of Stainless Alloys", EPRI Report NP-7275, Electric Power Research Institute, Palo, Alto, CA, May, 1991.
20. Buchanan, R. A., et. al., "Electrochemical Studies of Microbiologically Influenced Corrosion", EPRI Report NP-7468, Electric Power Research Institute, Palo Alto, CA, September, 1991.

Robert E. Melchers¹

MODELING OF MARINE CORROSION OF STEEL SPECIMENS

REFERENCE: Melchers, R.E., “**Modeling of Marine Corrosion of Steel Specimens,**” Corrosion Testing in Natural Waters: Second Volume, ASTM STP 1300, Robert M. Kain, Walter T. Young, Eds., American Society for Testing and Materials, 1997.

ABSTRACT: Phenomenological modeling of the long term general corrosion of mild and low alloy steel specimens under marine conditions is considered, using weight loss as a function of time. A conceptual model for immersion corrosion, tidal corrosion and atmospheric corrosion under marine conditions is proposed. The model uses accepted theories for short term surface corrosion and employs modern understanding of the action of bacterial colonisation of the surfaces of specimens, including the development of anaerobic conditions. Kinetic, diffusion, nutrient and anaerobic components of the model are identified and mathematical descriptions given. The model is compared to some data available in the literature. Some observations are made about data requirements for further development of models of the type proposed.

KEYWORDS: corrosion, modeling, marine, immersed, half-tide, atmospheric, diffusion, kinetic, nutrients, anaerobic

INTRODUCTION

In the design of steel structures such as off-shore jackets and ships, allowance must be made for corrosion, even when protective coatings and cathodic protection are applied. Reference to corrosion engineering handbooks and trade literature typically shows order of magnitude design allowances for corrosion loss of material. Constant corrosion rates are implied, often quoted with rather limited guidance about their applicability.

There are increasing requirements for life-time predictions of structural safety. These demand reasonably accurate prediction of the likely future degree of corrosion. Unfortunately, methods such as the measurement of corrosion potentials for an existing structural element are of limited practical use at the design stage for a new project. The present paper is an attempt to begin to construct a model for the marine corrosion of mild and low alloy steel structures. It will be argued that there is likely to be a high degree of integration between immersion, tidal and atmospheric corrosion behavior for such structures and that a common model can be used. Comments will be made also about data needs for the further development of the model.

¹Professor of Civil Engineering, Department of Civil, Surveying and Environmental Engineering, The University of Newcastle, NSW, Australia, 2308.

PREVIOUS MODELS

The non-linearity of corrosion material loss as a function of time was noted for steel by Larrabee [1] for atmospheric corrosion conditions. Experimentally this has been demonstrated repeatedly also. It has led to several attempts to model the material loss with time as a function of environmental factors, with most emphasis on the effect of sulphur oxides [2,3].

Similarly, for immersion corrosion of steel in relatively shallow sea-water, the evidence that the relationship is actually non-linear has been available for some time [4], although for design purposes it is often represented as a given rate of material loss (implying a linear model). Until recently, the only (non-linear) mathematical model for immersion corrosion of steel specimens which appears to have been proposed is the bi-linear model of Southwell *et. al.* [5] for Panama Canal zone data:

$$d_w = a + bt \quad (1)$$

where d_w is the mean depth of corrosion as obtained from specimen weight-loss, t denotes time and a and b are constants. No similar attempt appears to have been made to fit corrosion data for specimens exposed to tidal conditions.

In a review of all available data sources it was suggested that contrary to the conventional wisdom, correction of immersion corrosion data for sea-water temperature is justified [6]. The following relationship was proposed:

$$d_2 = [(t_2 - t_0) / (t_1 - t_0)] d_1 \quad (2)$$

where d_2 is the mean corrosion depth at mean temperature t_2 , d_1 is the corresponding depth at t_1 and t_0 is the mean annual temperature below which the maximum seawater temperature never exceeds the freezing point of sea-water (approximately -2.5 °C). On the basis of the available data $t_0 = -10$ °C was chosen. This correction is consistent with recently reported laboratory observations for small scale immersion specimens [7]. All known and consistent immersion corrosion data for mild steel [6], corrected using (2), is plotted in Figure 1. Laboratory observations are not included. A recently proposed alternative bilinear (probabilistic) model [8] is also shown in terms of the function for the mean m_d and for the standard deviation function s_d :

$$m_d = 0.09 t \quad 0 < t < 1.46 \text{ years} \quad (3a)$$

$$m_d = 0.076 + 0.038 t \quad 1.46 < t < 16 \text{ years} \quad (3b)$$

$$s_d = 0.062 t \quad 0 < t < 1.46 \text{ years} \quad (3c)$$

$$s_d = 0.035 + 0.017 t \quad 1.46 < t < 16 \text{ years} \quad (3d)$$

Both models (1) and (3) are conservative in the period 1 - 3 years, that is, they over-estimate the average immersion corrosion rate, see Figure 1.

A further non-linear model based on the exponential model widely adopted for atmospheric work was also considered for immersion corrosion [8], with mean corrosion depth given by:

$$m_d = 0.084 t^{0.823} \quad (4a)$$

and the standard deviation function:

$$s_d = 0.056 t^{0.823} \quad (4b)$$

It was found [8] that a log-normal probability distribution model for the corrosion depth was not inconsistent with the data. However, the coefficients and the exponents of the empirical model (4) were found to be extremely sensitive to data points at longer exposure times. This indicates that the exponential model is not a good one, at least for immersion corrosion.

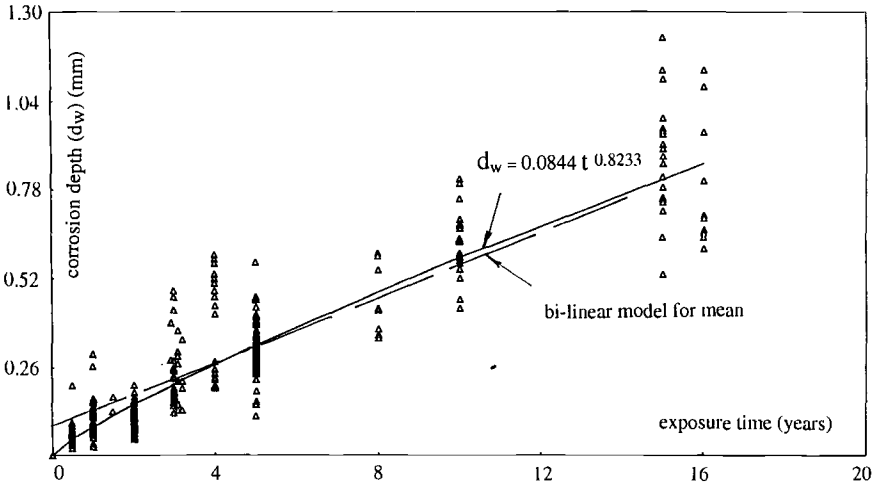


FIG. 1 - Immersion corrosion data points corrected for temperature with (i) fitted bi-linear model (eqn 1), and (ii) fitted exponential model for mean (eqn 4a).

CONCEPTUAL MODEL FOR MARINE CORROSION

Assumptions

Only general or uniform corrosion (as characterised by weight-loss) of specimens under marine conditions will be considered. This is obviously an idealization. For convenience inhomogeneity due to the formation of localized corrosion "cells" will be ignored herein.

The factors which influence corrosion of steel by sea-water include biological agents, temperature, salinity, dissolved oxygen, pH, wave action, water velocity, presence of pollutants, etc. Detailed reviews are available [4, 6]. However, the important influences of biological agents requires some comment and observations.

Biomass and Bacteria

It is now generally accepted that immediately upon being placed in seawater, the physical and chemical properties of the material surface are modified such that dissolved organic material are absorbed/adsorbed onto the surface. Bacteria, diatoms and other micro-organisms begin to colonise the substratum [9]. Observations in the North Sea suggest that micro-algal communities tend to develop on all substrates, with some seasonal dependence. Colonization tends to be rapid with micro-algal colonizers, mainly diatoms, present in large numbers within a few days of immersion. This colonization form what is known as the primary biofilm. Usually it is overgrown by different species, giving a

layered pattern. Generally, colonization tends to be relatively uniform on continuously submerged substrata, but is more clumped and patchy on inter-tidally exposed substrata [9].

In terms of oxygen diffusion to a corroding surface, it is important to note that most bacteria in situ are now considered to be small, passing through pores of 0.45 μm diam bacteriological filters. The cells also appear to be highly motile, suggesting that bacterial activity can occur within the corrosion products [10].

The biomass contains aerobic and anaerobic bacteria and other constituents in microbial communities or "consortia". Interactions between the constituents in the consortia are important for the growth, development and survival (and death) of the anaerobic bacteria. In particular, the aerobic bacteria appear to be important for reaching the required threshold level of supply of nutrients for the anaerobic bacteria [11,12].

Primary biofilms contain a variety of material, including aerobic and facultative heterotrophs, anaerobes and, importantly, sulphate reducing bacteria. It has been suggested that after a relatively short time, the uptake of oxygen by the aerobic species is controlled by the rate of oxygen diffusion through the primary biofilm (and subsequent corrosion products and biological material) and that when the oxygen supply is sufficiently low, anaerobic conditions begin to develop in the region of the corrosion interface [12].

Most marine bacteria are thermosensitive. There is a small positive growth response to mild increases in temperature, such as might be the result of seasonal and daily changes. However, the bacteria begin to die when the temperature is much above normal for any length of time [13, 14]. UV (or solar) radiation (which is generally high above or on water surfaces, but reduces very quickly with water depth) can have both lethal and non-lethal effects on bacteria [15]. Also, there is the possibility of dormancy (i.e. cells survive but are inactive). For example, natural bacterial communities in seawater were found to react rapidly to enrichment with organic nutrients, with good kinetic response within 12 hours and most responding after 20-36 hours. Such a response times suggest that some cells in the consortium were functionally switched-off or dormant, since substantial cell multiplication in this time frame is unlikely [15]. These matters are introduced here for further discussion, mainly when considering tidal corrosion.

Phenomenological Model

The model for marine corrosion to be considered herein is a development of the various earlier phenomenological models outlined above. The model attempts to take account somewhat more closely the phenomenological features which are now evident about marine corrosion. Thus, detailed modeling of electrochemical reactions and surface and biological activity is not attempted, although there is an interesting literature on mathematical models related to biofilms [16].

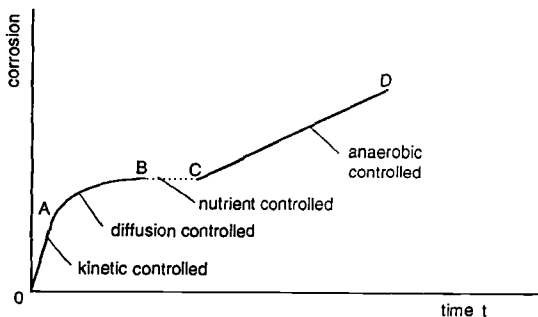


FIG. 2 - Proposed conceptual phenomenological model for marine corrosion

Figure 2 shows the main features of the proposed phenomenological model. A discussion of each of the components of the model is given below. The application of the model to a specific situation will be described later in the paper. In the discussion to follow it will be assumed that seawater is present on the corroding surface, through full continuous immersion or through periodic or continuous wetting in tidal conditions at sea or in atmospheric conditions at sea or close to it.

Initial Corrosion (Kinetic)

When a steel specimen is first exposed to sea-water, the reaction is likely to follow conventional electrochemical rules in which iron molecules are changed to various forms of ferrous hydroxides [4]:



Also, the corrosion product mass m_{cp} is a linear function of the amount of material consumed in the corrosion process:

$$m_{cp} = \alpha \cdot \gamma_s \cdot x \quad \text{per unit area} \quad (6)$$

where x is the loss of material (steel) due to corrosion (obtained from weight-loss and expressed in millimetres), γ_s is the density of steel and α is a constant.

Experimental evidence suggests that x is a linear function of the amount of dissolved oxygen in the sea-water [4]. Assuming that oxygen can reach the surface where the electrochemical reaction occurs, the rate of the reaction (5) can be expressed as:

$$x = \lambda \cdot k_i \cdot C_i^n \quad (7)$$

where C_i is the oxygen concentration at the corrosion interface, n is an exponent (the *order* of the reaction), k_i is a constant for the rate of corrosion and λ is a surface roughness coefficient to allow for the effect of surface roughness on corrosion rate. Field data for general corrosion shows that kinetic corrosion is a first order rate process [4] (i.e. the amount of corrosion is linearly proportional to the oxygen available), thus $n = 1$ and the material loss due to corrosion is a linear function of time. This is the first part of the model shown in Figure 2.

Diffusion-limited Corrosion

The kinetic rate reaction will continue to determine the rate of metal loss until the rate of oxygen supply becomes limited by the diffusion capacity of the (increasing) thickness of corrosion product and, interstitial micro-organisms and biological products. The time when this transition occurs will be influenced by various factors. These include the removal of corrosion and biological products due to impact, abrasion or erosion (such as due to water current) and the effects on the bio-matter of UV radiation, pollutants and, possibly, drying-out (as in tidal and atmospheric conditions - see below).

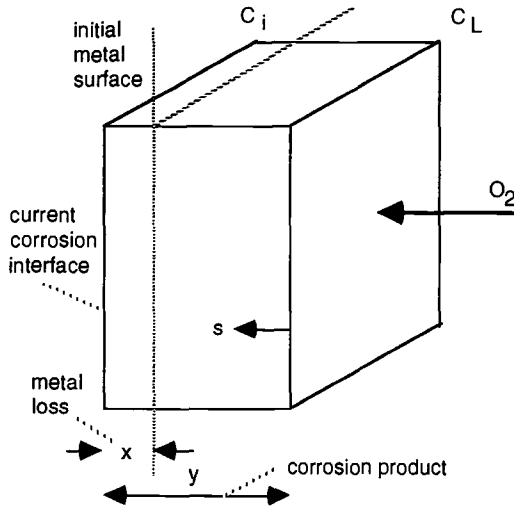


FIG. 3 - Element of corrosion product showing oxygen transfer, moving corrosion interface and mathematical notation

The diffusion-kinetic reaction system governing this part of the corrosion behaviour can be idealized as a series system. This means that the rate of the overall process is controlled by the slowest link of the component processes. From this follows the common observation that corrosion is either kinetically or diffusion controlled [17].

In previous work on corrosion modeling in the context of atmospheric corrosion [2, 3], the formulation for diffusion of oxygen through the corrosion product layer was referred back to the work of Tammann in 1923 [18] on tarnish layers and on the observations of Copson [19] for atmospheric corrosion, as well as on experimental observations. Various efforts have been made to extend the formulation to allow for relevant environmental related factors [e.g. 2,3]. The work by Evans [17], which has some similarities with that to be outlined below, appears to have been largely overlooked.

The basic case of diffusion limited corrosion may be represented as follows. Let it be assumed that the corrosion and biological products discussed earlier are intimately intermixed and together form the layer through which oxygen diffusion to the corroding surface must occur: let this be assumed to follow conventional diffusion laws:

$$\frac{dO_2}{dt} = \text{oxygen mass flow} = \frac{k_1(C_L - C_i)}{R} \quad (8)$$

where O_2 represents the mass of oxygen transfer, C_L and C_i are the concentrations of oxygen in the seawater and at the corrosion interface respectively, R is the resistance to diffusion and k_2 is a constant. The "driving force" for the mass transfer of oxygen is the difference in the oxygen concentrations: for an on-going corrosion process in well-oxygenated conditions this can be taken as sensibly constant. Since the amount of corrosion is a linear function of the available dissolved oxygen content in the sea-water (see expression (5) above), it follows that:

$$\frac{dO_2}{dt} = \eta \cdot \frac{dx}{dt} \tag{9}$$

where η is a constant.

Although the corrosion and biological products are inter-mixed, let the resistance R be taken as the sum of the resistance provided by the corrosion products and of the resistance provided by the biomass:

$$R = R_{cp} + R_b \tag{10}$$

or

$$R = \int_0^y f_{cp}(s) \cdot \gamma_{cp}(s) \cdot ds + \int_0^y f_b(s) \cdot ds \tag{11}$$

where $\gamma_{cp}(s)$ is the density function for the corrosion products (see Figure 3), f_{cp} is a function obtained from diffusion experiments and $f_b(s)$ is a biomass diffusion resistance function. The variable s represents the distance from the exterior of the corrosion product layer measured towards the corrosion interface and y represents the total depth of corrosion products and biological matter inhibiting oxygen diffusion (see Figure 3).

$$R = \int_0^y [f_{cp}(s) \cdot \gamma_{cp}(s) + f_b(s)] ds \tag{12a}$$

$$\text{or } R = k_2 \cdot y \tag{12b}$$

Collecting equations (8 - 12) produces:

$$\frac{dx}{dt} = \frac{k_3}{y} \tag{13}$$

where k_3 is a constant incorporating earlier constants and assumptions. If it is now assumed that the density of corrosion products is uniform with depth, the average density $\bar{\gamma}_{cp}$ can be used, so that equation (6) becomes:

$$m_{cp} = \bar{\gamma}_{cp} \cdot y = \alpha \cdot \gamma_s \cdot x \tag{6a}$$

where now the biological products inhibiting oxygen diffusion are included in the total corrosion product. Substituting into (13):

$$\frac{dx}{dt} = \frac{k_4}{x} \tag{14}$$

which produces, on integration

$$x = \sqrt{k_5 \cdot t + c} \tag{15}$$

where k_4 , k_5 and c are constants. If the depth of corrosion x_1 at time t_1 is known, equation (15) may be written as:

$$x = \sqrt{2k_5(t - t_1) + x_1^2} \tag{15a}$$

Only if the curve passes through the origin (which means that the process is diffusion controlled from the very beginning, an extremely unlikely situation), will $x_I = t_I = 0$, so that

$$x = k_c \cdot t^{\frac{1}{2}} \quad (15b)$$

This is the standard diffusion-controlled corrosion rate equation widely used and quoted as the basis for the corrosion - time curves in the atmospheric corrosion literature (e.g. [2,18]). Surprisingly, very little attention has been given to the various important assumptions which must be made in its derivation, as given here. It is noted that Evans [19] did consider the effect of kinetic versus diffusion controlled behaviour and the implications this has for the corrosion curve.

Modifications of Basic Relationship

The results given above must be modified if allowance needs to be made for corrosion and biological product removal or for the possible increase in density of corrosion products with s (see Figure 3). At least three cases can be identified involving exposure of the specimen to both immersion and atmospheric conditions (e.g. at the half tide location). Each of these cases represent idealizations of the actual situations as they might occur in the field.

1. Exposure "at sea". Even without the aggravating conditions of wetting due to sea spray, spray impact, etc. it is likely that even an "atmospheric" specimen will remain continuously wet due to the high water vapour conditions and the hygroscopic property of sea-salt. Unless the sea conditions are extremely quiet, it is unlikely that rain or UV exposure will have much effect. The seawater is likely to be high in dissolved oxygen.

2. Exposure in protected sea conditions, such as in harbours, bays etc. In this case drying out of an "atmospheric" specimen is much more likely, with proportionally greater UV exposure, possible dormant states of the biomass and effects of rain in diluting the salt content and causing densification of the corrosion products. For tidal specimens the effect will be less and it will be less still for immersed specimens.

3. Exposure "inland". This is the case which has been described extensively in the literature for atmospheric corrosion, often in association with industrial pollution. Drying out of "atmospheric" specimens over lengthy periods is possible, depending on local climate and location. This will slow the rate of corrosion. The effect can be incorporated readily into the above model by noting that the slope of the corrosion-time curve will be reduced in direct proportion to the percentage of "wet" time compared to total time t [2]. On the other hand, the effect of UV radiation on any micro-organisms is likely to be considerable for atmospheric and tidal exposure and less so for immersion exposure conditions.

Each of these cases is more complex than the basic model for diffusion limited conditions described above since they involve periodic processes rather than continuous ones. The precise behaviour is also likely to be dependent on the timing of the various processes, particularly for the early corrosion behavior [2, 3, 4, 17, 20]. From a modeling viewpoint it may be sufficient to take annual average values, both for input variables and for the resulting corrosion. Account may need to be taken also of particular environmental conditions such as sea-spray effects, however these will not be considered specifically herein. Only the two important special cases will be discussed below - removal of corrosion product protection and corrosion product densification.

Removal of Corrosion and Biological Products

The effect of higher or lower rates of development of the biological products and the steady removal of corrosion products (such as due to water current, abrasion, erosion etc.) can be considered in a simple manner. If each of the densities of the biological and the corrosion products are constant with respect to s , then equation (14) will become

$$\frac{dx}{dt} = \frac{k_7}{x(1 + k_b/k_{cp})} \tag{16}$$

where k_{cp} and k_b are given by the first and second terms in equation (11) respectively, each constant in value with respect to s . It follows that

$$x = \sqrt{\frac{k_8 \cdot t}{1 + k_b/k_{cp}} + c_2} \tag{17}$$

Again, only when the curve is assumed (incorrectly) to pass through the origin, will the constant c_2 be zero. It is then evident that changes in biomass growth rate or steady removal of corrosion products affects only the constant k_8 in equation (15). The exponent is not effected, contrary to what has been suggested in the literature [e.g. 2].

Densification

Densification of the corrosion products with closeness to the corrosion interface region is considered to be the result of rain [2,3] and, possibly, the initial stage of dry conditions at the interface [20]. However, there appears to be no data to help form a model of the density function $\gamma_{cp}(s)$ or the function $f_{cp}(s)$ which measures the porosity (see equation 11). A first approximation might be made by reference to considerations of porosity involving spherical particles (e.g. [21]). These suggest that the resistance to fluid flow is inversely proportional to (square of) the "hydraulic radius", a measure of pore area to pore perimeter, with wide, low aspect ratio pores having a very low radius. It also suggests that the resistance is proportional to (the square of) the "tortuousness" of the flow path.

A preliminary estimate of the effect of corrosion product densification might be made by reference to the geomechanics literature and using some reasonable estimates [21]. In particular, it will be assumed that $\gamma_{cp}(s)$ is proportional to s^2 and that

$[f_{cp}(s) \cdot \gamma_{cp}(s) + f_b(s)]$ is proportional to s^n with n in the range 3 - 4. It then follows that

$$R = K_1 \cdot \int_0^y s^n \cdot ds = K_2 y^{n+1} \tag{18}$$

where K_i ($i=1,2$) are constants. Also, the mass balance requires that

$$\alpha \cdot \gamma_s \cdot x = \int_0^y \gamma_{cp}(s) \cdot ds = \frac{1}{3} y^3 \tag{19}$$

Using these two expressions in equation (8) together with (9) produces eventually:

$$\frac{x^{m+1}}{m+1} = K_4 \cdot t + c_3 \tag{20}$$

with the parameter m in the range 1 - (about) 2. Evidently, if $m = 1$, the standard result (equation 15) is obtained; if $m = 2$, there is obtained:

$$x = [K_5 \cdot t + c_4]^{\frac{1}{2}} \quad (21)$$

which shows that (with $c_4 = 0$) the exponent is reduced compared to the standard case, as has been suggested in the atmospheric corrosion literature [e.g. 2]. Evidently, the precise form of the densification function is critical in the value of the exponent n which results.

Anaerobic Corrosion

The final part of the proposed model consists of anaerobic corrosion under the action of sulphate reducing bacteria (SRB). Southwell *et. al.* [5] noted already in the 1970's that the slope of the corrosion curves for immersed and for tidal conditions were very similar for the Panama Canal Zone data. They suggested that anaerobic conditions were critical in long term corrosion behaviour. Since then it has become clear that the action of the SRB is to create sulfides at or near the corrosion interface and that it is this rather than any biological interaction with the steel which creates the observed corrosion conditions [12].

In view of the observations of Larrabee and Mathay [22] that long term atmospheric corrosion of steel is well described by a linear function (rather than the exponential function widely applied for shorter exposure times), it is possible that atmospheric corrosion, under the marine conditions considered herein, also eventually becomes anaerobic. The rate at which anaerobic activity occurs (i.e. the slope of the line CD in Figure 2) will depend on the availability of moisture at the corrosion interface. It might be expected that in conditions of continuous availability of moisture the slope of the line will be similar to that for immersion corrosion conditions.

Figure 2 suggests that the anaerobic state does not necessarily commence at the "end" of the diffusion state (i.e. when oxygen diffusion might be considered to be at a rate insufficient to support aerobic activity). As noted above, there is some evidence that anaerobic activity requires a threshold supply of nutrients and that this depends on the sufficient development of aerobic bacteria. It is therefore possible that a period of essentially zero corrosion could occur between the effective end of oxygen diffusion and the satisfaction of the nutrient threshold as governed by the growth of aerobic bacteria. In practice the slope of the curve will not reach zero since it would not be expected that all corrosion cells will reach the anaerobic state at the same time. Hence a transition region might be expected.

Anaerobic corrosion can be represented by

$$x = \mu D(t - t_i) + E \quad (22)$$

where μ describes the availability of moisture, D is a rate constant and E is a constant describing the depth of corrosion at time t_i at which time anaerobic activity concludes or nutrient requirements for the anaerobic bacteria are satisfied. Data for the Panama Canal Zone [5] suggests that μD is about 0.07 mm/year.

AN APPLICATION

The model described above can be applied in a preliminary way to immersion, tidal corrosion data and atmospheric corrosion conditions using the Panama Canal Zone data [5] and data for Kure Beach [4]. The tidal case is for protected waters only, due to the scarcity of data for near- and at- sea situations. The curves are sketched in Figure 4. Corrections for temperature and other conditions did not need to be applied. Two curves are shown for

atmospheric corrosion. The 250m curve was obtained at Kure Beach and represents, in a qualitative way, the variation from the "at sea" curve as the influence of drying out, and wetness time become more important.

Some qualitative observations can be made. It seems plausible that when the corrosion reaches about 0.25 mm in depth (approx 10 mils) oxygen transfer is reduced to a level to allow anaerobic conditions to take over. This appears to be the situation for all curves, except where there are significant periods of dryness (as would be expected in the 250m data set). Unfortunately, the transition point does not arise naturally from the theory presented above.

Although the data so far appear to be insufficient to show that atmospheric corrosion develops into the anaerobic state, the data for longer exposure times is not inconsistent with such a hypothesis, given that the exposure to moisture is the same. This would suggest that the anaerobic corrosion rate is about the same for each environment. One reason for this is that bacterial action is likely to be a factor also for atmospheric corrosion under severe marine conditions, since there is likely to be some airborne transport (spray / mist) of bacteria, particularly when the specimens are close to the sea.

The rate of corrosion in tidal conditions would be expected to be affected by wave action and the possibility of oil on the water surface [8]. These matters do not appear to have been factors in the data shown in Figure 4, but would need to be considered in further analyses.

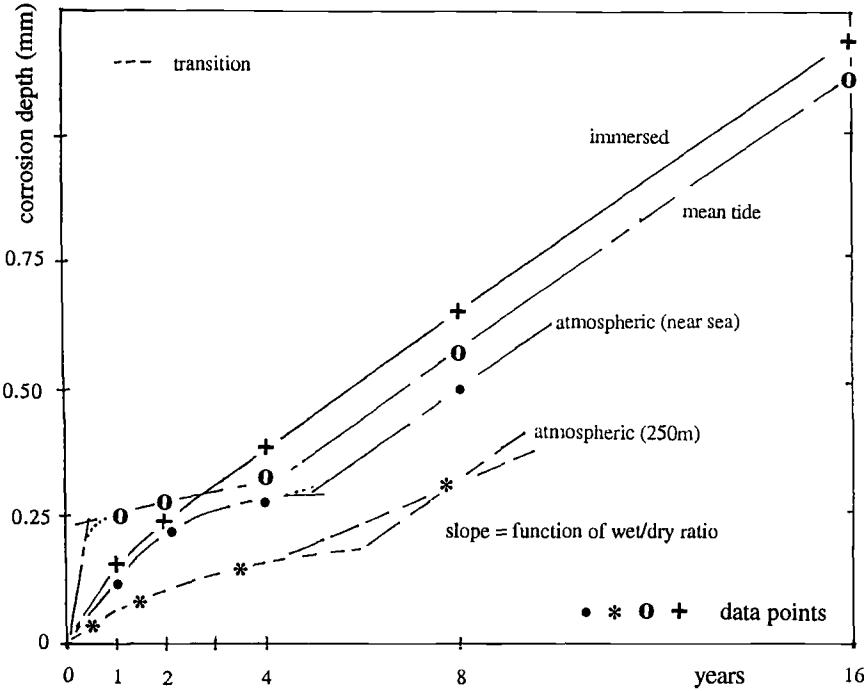


FIG. 4 - Fitted relationships for Panama Canal zone and Kure Beach (250m) data.

DISCUSSION

The curve for tidal corrosion conditions in Figure 4 has been drawn for the specimen at the mean-tidal level. Clearly, as the specimen level is lowered, the corrosion behaviour would be expected to approach that of the fully immersed specimen at that location. Similarly, as the specimen level is raised, the corrosion behaviour would be expected to take on more of the properties of atmospheric corrosion at the same location. Hence the precise definition in test programs of what is actually the location of such partially exposed specimens is important for theoretical interpretation. For atmospheric corrosion the micro-climatic conditions are important [2,3] as is the specimen orientation and inclination [1,5]. Very high atmospheric corrosion rates have been recorded for specimens close to, or at sea [5,22,23]. Thus, tidal corrosion rates at sea are also likely to exhibit very high corrosion rates, probably somewhere between the immersion rates and the atmospheric rates. This supports the hypothesis that there is a transition from immersion corrosion to tidal corrosion to atmospheric corrosion at (or very near to) the sea. It also points up the need to record relevant parameters such as location and micro-climatic indicators.

For immersion corrosion, it appears that the early, diffusion controlled part of the process is established rather rapidly [24]. In view of equation (15), a smooth transition between kinetic controlled and diffusion controlled corrosion would not necessarily be expected (see point A in Figure 2). However, the data in Figure 4 suggests that the transition is relatively smooth, presumably because the kinetic state controls for only a relatively short time. More data in these regions would be useful.

Corrosion data [5] show that the transition from immersion aerobic to anaerobic corrosion is apparently smooth. The transition for tidal and atmospheric corrosion appears to be more pronounced (see Figure 4). At this stage it does not appear possible to suggest precisely when the transition from aerobic to anaerobic conditions will occur.

The high initial corrosion period observed for tidal corrosion specimens has not been recorded for immersion corrosion except for one (reported) case (see Naos Island [ref 5, p 379, Fig. 5]). This observation tends to support the contention that there is a transition between fully immersed and tidal specimen corrosion behaviour.

For atmospheric corrosion, the diffusion part of the proposed model appears to be the only part which has been considered in the literature, but with the theoretical exponent 0.5 replaced by a number obtained from curve fitting. Curve fitting exercises in the past appear to have ignored the possibility that the relationship between material loss and time may change with time, and in particular the possibility of a kinetic reaction governing early corrosion behaviour, and anaerobic activity possibly governing later behaviour. The result is that purely empirical constants have been obtained for the assumed exponential relationship. As has already been noted, these constants are extremely sensitive to changes in data, history, etc.

It is suggested that one reason for the lack of observation of some of the features predicted by the idealised model is that the early part of the corrosion process in real sea-water environments generally has not been observed. In some in-situ test programs the first observations were made at 6 months; in most, however, there were no observations before 12 months [5, 6]. Hence it is easy not to discern any short-term peculiarities in the data and which may assist in model development. A further, complicating, factor is that there is a lot of scatter in the data which has been reported from various sources (see Figure 1), mainly, it is suggested, as a result of the unrecorded influences of environmental variables.

Reanalysis of all available data, using some reasonable assumptions about data which appear in many cases not to have been recorded, is necessary for further development of the proposed model. This work is currently being undertaken.

Finally, as indicated in the first part of the paper, it will be necessary to adopt a probabilistic (and iterative) approach to model development. A necessary precursor to such work is the development of a deterministic model of reasonable quality. This will help focus more clearly on the data required and in turn such data should help refine the model.

CONCLUSION

The development of an integrated phenomenological model for "uniform" corrosion of mild and low alloy steels under various marine conditions requires account to be taken of the main factors influencing corrosion behaviour. These include chemical and physical aspects (which are well-known) and also biological factors. It is argued that the latter have an important effect and that consideration of their influence allows a plausible model to be proposed. The model consists of kinetically controlled, oxygen diffusion controlled, possibly a nutrient controlled and anaerobic controlled corrosion zones. Under various conditions this model was shown to be compatible with consistent long-term corrosion data. It was shown also that some data-based curve-fitting approaches to model development are theoretically inconsistent. The extent to which this is a serious matter awaits both high quality short-term and high quality long-term corrosion data. Finally, the proposed model should be seen as part of an on-going process involving attainment of reasonable consistency between corrosion data and theoretical corrosion models.

ACKNOWLEDGMENT

This work is part of a project supported financially by the Australian Research Council under grant A89530940. The support of Professors L. Boswell, City University, London, England and P. Grundy, Monash University, Melbourne, Australia in providing facilities and support for the continuation of this project while the author visited their institutions during June-July and August - September, 1995 respectively is gratefully acknowledged.

The Author is indebted to a number of referees for their various observations, corrections and suggestions. Their input is acknowledged with gratitude.

REFERENCES

- [1] Larrabee, C.P. "Mechanisms by which Ferrous Metals Corrode in the Atmosphere," Corrosion - NACE Vol. 15, No. 10, 1959, pp 526t-529t.
- [2] Benarie, M. and Lipfert, F.L. "A General Corrosion Function in Terms of Atmospheric Pollutant Concentrations and Rain pH," Atmospheric Environment, Vol. 20, No. 10, 1986, pp 1947-1958.
- [3] Feliu, S., Morcillo and Feliu, Jr. S. "The Prediction of Atmospheric Corrosion From Meteorological and Pollution Parameters - 1. Annual Corrosion & - 2 Long-Term Forecasts," Corrosion Science, Vol. 34, No. 3, 1993, pp 403-422.
- [4] Schumacher, M. (Ed.) Seawater Corrosion Handbook, Noyes Data Corporation, New Jersey, 1979.
- [5] Southwell, C.R., Bultman, J.D. and Hummer, Jr., C.W., "Estimating Service Life of Steel in Seawater", Schumacher, M. (Ed.) Seawater Corrosion Handbook, Noyes Data Corporation, New Jersey, 1979, pp 374 - 387.
- [6] Melchers, R.E. and Ahammed, M. "Nonlinear Modelling of Corrosion of Steel in Marine Environments," Research report 106.09.1994, Department of Civil Engineering and Surveying, The University of Newcastle, 1994.
- [7] Mercer, A.D. and Lumbard, E.A. "Corrosion of Mild Steel in Water," British Corrosion Journal, Vol. 30, No. 1, 1995, pp 43-55.

- [8] Melchers R.E. (1995) "Probabilistic modelling of Marine Corrosion of Steel Specimens", Conference Proceedings, ISOPE-95, International Society for Offshore and Polar Engineering, the Hague, the Netherlands, June 12-15, 1995.
- [9] Edyvean, R.G.J. "Diatom Communities on Steel Protected from Corrosion in Seawater", L.V. Evans and K.D. Hoagland, (Eds) Algal Biofouling, Elsevier, Amsterdam, 1986, pp. 231-246.
- [10] Silverman, M., Belas, R. and Simon, M. "Genetic Control of Bacterial Adhesion," K.C. Marshall, (Ed) Microbial Adhesion and Aggregation, Springer-Verlag, Berlin, 1984, pp 95 -108.
- [11] Carlucci, A.F. Nutrient and Microbial Response to Nutrients in Seawater, R.R. Colwell and R.Y. Morita (Eds), Effect of Ocean Environments on Microbial Activities, Uni. Park Press, Baltimore, 1974.
- [12] Hamilton, A.W., "Bio-corrosion: the Action of Sulphate Reducing Bacteria," Ratledge, C. (Ed) Biochemistry of Microbial Degradation, Kluwer Academic Publishers, Dordrecht, the Netherlands, 1994, pp 555-570.
- [13] Morita, R.Y., "Temperature Effects on Marine Organisms," R.R. Colwell and R.Y. Morita (Eds), Effect of Ocean Environments on Microbial Activities, Uni. Park Press, Baltimore, 1974, pp 75-79.
- [14] Breznak, J.A., "Activity on Surfaces," K.C. Marshall, (Ed) Microbial Adhesion and Aggregation, Springer-Verlag, Berlin, 1984, pp 203 -222.
- [15] Austin, B., Marine Microbiology, Cambridge University Press, Cambridge, 1988.
- [16] Characklis, W.G. and Marshall, K.C., Biofilms, John Wiley & Sons, New York.
- [17] Evans, U.R., The Corrosion and Oxidation of Metals: Scientific Principles and Practical Applications, Edward Arnold (Publishers) Ltd., London, 1960.
- [18] Tammann, G., Lehrbuch der Metallographie, 2nd Edn, Leipzig, 1923.
- [19] Copson, H.R., "A Theory of the Mechanism of Rusting on Low Alloy Steels in the Atmosphere", Proceedings, ASTM, Vol. 45, 1945, p 554.
- [20] Lloyd, B. and Manning, M.I. The Episodic Nature of the Atmospheric Rusting of Steel, Corrosion Prevention and Control, Vol. 38, No. 2, 1991, pp 29-35.
- [21] Wu, T.H., Soil Mechanics, Allyn and Bacon, Inc. Boston, 1966.
- [22] Larrabee, C.P. and Mathay, W.L., "Iron and Steel," F.L. LaQue and H.R. Copson, (Eds) Corrosion Resistance of Metals and Alloys, Second Edition, Reinhold Publishing Corp. New York, 1963, pp 305-353.
- [23] Roy, S.K. and Ho, K.H., "Corrosion of Steel in Tropical Marine Atmospheres," British Corrosion Journal, Vol. 29, No. 4, 1994, pp 287-291.
- [24] Ho, K.H. and Roy, S.K., "Corrosion of Steel in Tropical Sea Water", British Corrosion Journal, Vol. 29, No. 3, 1994, pp 233-236.

Bopinder S. Phull,¹ Stanley J. Pikul,² and Robert M. Kain³

SEAWATER CORROSIVITY AROUND THE WORLD: RESULTS FROM FIVE YEARS OF TESTING

REFERENCE: Phull, B. S., Pikul, S. J., and Kain, R. M., “Seawater Corrosivity Around the World: Results from Five Years of Testing,” Corrosion Testing in Natural Waters: Second Volume, ASTM STP 1300, Robert M. Kain and Walter T. Young, Eds., American Society for Testing and Materials, 1997.

ABSTRACT: A world-wide test program was undertaken by ASTM Task Group G1.09.02.03 to assess the relative corrosivity of seawater at 14 test sites. Aluminum alloy 5086 (UNS A95086), 90/10 copper-nickel (UNS C70600), and copper-bearing carbon steel (UNS K01501) test specimens were prepared at one location, shipped to the various sites, and returned to the original location for final evaluations. Results obtained through five years of testing indicate that corrosion behavior was generally within the limits of previously published results. The results show that while seawater is a ubiquitous environment, and quite similar in terms of chloride content and pH, the corrosivity is site-specific, and likely to be influenced by a myriad of other factors such as temperature, dissolved oxygen concentration, flow, degree of fouling, bacterial activity, pollution, etc. All of these factors are themselves often interrelated. The cooperation of all program participants has contributed much toward accomplishment of the objectives. More frequent monitoring of seawater variables at an exposure site is always helpful in better interpretation of the results of corrosion tests performed there. All of the 0.5 through 5-year exposure data are presented here; any typographical errors in the 0.5 through 3-year exposure data published previously have been corrected.

KEY WORDS: seawater, corrosivity, world-wide, aluminum alloy, copper-nickel, steel, localized corrosion, erosion, velocity, biofouling

¹Principal Corrosion Scientist, ²Senior Research Technologist, ³Senior Corrosion Scientist, LaQue Center for Corrosion Technology, Inc., Wrightsville Beach, NC 28480.

INTRODUCTION

Within ASTM Subcommittee G1.09 on Corrosion in Natural Waters, a task group (G1.09.02.03) was appointed in 1980 to organize a world-wide seawater corrosivity test program. The objective of the task group was to apply existing standards for conducting corrosion tests in seawater to compare the relative corrosivities at a variety of natural coastal sites around the world. This was accomplished by exposure of aluminum alloy A95086, copper-nickel alloy C70600, and K01501 steel specimens at the 14 test sites listed in Table 1 and shown on a world map (Fig. 1). A 5-year exposure program was initiated in 1983 and duplicate specimens of each alloy were removed after nominally 0.5, 1, 3, and 5-year durations in most instances. The LaQue Center for Corrosion Technology, Inc. agreed to handle the initiation of the program as well as the final evaluations. The 3-year results were reported previously [1]. This report summarizes the results of the 5-year test program.

EXPERIMENTAL PROCEDURE

Test Method

The test program was conducted according to the guidelines provided in ASTM G52: Standard Practice for Conducting Surface Seawater Exposure Tests on Metals and Alloys. One exception occurred at the Hawaii site where, despite a requirement to the contrary, the test panels were exposed horizontally rather than vertically, with the test rack being mounted to a nonmetallic pipe resting on the seabed. Although no immersion depth was specified, the participants were requested to ensure that the racks and specimens were fully submerged at all times. Typical seawater characteristics provided by the participants at all sites are summarized in Table 2. Initial exposure dates are given in Table 3. For the Australian test site, the original set of specimens exposed were all lost, reportedly during a cyclone.

Test Materials

The materials used in the test program are listed in Table 4 with their respective compositions. Specimens (6 x 100 x 300 mm) of each material were supplied as-sheared to size. They were notch-coded for identification, for example, as shown in Fig. 2. Table 5 outlines the cleaning procedures used for each material. Following cleaning, the specimens were weighed to the nearest 0.1 g.

Test Racks

The specimens were mounted on metallic test racks using nylon bolts and washers for electrical isolation as illustrated in Fig. 3. The bolts were tightened to a torque of 1.7 Nm. Eight specimens of each material were attached to three individual racks for exposure at each site. The A95086 aluminum specimens were mounted on a 1.3 m-long

TABLE 1--Test sites for world-wide seawater corrosivity evaluations.

Site	Original Contact/Affiliation
Ocean City, New Jersey Bar Graph Code: NJ	G. A. Gehring, Jr. Ocean City Research Corporation
Wrightsville Beach, North Carolina Bar Graph Code: NC	S. J. Pikul LaQue Center for Corrosion Technology, Inc.
Key West, Florida Bar Graph Code: FL	M. H. Peterson U.S. Naval Research Laboratory
Freeport, Texas Bar Graph Code: TX	C. Arnold The Dow Chemical Company
Port Hueneme, California Bar Graph Code: CA	J. F. Jenkins U.S. Naval Civil Engineering Laboratory
Talara, Peru Bar Graph Code: PE	K. D. Eford Occidental Oil and Gas Company
KeAhole, Kona, Hawaii Bar Graph Code: HI	J. Larsen-Basse/T. Daniel University of Hawaii at Manoa
Australia, Innisfail Bar Graph Code: AU	J. J. Batten Materials Research Laboratories
Sakata Harbor, Japan Bar Graph Code: JA	S. Sato Sumitomo Light Metal Industries, Inc.
Genoa, Italy Bar Graph Code: IT	E. Mor Istituto per la Corrosione Marinadei Metalli-del C.N.R.
Sjaelland, Denmark Bar Graph Code: DE	H. Arup Korrosionscentralen, ATV
Studsvik, Sweden Bar Code: ST	S. Henrikson/E. Mattsson Swedish Corrosion Institute
Bohus-Malmon, Sweden Bar Code: BM	S. Henrikson/ E. Mattsson Swedish Corrosion Institute
Isle of Wight, England Bar Code: EN	P. E. Francis National Physical Laboratory

TABLE 2--Worldwide seawater exposure sites: Typical seawater characteristics.

Site	Rack Location	Range of Environmental Constituents ^a			pH
		Dissolved Oxygen, ppm	Salinity	Temperature °C	
Ocean City, NJ	from raft 0.3 m below surface	5.2 - 11.7	31 - 34	1 - 29	7.5 - 8.2
Wrightsville Beach, NC	from wharf in channel	5.0 - 9.6	31.8 - 37.6	7 - 30	7.9 to 8.2
Banks Channel					
Key West, FL	under pier	4 - 8	33 - 39	16 - 31	8.0 - 8.2
Fleming Key					
Freeport, TX	intake flume	1.5 - 6.0	11.7 - 19.4 ^b	15 - 27	7.5 - 8.6
Port Hueneeme, CA	from bulkhead	3.6 - 5.3	33	14 - 21	7.9 - 8.1
Port Hueneeme Harbor					
Talara, Peru	from pier 180 m from shore	5 - 6	19.8 ^b	18 - 22	8.2
KeAhole, Kona, Hawaii	45 m from shore on pipe	6 - 14	34.6 - 35	24 - 28	8 - 8.3
Australia, Innisfail	from raft	5.1 - 6.5	31.7 - 37.2	23 - 30	8 - 8.5
North Bamard Islands					
Japan	off docking pier	7.1 - 13	16.8 - 18.3 ^b	2 - 28	8.4
Sakata Harbor					
Italy	from raft	4.5 - 6.0	35	11 - 25	8.1
Genoa Harbor					
Denmark, Sjaelland	from raft in Fjord	NA ^c	18 - 28	0 - 18	7.5 - 8.0
Kyndby Isefjord					
Sweden					
Studsvik (Baltic Sea)	from wooden bulkhead	6 - 10	7.8 - 8.1	2 - 20	7.4 - 7.6
Bohus-Malmon (North Sea)	from raft	6 - 10	21 - 28	2 - 20	8.0 - 8.2
England, Isle of Wight	from raft				
Langstone Harbour		88 - 118 ^d	34 - 34.6	5 - 22	7.8 - 8.4

^a compiled from information provided by participants^b chlorinity, g/L^c NA = not available^d reported as % saturation

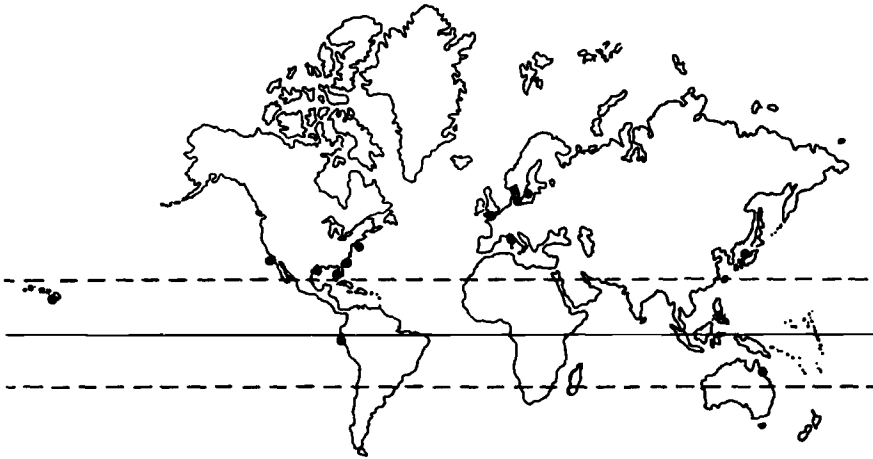


FIG. 1--General location of exposure sites. Solid line indicates Equator; dashed lines indicate the Tropics.

TABLE 3--Summary of initial exposure dates

Test Site	Initial Exposure Date
Ocean City, NJ	July 1983
Wrightsville Beach, NC	May 1983
Key West, FL	May 1983
Freeport, TX	October 1983
Port Hueneme, CA	May 1983
Talara, Peru	March 1984
KeAhole, Kona, Hawaii	July 1983
Australia, Innisfail	July 1986*
Sakata Harbor, Japan	August 1983
Genoa, Italy	September 1983
Sjaelland, Denmark	October 1983
Studsvik, Sweden	August 1983
Bohus-Malmon, Sweden	August 1983
Isle of Wight, England	August 1983

* Second complete set of specimens, since original set lost in cyclone.

TABLE 4--Test materials chemical analyses.

Alloy	Composition, weight %	Supplier
5086 Al (UNS A95086) (H116 temper)	0.14 Si	Kaiser Aluminum and Chemical Corporation
	0.33 Fe	
	0.030 Cu	
	0.57 Mn	
	3.89 Mg	
	0.13 Cr	
	BAL Al	
90/10 Cu-Ni (UNS C70600) (hard)	9.44 Ni	Revere Copper Products, Inc.
	1.40 Fe	
	0.29 Mn	
	0.008 P	
	0.007 S	
	BAL Cu	
Carbon Steel (UNS K01501)	0.046 C	Armco, Incorporated
	0.32 Mn	
	0.006 P	
	0.009 S	
	0.003 Si	
	0.19 Cu	
	0.019 Ni	
	0.020 Cr	
	<0.002 Sn	
	<0.004 V	
	<0.011 Mo	
	<0.006 Ti	
	0.008 Al	
<0.002 Cb		
<0.0001 B		
<0.002 Zr		
0.004 Co		
<0.006 Pb		
<0.004 Te		
<0.004 Ce		
0.0004 As		
BAL Fe		

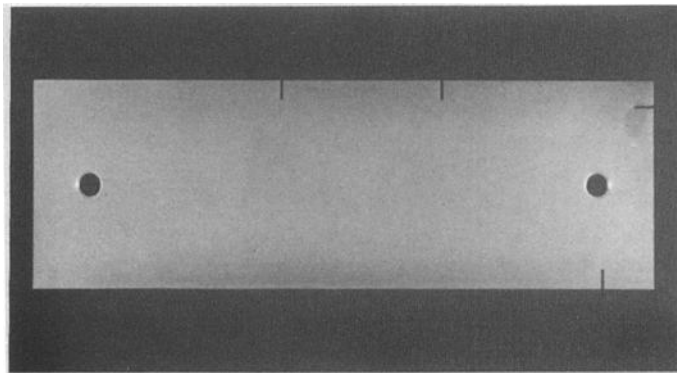


FIG 2--Typical appearance of a test specimen prior to exposure showing notches used as identification codes. The two specimen mounting holes are also apparent.

TABLE 5--Cleaning procedures for the test specimens.

<u>Prior to Exposure:</u>		
<u>A95086</u>	<u>C70600</u>	<u>K01501</u>
Acetone degrease	Acetone degrease	Sand blasted
30% HNO ₃ pickle (3 min)	Water rinse	Inhibited conc. HCl pickle (15 to 45 min)
Water rinse	Pumice scrub (light)	Water rinse
Pumice scrub	Water rinse	Pumice scrub
Water rinse	10% H ₂ SO ₄ pickle (3 to 5 min)	Water rinse
Alcohol rinse	Water rinse	Alcohol rinse
Dry with towel	Pumice scrub	Acetone rinse
Forced hot air dry	Water rinse	Dry with towel
Oven dry at 120°C	Alcohol rinse	Forced hot air dry
	Dry with towel	Oven dry at 120°C
	Forced hot air dry	
	Oven dry at 120°C	

After Exposure:

After seawater test exposures, all the specimens were lightly scraped to remove marine biofouling and loose corrosion products. This was followed in each case by pickling, pumice and detergent scrubbing and the remainder of the cleaning procedure for each alloy above.

NOTE: No detectable mass loss was noted on control specimens in any pickling treatment.

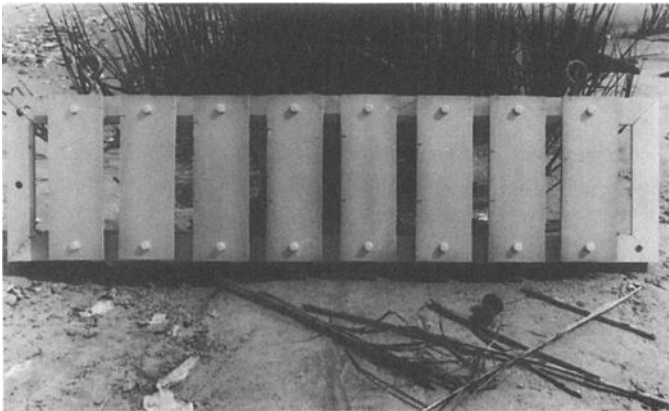


FIG. 3--Assembled test rack prior to exposure.

aluminum alloy test rack. Two Ni-Cu alloy-400 test racks (each 1.3 m-long) were used to separately accommodate the C70600 copper-nickel and K01501 steel specimens.

Eye bolts were affixed to the racks to facilitate exposure, from a fixed structure at each site, with the aid of ropes. The test racks with the mounted specimens were wrapped in polyethylene sheet and closed in with two bags of desiccant, crated, and shipped to each test site.

Exposures

At each of the 14 test sites, the test racks were exposed and retrieved by local site personnel. Duplicate specimens of each alloy were requested to be removed after exposures of nominally 0.5, 1, 3, and 5 years. Participants were requested to remove the specimens after the appropriate exposure periods, lightly brush and scrape them on site to remove heavy biofouling attachments, and dry them before packaging and return to the LaQue Center for evaluation. Participants were also requested to photographically document the as-removed appearance of specimens where possible, and provide environmental data for the site if it was available.

Evaluations

Upon receipt of the specimens from each site, the “before-cleaning” appearance was photographically documented for all but the 5-year specimens. The specimens were then cleaned to remove corrosion products and any remaining biofouling attachments using the following chemicals per ASTM G1: Standard Practice for Preparing, Cleaning, and Evaluating Corrosion Test Specimens.

for A95086 -- ambient temperature, 30% nitric acid

for C70600 -- ambient temperature, 10% sulfuric acid

for K01501 -- ambient temperature, concentrated hydrochloric acid inhibited with antimony trioxide

Further details of the cleaning procedures are given in Table 5.

The specimens were reweighed to determine mass loss (± 0.1 g). Measurements of thickness loss and localized depth of attack were obtained using a micrometer (± 0.01 mm) and depth gage (± 0.01 mm), respectively. As-measured maximum depths of attack, where the surrounding areas represent the datum, are reported. They have not been normalized with respect to decrease in original specimen thickness due to general corrosion. Selected specimens were also photographed after cleaning to illustrate variations observed in the type or extent of corrosion incurred.

RESULTS AND DISCUSSION

The corrosion data range for each material and exposure time are summarized in Table 6. To enable detailed comparisons for each and among the 14 test sites, the data for all specimens in the test program are tabulated in the Appendix, Tables 7 through 20. Also, much of the corrosion data are summarized in bar-graph form in Figures 4-6, and 11 and 12. As stated earlier, the original specimens sent to Australia were reportedly lost in a cyclone and a replacement set was provided. Unfortunately, the 6-month specimens from the replacement set were not received at the LaQue Center either. Apparently, they were lost during return shipment. Only one 6-month exposure specimen of each alloy was returned, instead of two, from the Freeport, Texas, site. This resulted in the return of three, instead of two, 5-year exposure specimens. The second set of specimens at the Port Hueneme, California, site were subjected to two years' exposure instead of one; and only one of duplicate 5-year specimens was returned. In several other cases, the test specimens were not exposed for the precise periods requested.

Aluminum Alloy A95086

Aluminum-magnesium alloys (5000 series) typically exhibit good resistance to both general and localized corrosion in seawater [2]. Some pitting or crevice corrosion, however, can be expected but the extent of such attack in surface seawater is affected by a number of factors, including oxygen content, temperature, velocity, and crevices such as those areas shielded by the attachment of biofouling organisms or deposits of sand or silt [2,3,4]. Since the corrosion resistance depends on the maintenance of a passive oxide film, aluminum-magnesium alloys are expected to be most resistant in seawater that is well aerated, for example, near the ocean surface.

Mass loss data from this program (detailed in the Appendix) show that the average corrosion rate of alloy A95086 decreased from 11 $\mu\text{m}/\text{yr}$ after 0.5 year to 7 $\mu\text{m}/\text{yr}$ after 1 year, 3 $\mu\text{m}/\text{yr}$ after three years, and about 2 $\mu\text{m}/\text{yr}$ after 5 years. These corrosion rates are generally within the range of published data referenced previously. Although general corrosion rates were calculated from mass loss to provide some overall idea of corrosivities at the various test sites, they should be interpreted very cautiously for service applications because the mode of attack was highly localized. At most of the test sites, a significant portion of the mass loss occurred during the initial 6 months of exposure, except in California, Denmark and England. Maximum depth of localized attack data are summarized in Fig. 4. With the exception of California and Sweden (Studs vik site), the maximum depths of attack over 5 years of exposure at each of the other test sites was less than 0.5 mm. It is not meaningful to compare depth of attack as a function of time, at any given test site, because the measurements were made on different specimens. In other words, it was not the same pits being monitored after initiation of attack. Even with minimal general corrosion, decreasing values of maximum pit depths measured on different test specimens, as a function of time, can lead to the erroneous interpretation that the pits are getting shallower. This is an idiosyncrasy of the stochastic nature of localized corrosion.

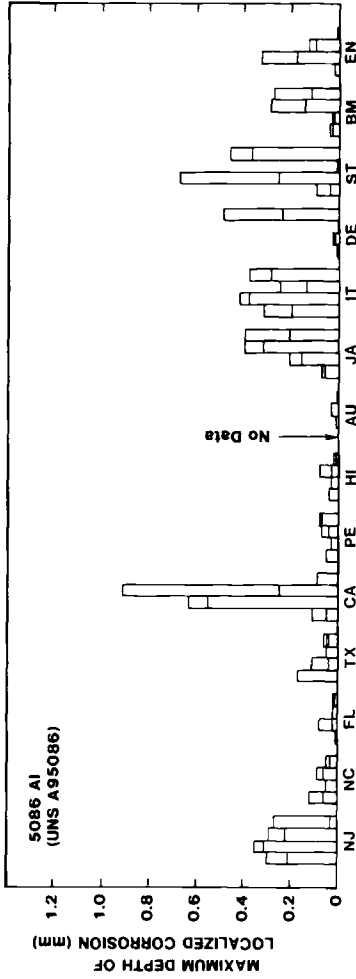


FIG. 4--Localized corrosion data for A95086 aluminum alloy in seawater at the 14 test sites. For key to site abbreviations, see Table 1. For each location, the 1st, 2nd, 3rd and 4th bars from the left correspond to exposure periods of nominally 0.5, 1, 3 and 5 years, respectively. (Note that the second bar for the California and Denmark sites represent exposure data for 2 and 1.5 years, respectively.)

TABLE 6--Summary of corrosion data for 14 worldwide seawater test sites.

Alloy	Exposure Period, year	Mass Loss Corrosion Rate Range, $\mu\text{m}/\text{yr}$	Average Thickness Loss Range, mm	Maximum Thickness Loss Range, mm	Max. Depth of Localized Attack Range, mm
A95086	0.5	3 - 19	0.01 - 0.32
	1.0	3 - 12	0.02 - 0.68
	3.0	1 - 12	0.03 - 0.91
	5.0	1 - 6	0.01 - 0.46
C70600	0.5	6 - 374	0.03 - 0.46
	1.0 ^a	4 - 29	0.01 - 0.35
	3.0	2 - 24	0.01 - 2.68
	5.0	2 - 17	0.01 - 1.01
K01501	0.5	82 - 550	0.08 - 0.59	0.16 - 0.95	...
	1.0	86 - 536	0.01 - 1.51	0.22 - 6.07	...
	3.0	62 - 224	0.72 - 2.58	0.92 - 6.07	...
	5.0	56 - 224	0.66 - 2.51	1.00 - 4.11	...

a - Excludes 1.5 and 2.0-year data from Denmark and California sites, respectively.

The maximum depth of localized attack on a boldly exposed surface (~0.9 mm after 3 years) occurred at Port Hueneme, California, a site where the test racks were subjected to constant wave action. On the one hand, this would normally bring a greater oxygen supply to the specimen surfaces and help maintain or reheel the protective oxide film disrupted, for example, by chloride ions or by impingement. On the other hand, it could encourage growth of marine fouling organisms because of increased aeration and nutrient supply. The shielding effects of the naturally created crevices interfere with the diffusion of oxygen, necessary to maintain passivity, and consequently leads to localized corrosion. This is the most likely mechanism for pitting and crevice corrosion of aluminum alloys in seawater and was previously observed and documented by Ailor [2]. The maximum pit depth reported by Brouillette [4] for another aluminum alloy, A95052, at the same Port Hueneme Harbor location, on a test specimen recovered from the seafloor after 30 months' exposure, was about 1.2 mm.

The second greatest depth of localized attack (~0.7 mm) occurred after one year at Studsvik, Sweden, a brackish water site with about one-fourth the salinity of "normal" seawater. Even more noteworthy is the fact that no measurable localized attack was noted on the two Studsvik specimens removed after three years; yet the maximum depth of

attack (0.46 mm) was the second highest of all the test sites after 5 years. Conversely, the 5-year specimens from England and Australia exhibited virtually no localized attack.

In regard to seawater temperature, there appears to be some evidence of lesser attack at the warmer sites, for instance in North Carolina, Florida, Texas, Peru, Hawaii, and Australia. However, the slight attack at the colder Denmark site for the 3-year exposures illustrates that seawater corrosivity isn't dictated by just this single variable. The lack of much more detailed information on seawater characteristics (e.g., silting, pollutants, biofouling, flow rate, etc.) at each test site precludes explanation of these observations in terms of seawater corrosivity.

Copper-Nickel Alloy C70600

The 90/10 Cu-Ni alloy C70600 is known for its good resistance to corrosion in seawater and to biofouling [5-11]. The corrosion resistance is usually attributed to the formation of a visible, protective corrosion product film on the exposed surfaces. Film formation, which initiates quickly on exposure to clean, aerated seawater may take long times to reach steady state where the corrosion rate is very low, on the order of 3 $\mu\text{m}/\text{year}$ [7]. As in the case of aluminum alloys, many factors associated with the seawater environment can affect the corrosion behavior of this alloy. However, the antifouling properties of 90/10 Cu-Ni appear to eliminate the confounding effects of localized corrosion under macrofouling; and, consequently, permit potentially better comparisons of seawater corrosivities of the various test sites. It is apparent from the data summarized in Table 6 that there are large site-to-site variations in corrosivity.

The corrosion rate data shown in Fig. 5 indicate a general trend toward decreasing mass loss corrosion rate as a function of exposure time for most of the test sites. For Hawaii, the corrosion rate didn't appear to decrease further for the 3 and 5-year exposures; whereas, there was a slight trend toward increase in corrosion rate with time for Sweden, (Bohus-Malmon), England, Italy, and to a lesser extent Denmark. In contrast to the very low corrosion rate mentioned previously, specimens from only half of the test sites exhibited a rate less than 10 $\mu\text{m}/\text{year}$ after three years. Reinhart [12] reported corrosion rates decreasing from 25 to 13 $\mu\text{m}/\text{year}$ for 6 months to two years of exposure for this alloy at Point Mugu, California, not far from Port Hueneme. It is interesting to observe that the low rates for the 3 and 5-year exposures at the North Carolina site are very similar to those reported for the same site in long-term tests concluded seventeen years earlier [7].

The highest corrosion rate was noted at Port Hueneme, California, on one specimen removed after six months. The validity of the extremely high rate was questioned, but thorough review of the specimen history (original and final weights and dimensions) confirms this observation. Once again the constant wave action at this site appears to be the reason for the severe corrosion. The specimen in question was mounted on the end of the rack and, consequently, subjected to high seawater velocities on the leading edge. The companion specimen also exhibited a high corrosion rate of 40 $\mu\text{m}/\text{year}$

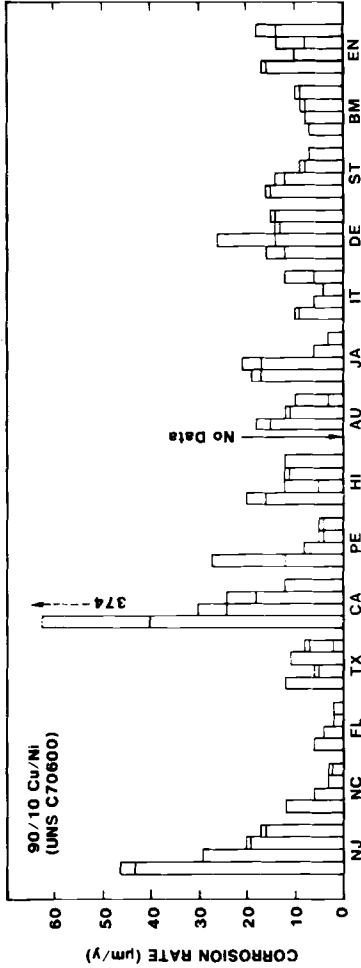


FIG. 5- Corrosion rate data for copper-nickel alloy C70600 in seawater at the 14 test sites. For key to site abbreviations, see Table 1. For each location, the 1st, 2nd, 3rd, and 4th bars from the left correspond to exposure periods of nominally 0.5, 1, 3, and 5 years, respectively. (Note that the second bar for the California and Denmark sites represent exposure data for 2 and 1.5 years, respectively.)

but appears to have had the benefit of being shielded by the first specimen. In each successive removal, the leading edge specimen exhibited more corrosion (much of it on the leading edge) than its companion. The end of the rack, of course, shielded all specimens except the first one from the most severe wave action.

The greatest depth of localized corrosion, noted in Fig. 6, occurred at the California site on one of the specimens removed after three years' exposure. A maximum depth of 2.68 mm was measured at the mounting washer as shown in Fig. 7 and is attributed to "wear" caused by the specimen coming loose at the mounting hole and "vibrating" in the seawater flow. It is not known if corrosion beneath the mounting washer was responsible for this loosening effect. For the other test sites, attack under the washers was generally minimal. However, in many instances, crevice-related attack was observed immediately outside the crevice area; i.e., adjacent to the washers. This is ascribed to the metal-ion concentration-cell mechanism where the buildup of copper ions results in the crevice being cathodic, while the area immediately outside becomes anodic.

Deep pitting occurred only on the upward facing sides of the horizontally exposed specimens at the Hawaii site as illustrated in Fig. 8. The bottom surfaces of these specimens were not pitted. Pitting corrosion is attributed to attack under deposits which settled on the top surface.

It is difficult to accurately assess any effects of seawater temperature since much of the information reported for the test sites was based on ranges, averages, or estimates, and because of the influence of other undocumented variables. There is some indication, however, that general corrosion rates were less at the warmer sites, possibly due to lower oxygen levels. Although alloy C70600 generally displays good resistance to biofouling, some attachments were noted. Under very low flow velocity or static conditions, some biofouling of C70600 can occur. Depending upon the biological nature of the deposits, and particularly if they die, sulfides can cause severe corrosion of C70600. Figure 9 shows the test specimens at the North Carolina site immediately after the rack was lifted from the water after three years of exposure. Most of the biofouling is attached to the rack or the plastic fasteners and overhangs the test specimens. A few isolated instances of attachment and growth, however, can be noted. This is in marked contrast to the appearance of the steel specimens (Fig. 10) which are prodigiously fouled after the same exposure period.

It is well known that the corrosion of copper-base alloys is influenced by the presence of sulfide in seawater [12-15]. Although none of the sites reported the presence of sulfide, it is known that even brief contact with, for example, sulfide-containing silt, stirred up from bottom anaerobic sediments, can be detrimental to the normally protective corrosion product films on alloy C70600.

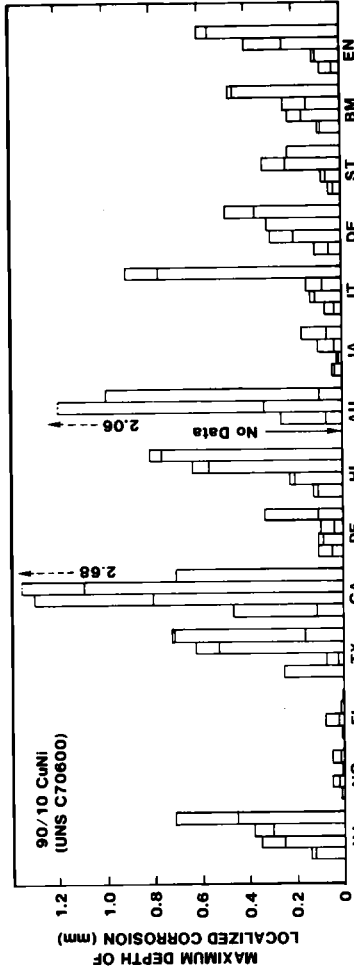


FIG. 6--Localized corrosion data for copper-nickel alloy C70600 in seawater at the 14 test sites. For key to site abbreviations, see Table 1. For each location, the 1st, 2nd, 3rd, and 4th bars from the left correspond to exposure periods of nominally 0.5, 1, 3, and 5 years, respectively. (Note that the second bar for the California and Denmark sites represent exposure data for 2 and 1.5 years, respectively.)

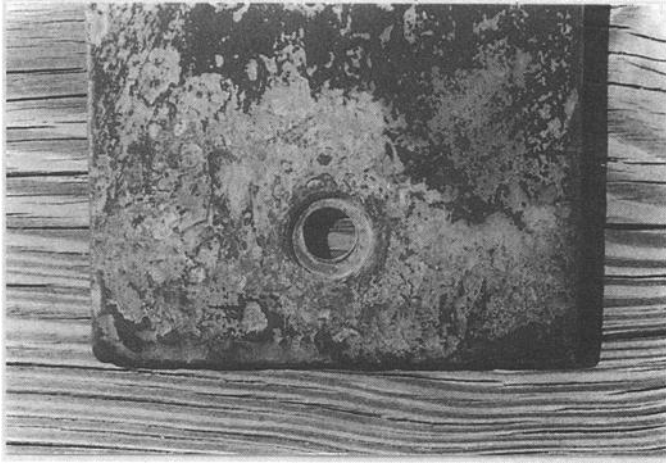


FIG. 7--Erosion under the mounting washer on one of the alloy C70600 specimens exposed at Port Hueneme, California for 3 years.

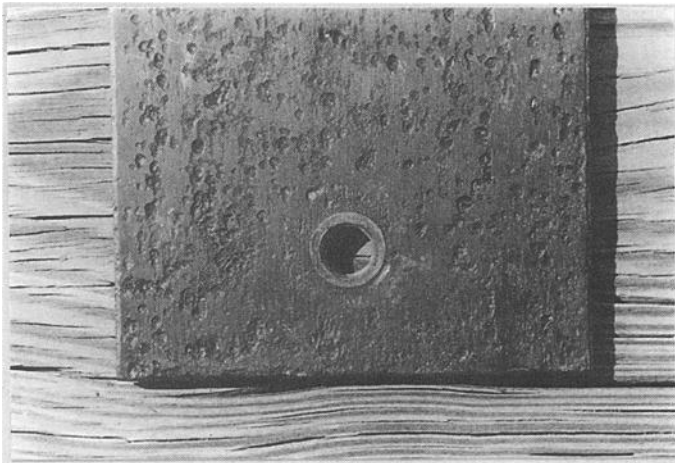


FIG. 8--Typical pitting after 3 years on the upper side of horizontally exposed alloy C70600 specimens exposed at KeAhole, Kona, Hawaii.

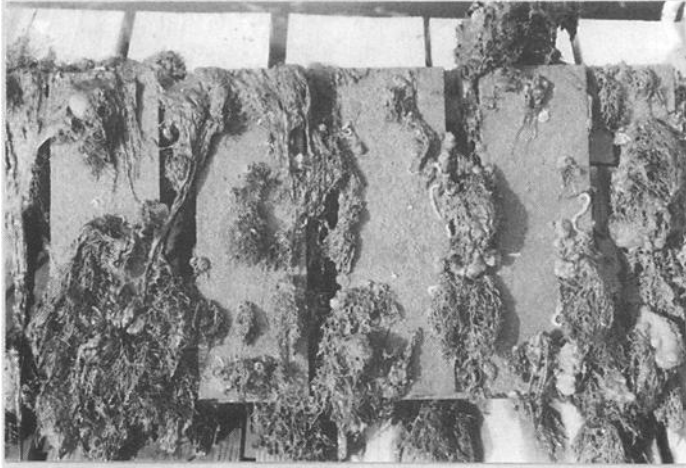


FIG 9--90/10 CuNi after 3 years at Wrightsville Beach, North Carolina. Most of the biofouling is attached to the test rack and nonmetallic fasteners, and hangs over the specimens.



FIG. 10--Typical biofouling on carbon steel specimens after 3 years' exposure at Wrightsville Beach, North Carolina.

Carbon Steel K01501

The corrosion of carbon steel in seawater is generally governed by the rate of diffusion of oxygen through the layers of rust and marine organisms that attach and grow on exposed surfaces. Corrosion rates in the range of 75 to 200 $\mu\text{m}/\text{yr}$ are reported in the literature [3,5,6,16,17] for exposure times of at least six months. Although carbon or structural steels corrode over 100% of the surface exposed, the result is usually general but not uniform thickness loss in seawater.

The average corrosion rates of carbon steel at all the test sites, considered collectively, in this program were similar after six months and one year (168 and 172 $\mu\text{m}/\text{yr}$), decreasing to 117 $\mu\text{m}/\text{yr}$ after three years, and 107 $\mu\text{m}/\text{yr}$ after 5 years. The general corrosion rates based on mass loss are depicted graphically in Figure 11. The lack of any simple trends as a function of time collectively for all the test sites confirms previously documented experience [18].

The measured maximum thickness-loss values for the various exposure periods are plotted graphically in Fig. 12. For most of the test sites, there is a general trend toward increasing maximum thickness loss with time. However, again caution is advised in interpretation because the data are for different specimens as discussed previously. Based on experience [16,17], however, the overall behavior is typical of carbon steels in seawater. Complete penetration through the ~6 mm thick specimen was noted on one specimen removed from the Hawaii site after only one year (Fig. 13). This specimen, exposed horizontally, was subjected to deposits such as sand and silt settling out of the water on to its upper surface. Biofouling was also profuse, at all of the test sites. A typical illustration of this was shown in Fig. 10. An example of rather severe localized penetration of a steel H-beam piling has been described by LaQue previously [19]. In that case, sea urchins were noted to have settled on the steel surface and they remained there for a long period of time. It was observed that their periodic movement was sufficient to brush away corrosion products so that the freshly exposed steel beneath the urchins was continually corroding at the relatively high rate characteristic of the early stages of corrosion of steel in seawater. The surrounding steel surfaces were at least partially covered and protected by the barrier layers of biofouling (hence, a feeding ground for the sea urchins). It is not known if this type of mechanism caused perforation of the steel specimen at the Hawaii site in this program, because there was significant corrosion product still in place in the severely corroded area when the specimen was received back at the LaQue Center.

Another perforation of a steel specimen occurred after 3 years' exposure at the Genoa, Italy site, where the test racks were exposed vertically. The companion specimen suffered a maximum thickness loss of 4.4 mm in a rather broad area, as noted in Fig. 14. These specimens also displayed evidence of heavy biofouling over their surfaces, and rust encrustation in the severely corroded area. This severe localized penetration could have been caused by the same mechanism described previously, particularly since LaQue's observation [19] was also on a vertical surface.

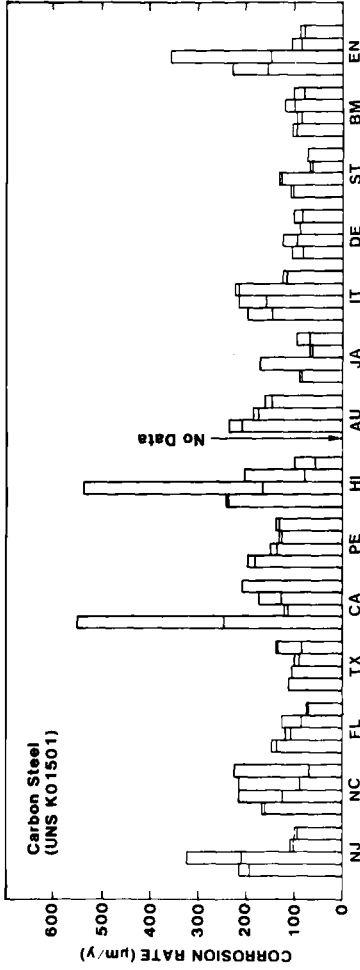


FIG. 11--Corrosion rate data for K01501 steel in seawater at the 14 test sites. For key to site abbreviations, see Table 1. For each location, the 1st, 2nd, 3rd, and 4th bars from the left correspond to exposure periods of nominally 0.5, 1, 3, and 5 years, respectively. (Note that the second bar for the California and Denmark sites represent exposure data for 2 and 1.5 years, respectively.)

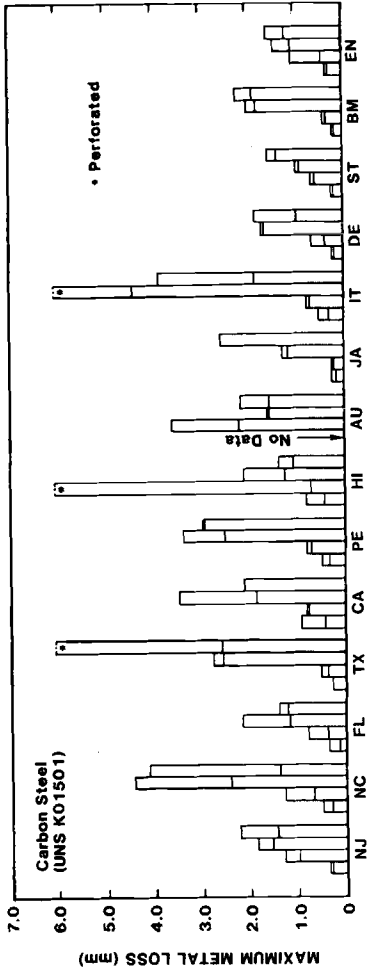


FIG. 12--Maximum metal thickness-loss data for K01501 steel in seawater at the 14 test sites. For key to site abbreviations, see Table 1. For each location, the 1st, 2nd, 3rd, and 4th bars from the left correspond to exposure periods of nominally 0.5, 1, 3, and 5 years, respectively. (Note that the second bar for the California and Denmark sites represent exposure data for 2 and 1.5 years, respectively.)



FIG. 13--Steel perforated after 1 year of exposure at the Hawaii test site. The specimen was mounted horizontally.

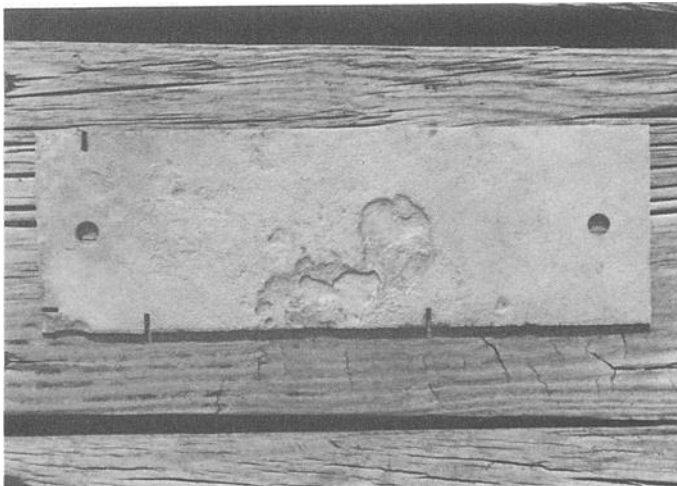


FIG. 14--Corrosion of carbon steel specimen after 3 years at Genoa, Italy.

Figure 12 shows that two of the three 5-year specimens from this Texas site were also perforated.

Although theory predicts that an increase in the corrosion rate of carbon steel may be expected with increased water temperature [3,20], no clear evidence of this is apparent from this test program. It may be noted, however, that maximum metal thickness loss greater than 1.5 mm occurred at 12 of the 14 test sites in 5 years, independent of warm water versus cold water sites. As stated previously, variables other than temperature and their complex interactions, particularly attack underneath the biofouling, probably account for the differences in corrosion behavior for replicate specimens and various exposure times at the same or the other test sites.

Heavy growths of biofouling are also known to slough off steel surfaces and expose the underlying metal [6]. If the bare steel is exposed to flowing seawater, before any barrier layer of biofouling forms, acceleration of general corrosion can be expected. Copson [21] demonstrated a tripling of the corrosion rate of carbon steel even at a velocity of less than 2 m/s velocity, but in the absence of fouling or corrosion products. Adherent corrosion products and/or macrofouling growths tend to significantly reduce the effect of seawater velocity on general corrosion, but promote localized corrosion. Thus, reduction in the general mass loss corrosion rate may be offset by deep local penetrations and even perforation in the absence of corrosion-control measures.

CONCLUSIONS

1. A worldwide seawater corrosivity test program was conducted from 1983 to 1988. Fourteen host sites were selected and identical test racks comprising multiple test specimens of 3 alloys (Al alloy UNS A95086, CuNi alloy UNS C70600, and steel UNS K01501) were provided to each site for exposure to seawater. It was requested that duplicate specimens of each alloy be removed and returned to the evaluating laboratory after exposures of 0.5, 1, 3, and 5 years.
2. Despite "standard" instructions, there were a number of departures from the requirements pertaining to the exposure and return of the test specimens. For example, at one site the racks were exposed such that the test specimens were horizontal instead of vertical. In a number of cases, test specimens were not removed in a logical, sequential numbering order. In others, the exposure periods were "non-standard", e.g., 2 years instead of 1. In some cases, only one instead of duplicate specimens were removed after 6 months' exposure, ultimately resulting in triplicate instead of duplicate 5-year specimens. In another, the duplicate specimen of each 5-year set was never returned.

These foregoing nuances indicate the influence of "human factors" and highlight the difficulties in conducting even seemingly simple field corrosion tests. Nature can also have an impact on such testing. For example, the original set of racks at the Australian test site were lost in a cyclone.

3. The average corrosion rates of the 3 test materials for all the test sites, based on mass loss were in general agreement with previously published corrosion data for seawater. However, the actual corrosion rates exhibited wide variations between many of the test sites, and often as a function of time even at the same site. Overall, at any given test site, aluminum alloy A95086 exhibited appreciably lower mass loss than the copper-nickel alloy C70600, which in turn was lower than the copper-bearing steel K01501. However, attack on the aluminum alloy A95086 was highly localized relative to the other two.
4. Corrosion data do not always provide a direct indication of exposure-environment corrosivity. This is particularly the case in long-term testing of materials in seawater. It is quite probable that the differences in seawater corrosivity at the different test sites are not particularly significant. This could be determined, for example, by conducting very short-term tests --- such as potentiodynamic polarization --- on clean, bare metal surfaces before any corrosion product films and/or fouling attachments develop.

However, in long-term immersion tests, the influence of corrosion products and/or fouling probably outweighs the corrosivity of seawater per se. In other words, local conditions underneath the deposits play a more important role than the bulk composition/properties of seawater. The corrosion rate of copper-nickel alloy C70600, which exhibits good anti-fouling properties under certain exposure conditions, probably represents the "best" indicator of relative worldwide seawater corrosivities at the various test sites.
5. There are complex interactions, between the seawater variables such as degree and types of fouling, silting, bacterial activity, temperature, dissolved oxygen, flow rate, pH, etc., which tend to be site-specific.

The results of this test program show that the corrosion behavior of materials in seawater cannot always be reliably predicted for a particular site on the basis of corrosion data from another site. For critical applications, longer-term corrosion testing (e.g., at least 1 year) is recommended at the specific site of interest.

ACKNOWLEDGMENTS

The commitment and support of numerous people, especially the individual site representatives and the material suppliers, is gratefully acknowledged. Special thanks are also given to the following: C. E. Bancroft and K. B. Horrell, and the many staff members and technicians at the LaQue Center for Corrosion Technology, Inc. who worked on the test program; A.G.S. Morton, Naval Surface Warfare Center (Annapolis, MD); W. W. Kirk, President Emeritus, LaQue Center for Corrosion Technology, Inc.; and T. S. Lee, III, the original task group chairman, presently at Instrument Society of America, Raleigh, NC.

REFERENCES

- [1] Kirk, W. W. and Pikul, S. J., "Seawater Corrosivity Around the World: Results from Three Years of Testing," Corrosion in Natural Waters, STP 1086, C. H. Baloun, Ed., American Society for Testing and Materials, Philadelphia, 1990, pp. 2-36.
- [2] Ailor, W. H., "Ten-Year Seawater Tests on Aluminum," Corrosion in Natural Environments, STP 558, American Society for Testing and Materials, Philadelphia, 1974, p. 117.
- [3] Beavers, J.A., Koch, G. H., and Berry, W. E., "Corrosion of Metals in Marine Environments -- A State of the Art Report," MCIC Report 86-50, Metals and Ceramics Information Center, Battelle Memorial Institute, Columbus, OH, July 1986 (now available from DOD, Materials Information Analysis Center, at CINDAS/Purdue University, West Lafayette, IN).
- [4] Brouillette, C. V., Corrosion, NACE International, Vol. 14, No. 8, 1958, p. 352t.
- [5] LaQue, F. L., Marine Corrosion Causes and Prevention, John Wiley & Sons, New York, 1975, pp. 143-149.
- [6] Efrid, K. D., Materials Performance, NACE International, Vol. 15, No. 4, 1976, p. 16.
- [7] Efrid, K. D. and Anderson, D. B., Materials Performance, NACE International, Vol. 14, No. 11, 1975, p. 37.
- [8] Bailey, G. L. J., Journal of the Institute of Metals, Vol. 79, 1951, p. 243.
- [9] Kirk, W. W., Lee, T. S., and Lewis, R. O., "Corrosion and Marine Fouling Characteristics of Copper-Nickel Alloys," Proceedings, Copper Development Association Conference on Copper Alloys in Marine Environments, Birmingham, England, April 1985.
- [10] Steward, W. C. and LaQue, F. L., Corrosion, NACE International, Vol. 8, No. 8, 1952, p. 259.
- [11] Gilbert, P. T., Paper No. 194, NACE Annual Conference, NACE International, Houston, TX, 1981.
- [12] Reinhard, F. M., "Corrosion of Copper Alloys in Hydrospace," Corrosion in National Environments, STP 558, American Society for Testing and Materials, Philadelphia, 1974, p. 135.

- [13] Gudas, J. P. and Hack, H. P., Paper No. 93, NACE Annual Conference, NACE International, Houston, TX, 1977.
- [14] Gudas, J. P., Danek, G. J., and Niederberger, R. B., Paper No. 76, NACE Annual Conference, NACE International, Houston, TX, 1976.
- [15] Efird, K. D. and Lee, T. S., Paper No. 24, NACE Annual Conference, NACE International, Houston, TX, 1978.
- [16] Tuthill, A. H. and Schillmoller, C. M., "Guidelines for Selection of Marine Materials," Marine Technology Society Conference, Washington, DC, June 1965.
- [17] Di Gregorio, J. S. and Fraser, J. P., "Corrosion Tests in the Gulf Floor," Corrosion in Natural Environments, STP 558, American Society for Testing and Materials, Philadelphia, 1974, p. 185.
- [18] "General Seawater Corrosion," Bulletin A-1276, The International Nickel Company, New York, March 1978.
- [19] LaQue, F. L., "Corrosion and Fouling," Proceedings, Third International Congress on Marine Corrosion and Fouling, Gaithersburg, MD, October 1972.
- [20] The Corrosion Handbook, H. H. Uhlig, Ed., Electrochemical Society, John Wiley & Sons, New York, 1948.
- [21] Copson, H. R., Corrosion, NACE International, Vol. 16, No. 2, 1960, p. 86t.

APPENDIX

Table 7 - Corrosion data for specimens exposed in Ocean City, New Jersey

Alloy	Exposure Duration, year	Mass Loss		Corrosion Rate(a) $\mu\text{m}/\text{year}$	Thickness Loss(b)		Max. Depth of Localized Attack(b) mm	Observations(d)	
		g	g/m^2		Average(c) mm	Maximum mm			
5086 aluminum (UNS A95086)	0.5	0.9	12.7	10	--	--	0.30(*)	CC, P	
	0.5	0.7	9.9	8	--	--	0.21(*)	CC, P	
	1.0	0.9	12.5	5	--	--	0.31	P	
	1.0	0.8	11.1	4	--	--	0.35	P	
	3.0	1.5	21.3	3	--	--	0.22(*)	CC, P	
	3.0	1.4	19.9	2	--	--	0.29	CC, P	
	5.0	1.4	19.9	1	--	--	0.03	CC, P	
	5.0	2.0	28.4	2	--	--	0.27	CC, P, EA	
	90/10 CuNi (UNS C70600)	0.5	14.2	197	46	--	--	0.14	P
		0.5	13.2	183	43	--	--	0.12	P
1.0		18.6	263	29	--	--	0.35	P	
1.0		18.7	265	29	--	--	0.25	P	
3.0		37.1	515	20	--	--	0.38	GC, P, EA	
3.0		36.2	503	19	--	--	0.30	GC, P, EA	
5.0		052.1	725	17	--	--	0.71	GC, BP, EA	
5.0		49.2	683	16	--	--	0.45	GC, EA	
Carbon Steel (UNS K01501)		0.5	53.1	745	192	0.25	0.36	--	P
		0.5	58.7	824	213	0.25	0.33	--	P
	1.0	118.4	1655	209	0.54	1.00	--	GC	
	1.0	181.5	2553	322	0.63	1.31	--	GC	
	3.0	160.9	2260	100	1.11	1.57	--	GC	
	3.0	179.8	2525	107	1.12	1.87	--	GC	
	5.0	257.0	3609	92	1.15	2.24	--	GC, BP	
	5.0	280.0	3933	100	1.01	1.46	--	GC	

N.B. Key to footnotes and abbreviations in Tables 7-20 appears in Table 21.

Table 8 - Corrosion data for specimens exposed in Wrightsville Beach, North Carolina

Alloy	Exposure Duration, year	Mass Loss g	Mass Loss g/m ²	Corrosion Rate(a) µm/year	Thickness Loss(b)		Max. Depth of Localized Attack(b) mm	Observations(d)
					Average(c) mm	Maximum mm		
5086 aluminum (UNS A95086)	0.5	1.2	17.0	13	--	--	0.12	P
	0.5	1.2	17.0	13	--	--	0.06	P
	1.0	1.2	17.0	6	--	--	0.05	P
	1.0	1.1	15.6	6	--	--	0.05	P
	3.0	1.7	24.1	3	--	--	0.09	P, CC
	3.0	1.6	22.7	3	--	--	0.06	P, CC
	5.0	1.7	24.1	2	--	--	0.05	P
	5.0	1.7	24.1	2	--	--	0.03	P
90/10 CuNi (UNS C70600)	0.5	3.7	51.3	12	--	--	--	GC
	0.5	3.6	50.0	12	--	--	--	GC
	1.0	4.2	58.3	6	--	--	0.05	P
	1.0	4.1	56.9	6	--	--	0.02	P
	3.0	6.4	88.9	3	--	--	--	GC
	3.0	6.4	88.9	3	--	--	--	GC
	5.0	7.8	108	2	--	--	0.05(e)	GC, CC
	5.0	7.9	110	3	--	--	0.01	GC
Carbon Steel (UNS K01501)	0.5	44.6	626	161	0.15	0.31	--	GC
	0.5	45.5	639	165	0.22	0.50	--	GC
	1.0	69.6	976	123	0.30	0.68	--	GC
	1.0	117.5	1680	213	0.47	1.28	--	GC
	3.0	146.3	2055	87	1.36	2.44	--	GC, BP
	3.0	360.4	5062	214	2.58	4.44	--	GC, BP
	5.0	189.0	2654	68	0.71	1.39	--	GC, BP
	5.0	627.3	8811	224	2.51	4.11	--	GC, BP

N.B. Key to footnotes and abbreviations in Tables 7-20 appears in Table 21.

Table 9 - Corrosion data for specimens exposed in Key West, Florida

Alloy	Exposure Duration, year	Mass Loss		Corrosion Rate(a) $\mu\text{m}/\text{year}$	Thickness Loss(b)		Max. Depth of Localized Attack(b) mm	Observations(d)	
		g	g/m^2		Average(c) mm	Maximum mm			
5086 aluminum (UNS A95086)	0.5	0.6	11.7	6	--	--	--	GC	
	0.5	0.8	11.3	8	--	--	--	GC	
	1.0	0.6	8.3	3	--	--	0.08	P	
	1.0	0.5	6.9	3	--	--	0.02	P	
	3.0	0.9	12.8	2	--	--	0.02	P	
	3.0	0.8	11.4	1	--	--	0.02	P, CC	
	5.0	0.9	12.8	1	--	--	0.02	P	
	5.0	0.6	8.5	1	--	--	0.01(*)	CC	
	90/10 CuNi (UNS C70600)	0.5	2.0	27.7	6	--	--	--	GC
		0.5	1.7	23.6	6	--	--	--	GC
1.0		2.8	39.6	4	--	--	0.08	P	
1.0		2.7	38.2	4	--	--	0.02	P	
3.0		4.4	61.1	2	--	--	0.01	GC	
3.0		4.5	62.5	2	--	--	0.01	GC	
5.0		6.4	88	2	--	--	--	GC	
5.0		7.1	99	2	--	--	--	GC	
Carbon Steel (UNS K01501)		0.5	37.5	527	136	0.10	0.16	--	GC
		0.5	40.2	565	146	0.13	0.36	--	GC
	1.0	60.7	852	107	0.25	0.81	--	GC	
	1.0	67.1	941	119	0.24	0.39	--	GC	
	3.0	207.8	2919	124	1.31	2.17	--	GC, BP	
	3.0	140.2	1969	84	0.75	1.19	--	GC	
	5.0	208.4	2927	74	0.66	1.23	--	GC	
	5.0	210.8	2961	75	0.77	1.40	--	GC	

N.B. Key to footnotes and abbreviations in Tables 7-20 appears in Table 21.

Table 10 - Corrosion data for specimens exposed in Freeport, Texas (h)

Alloy	Exposure Duration, year	Mass Loss		Corrosion Rate, (a) $\mu\text{m}/\text{year}$	Thickness Loss(b)		Max. Depth of Localized Attack(b) mm	Observations(d)
		g	g/m^2		Average(c) mm	Maximum mm		
5086 aluminum (UNS A95086)	0.5	1.1	15.3	11	--	--	0.17	P
	1.0	1.4	19.4	7	--	--	0.04	P
	1.0	1.4	19.4	7	--	--	0.11	P
	3.0	1.8	25.6	3	--	--	0.05	P, CC
	3.0	1.9	27.0	3	--	--	0.05	GC
	5.0	1.9	26.3	2	--	--	0.05	GC
	5.0	1.8	26.7	2	--	--	0.06	GC
	5.0	1.9	26.8	2	--	--	0.04	GC
	5.0	1.9	26.8	2	--	--	0.04	GC
90/10 CuNi (UNS C70600)	0.5	4.0	56.6	12	--	--	0.25	P
	1.0	3.4	48.1	5	--	--	0.02	P, CC
	1.0	3.7	52.4	6	--	--	0.07	P, CC
	3.0	20.7	288	11	--	--	0.62(e)	P, CC
	3.0	20.1	279	11	--	--	0.52(e)	P, CC
	5.0	25.7	356	8	--	--	0.72(e)	P, CC
	5.0	7.1	98	2	--	--	0.16(e)	GC, CC
	5.0	22.3	310	7	--	--	0.71(e)	P, CC
	5.0	22.3	310	7	--	--	0.71(e)	P, CC
Carbon Steel (UNS K01501)	0.5	33.1	436	120	0.14	0.27	--	GC
	1.0	59.4	833	105	0.21	0.37	--	GC
	1.0	59.5	835	105	0.28	0.53	--	GC, BP
	3.0	151.9	2133	91	1.39	2.58	--	GC, BP
	3.0	165.5	2324	99	1.47	2.77	--	GC, BP
	5.0	382.7	5374	137	1.64	6.07(f)	--	GC, BP
	5.0	378.4	5314	135	2.15	6.07(f)	--	GC, BP
	5.0	241.9	3397	86	1.11	2.59	--	GC, BP
	5.0	241.9	3397	86	1.11	2.59	--	GC, BP

N.B. Key to footnotes and abbreviations in Tables 7-20 appears in Table 21.

Table 11 - Corrosion data for specimens exposed in Port Hueneeme, California (i)

Alloy	Exposure Duration, year	Mass Loss		Corrosion Rate(a) $\mu\text{m}/\text{year}$	Thickness Loss(b)		Max. Depth of Localized Attack(b) mm	Observations(d)
		g	g/m^2		Average(c) mm	Maximum mm		
5086 aluminum (UNS A95086)	0.5	1.7	24.1	18	--	--	0.05	P
	0.5	1.8	25.5	19	--	--	0.11	P
	2.0	5.1	70.7	13	--	--	0.55	P, CC
	2.0	3.1	43.0	8	--	--	0.63	P, CC
	2.9	6.8	96.6	12	--	--	0.91	P, CC
	2.9	3.7	52.5	6	--	--	0.25	P, CC
	5.0	4.7	66.8	5	--	--	0.09(*)	GC, CC
90/10 CuNi (UNS C70600)	0.5	115.5	1604	374	--	--	0.46	P, EA
	0.5	12.5	174	40	--	--	0.11	P
	2.0	38.7	548	30	--	--	1.30	P, CC, EA
	2.0	30.3	429	24	--	--	0.80	P, CC
	2.9	44.3	615	24	--	--	2.68(g)	P, GC, CC, EA
	2.9	32.6	453	18	--	--	1.09(g)	P, GC, CC, EA
	5.0	37.1	515	12	--	--	0.70(g)	P, GC, CC
Carbon Steel (UNS K01501)	0.5	151.7	2131	550	0.59	0.95	--	GC
	0.5	67.7	951	245	0.25	0.44	--	GC
	2.0	127.1	1783	113	0.51	0.80	--	GC
	2.0	136.3	1912	121	0.55	0.83	--	GC
	2.9	205.8	2890	125	1.44	3.5	--	GC
	2.9	284.4	3994	173	1.34	1.88	--	GC
	5.0	346.9	4873	207	1.31	2.12	--	GC

N.B. Key to footnotes and abbreviations in Tables 7-20 appears in Table 21.

Table 12 - Corrosion data for specimens exposed in Talara, Peru

Alloy	Exposure Duration, year	Mass Loss g	g/m ²	Corrosion Rate(a) $\mu\text{m}/\text{year}$	Thickness Loss(b) Average(c) mm	Maximum mm	Max. Depth of Localized Attack(b) mm	Observations(d)	
5086 aluminum (UNS A95086)	0.5	1.1	15.3	12	--	--	0.05	P	
	0.5	1.0	13.9	10	--	--	0.05	P	
	1.0	1.1	15.3	6	--	--	0.03	P	
	1.0	1.1	15.3	6	--	--	0.03	P	
	3.0	1.8	25.6	3	--	--	0.07	P	
	3.0	1.8	25.6	3	--	--	0.04	P	
	5.0	1.9	27.0	2	--	--	0.07	GC	
	5.0	1.8	25.6	2	--	--	0.08	GC	
	90/10 CuNi (UNS C70600)	0.5	8.7	123	27	--	--	0.10	P
		0.5	3.7	52.4	12	--	--	0.04	P
1.0		5.1	72.2	8	--	--	0.08	P	
1.0		4.9	69.4	8	--	--	0.10	P	
3.0		8.8	122	5	--	--	0.09	GC	
3.0		6.9	95.8	4	--	--	0.03	GC	
5.0		13.4	186	4	--	--	0.10(e)	GC, CC	
5.0		15.0	208	5	--	--	0.33(e)	GC, CC	
Carbon Steel (UNS K01501)		0.5	55.4	777	196	0.23	0.48	--	GC
		0.5	50.9	714	180	0.21	0.35	--	GC
	1.0	83.1	1166	147	0.39	0.73	--	GC	
	1.0	76.3	1070	135	0.34	0.84	--	GC	
	3.0	214.7	3015	129	1.66	3.40	--	GC, BP	
	3.0	209.5	2492	126	1.81	2.52	--	GC, BP	
	5.0	367.8	5165	131	1.48	2.98	--	GC, BP	
	5.0	381.4	5356	136	1.52	2.95	--	GC, BP	

N.B. Key to footnotes and abbreviations in Tables 7-20 appears in Table 21.

Table 13 - Corrosion data for specimens exposed in KeAhole, Kona, Hawaii

Alloy	Exposure Duration, year	Mass Loss		Corrosion Rate(a) $\mu\text{m}/\text{year}$	Thickness Loss(b)		Max. Depth of Localized Attack(b) mm	Observations(d)	
		g	g/m^2		Average(c) mm	Maximum mm			
5086 aluminum (UNS A95086)	0.5	1.2	17.0	13	--	--	0.04	P	
	0.5	1.3	18.4	14	--	--	--	P	
	1.0	1.3	18.0	7	--	--	0.03	P	
	1.0	1.3	18.0	7	--	--	0.03	P	
	3.2	1.5	21.3	3	--	--	0.03	P	
	3.2	1.4	19.9	2	--	--	0.08(*)	P, CC	
	5.0	1.4	19.9	2	--	--	0.02	GC	
	5.0	1.5	21.3	2	--	--	0.01	GC	
	90/10 CuNi (UNS C70600)	0.5	6.2	86.1	20	--	--	0.12	P
		0.5	5.0	69.4	16	--	--	0.10	P
1.0		7.4	102.8	12	--	--	0.20	P	
1.0		3.0	41.7	5	--	--	0.22	P, CC	
3.2		21.7	301	11	--	--	0.56	P, GC	
3.2		22.6	314	12	--	--	0.63	P, GC	
5.0		36.7	510	12	--	--	0.81	P, GC	
5.0		36.5	506	12	--	--	0.76	P, GC	
Carbon Steel (UNS K01501)		0.5	66.3	931	240	0.35	0.84	--	P
		0.5	65.1	914	235	0.12	0.44	--	P
	1.0	93.1	1306	165	0.51	0.73	--	P	
	1.0	303	4251	536	1.51	6.07(f)	--	P	
	3.2	345.7	4855	204	1.71	2.11	--	GC	
	3.2	133.7	1879	79	0.83	1.27	--	GC	
	5.0	154.2	2166	56	0.71	1.09	--	GC	
	5.0	266.8	3747	97	1.34	1.41	--	GC	

N.B. Key to footnotes and abbreviations in Tables 7-20 appears in Table 21.

Table 14 - Corrosion data for specimens exposed in Innisfail, Queensland Australia

Alloy	Exposure Duration, year	Mass Loss		Corrosion Rate(a) $\mu\text{m}/\text{year}$	Thickness Loss(b)		Max. Depth of Localized Attack(b) mm	Observations(d)
		g	g/m^2		Average(c) mm	Maximum mm		
5086 aluminum (UNS A95086)	1.0	1.4	19.9	8	--	--	0.01	P
	1.0	1.9	27.0	10	--	--	0.01	P
	3.0	1.8	25.1	3	--	--	--	GC
	3.0	1.9	27.6	3	--	--	0.03	GC
	5.0	2.6	36.8	3	--	--	--	GC
	5.0	2.3	32.8	2	--	--	--	GC
90/10 CuNi (UNS C70600)	1.0	9.3	129	15	--	--	0.07	GC, P
	1.0	11.1	154	18	--	--	0.26(e)	GC, NUC, P, CC
	3.0	20.9	291	11	--	--	0.33	GC, P, CC
	3.0	21.7	301	12	--	--	2.06	GC, NUC, CC
	5.0	32.7	453	10	--	--	1.01	GC, NUC, CC
	5.0	9.1	126	3	--	--	0.10	GC, P
Carbon Steel (UNS K01501)	1.0	112.1	1574	207	0.79	3.63	--	GC, BP
	1.0	125.9	1768	233	0.97	2.23	--	GC, BP
	3.0	292.5	4108	174	1.27	1.62	--	GC
	3.0	310.5	4362	185	1.15	1.59	--	GC
	5.0	451.7	6343	162	1.65	2.20	--	GC
	5.0	407.7	5726	146	1.35	1.59	--	GC

N.B. Key to footnotes and abbreviations in Tables 7-20 appears in Table 21.

Table 15 - Corrosion data for specimens exposed in Sakata Harbor, Japan (j)

Alloy	Exposure Duration, year	Mass Loss g/m ²	Corrosion Rate(a) $\mu\text{m}/\text{year}$	Thickness Loss(b)		Max. Depth of Localized Attack(b) mm	Observations(d)	
				Average(c) mm	Maximum mm			
5086 aluminum (UNS A95086)	0.5	0.7	7	--	--	0.06	CC, P	
	0.5	0.6	6	--	--	0.10	CC, P	
	1.0	0.9	9	--	--	0.16	P	
	1.0	0.9	9	--	--	0.21	P	
	3.1	1.1	2	--	--	0.40	CC, P	
	3.1	1.0	2	--	--	0.32	CC, P	
	5.0	1.0	1	--	--	0.21	CC, P	
	5.0	1.1	1	--	--	0.40(*)	CC, P	
	90/10 CuNi (UNS C70600)	0.5	5.3	17	--	--	0.04	P
		0.5	6.0	19	--	--	0.03	P
1.0		6.7	21	--	--	0.01	P	
1.0		5.3	17	--	--	0.02	P	
3.1		(j)	--	--	--	0.03	GC, EA	
3.1		11.0	6	--	--	0.10	GC, EA,	
5.0		10.6	3	--	--	0.17(e)	GC, CC	
5.0		7.9	3	--	--	0.06(e)	GC, CC	
Carbon Steel (UNS K01501)		0.5	24.2	86	0.10	0.18	--	P
		0.5	25.1	89	0.15	0.27	--	P
	1.0	47.3	168	0.10	0.22	--	GC	
	1.0	48.1	171	0.18	0.27	--	GC	
	3.1	117.9	68	0.87	1.32	--	GC	
	3.1	106.4	62	0.77	1.21	--	GC	
	5.0	261.1	94	1.14	1.98	--	GC, BP	
	5.0	188.0	68	0.93	2.61	--	GC, BP	

N.B. Key to footnotes and abbreviations in Tables 7-20 appears in Table 21.

Table 16 - Corrosion data for specimens exposed in Genoa, Italy

Alloy	Exposure Duration, year	Mass Loss g	Corrosion Rate(a) $\mu\text{m}/\text{year}$	Thickness Loss(b)		Max. Depth of Localized Attack(b) mm	Observations(d)	
				Average(c) mm	Maximum mm			
5086 aluminum (UNS A95086)	0.5	0.8	11.1	--	--	0.20	P	
	0.5	0.7	9.7	--	--	0.32	P	
	1.0	0.9	12.5	--	--	0.42	P	
	1.0	1.9	26.4	--	--	0.38	P	
	3.0	1.1	15.6	--	--	0.14	P	
	3.0	1.2	17.0	--	--	0.25(*)	P, CC	
	5.0	1.3	18.9	--	--	0.29	P, CC	
	5.0	1.4	20.2	--	--	0.38	P, CC	
	90/10 CuNi (UNS C70600)	0.5	3.0	42.5	--	--	0.03	P
		0.5	3.1	43.9	--	--	0.07	P
1.0		3.9	55.2	--	--	0.13	P	
1.0		3.6	51.0	--	--	0.11	P	
3.0		7.0	97.2	--	--	0.15	GC	
3.0		7.5	104	--	--	0.08	GC	
5.0		36.6	509	--	--	0.91(e)	P, NUC, CC, EA	
5.0		18.4	256	--	--	0.77	P, GC	
Carbon Steel (UNS K01501)		0.5	40.9	574	0.27	0.54	--	GC
		0.5	54.9	770	0.16	0.32	--	GC
	1.0	89.3	1253	0.35	0.79	--	GC	
	1.0	120.7	1698	0.48	0.75	--	GC	
	3.0	361.0	5070	2.38	4.42	--	GC, BP	
	3.0	376.6	5289	2.27	6.07(f)	--	GC, BP	
	5.0	323.1	4538	1.42	3.88	--	GC	
	5.0	343.4	4823	1.33	1.86	--	GC	

N.B. Key to footnotes and abbreviations in Tables 7-20 appears in Table 21.

Table 17 - Corrosion data for specimens exposed in Kyndby Isefford, Sjælland, Denmark (K)

Alloy	Exposure Duration, year	Mass Loss		Corrosion Rate(a) $\mu\text{m}/\text{year}$	Thickness Loss(b)		Max. Depth of Localized Attack(b) mm	Observations(d)	
		g	g/m^2		Average(c) mm	Maximum mm			
5086 aluminum (UNS A95086)	0.5	1.3	18.0	13	--	--	--	GC	
	0.5	0.4	5.5	4	--	--	--	GC	
	1.5	1.2	16.6	4	--	0.02	0.02	P	
	1.5	1.3	18.0	5	--	0.03	0.03	P	
	3.1	2.2	31.3	4	--	--	--	GC	
	3.1	2.2	31.3	4	--	--	--	GC	
	5.0	5.5	77.6	6	--	0.49	0.49	P	
	5.0	4.8	67.6	5	--	0.24	0.24	GC, P	
	90/10 CuNi (UNS C70600)	0.5	5.0	70.8	16	--	--	0.11(e)	P, CC(e)
		0.5	3.9	55.2	12	--	--	0.05(e)	P, CC(e)
1.5		12.3	174	14	--	--	0.20	P, CC(e)	
1.5		22.0	312	26	--	--	0.30	P, CC(e)	
3.1		27.7	385	14	--	--	0.31(e)	GC, NUC, CC	
3.1		24.4	339	13	--	--	0.30	GC, NUC, CC	
5.0		43.4	602	14	--	--	0.36(e)	NUC, CC, EA	
5.0		47.1	654	15	--	--	0.49(e)	NUC, CC	
Carbon Steel (UNS K01501)		0.5	23.2	325	82	0.17	0.25	--	GC
		0.5	30.0	421	106	0.14	0.22	--	GC
	1.5	68.6	962	95	0.30	0.41	--	GC	
	1.5	92.4	1296	122	0.39	0.70	--	GC	
	3.1	157.6	2213	91	0.98	1.69	--	GC, BP	
	3.1	155.3	2181	90	1.13	1.72	--	GC, BP	
	5.0	279.0	3918	100	1.20	1.00	--	GC, BP	
	5.0	220.6	3098	79	1.88	1.85	--	GC	

N.B. Key to footnotes and abbreviations in Tables 7-20 appears in Table 21.

Table 18 - Corrosion data for specimens exposed in Studsvik, Sweden

Alloy	Exposure Duration, year	Mass Loss g	Mass Loss g/m ²	Corrosion Rate(a) µm/year	Average(c) mm	Thickness Loss(b) Maximum mm	Max. Depth of Localized Attack(b) mm	Observations(d)	
5086 aluminum (UNS A95086)	0.5	0.3	4.2	3	--	--	0.04	P	
	0.5	1.4	13.9	14	--	--	0.10	P	
	1.0	1.9	26.4	10	--	--	0.68	P	
	1.0	1.2	16.6	6	--	--	0.26	P	
	3.2	1.3	18.5	2	--	--	--	GC	
	3.2	1.2	17.0	2	--	--	--	GC	
	5.0	1.5	21.4	2	--	--	0.46	P	
	5.0	1.5	21.4	2	--	--	0.37	P	
	90/10 CuNi (UNS C70600)	0.5	5.0	70.8	16	--	--	0.05	P
		0.5	4.7	66.6	15	--	--	0.03	P
1.0		7.7	109	12	--	--	0.06	P	
1.0		8.8	125	14	--	--	0.08	P	
3.2		18.6	258	9	--	--	0.33	GC, P	
3.2		16.2	225	8	--	--	0.23	GC, P	
5.0		21.3	296	7	--	--	0.22	GC, P	
5.0		22.7	315	7	--	--	0.22	GC, P	
Carbon Steel (UNS K01501)		0.5	30.6	429	108	0.16	0.25	--	GC
		0.5	29.1	408	103	0.15	0.22	--	GC
	1.0	72.2	1013	128	0.46	0.60	--	GC	
	1.0	74.1	1040	131	0.36	0.69	--	GC	
	3.2	122.8	1725	69	0.72	1.00	--	GC	
	3.2	111.0	1559	62	0.74	0.92	--	GC	
	5.0	203.8	2862	73	1.00	1.58	--	GC, BP	
	5.0	201.2	2825	72	0.98	1.40	--	GC	

N.B. Key to footnotes and abbreviations in Tables 7-20 appears in Table 21.

Table 19 - Corrosion data for specimens exposed in Bohus-Malmon, Sweden

Alloy	Exposure Duration, year	Mass Loss g	Mass Loss g/m ²	Corrosion Rate(a) µm/year	Thickness Loss(b)		Max. Depth of Localized Attack(b) mm	Observations(d)	
					Average(c) mm	Maximum mm			
5086 aluminum (UNS A95086)	0.5	1.1	15.6	11	--	--	0.03	P	
	0.5	1.0	14.1	10	--	--	0.04	P	
	1.0	1.6	22.1	8	--	--	0.02	P	
	1.0	1.5	20.8	8	--	--	0.03	P	
	3.1	2.4	34.1	4	--	--	0.29	P	
	3.1	2.5	35.5	4	--	--	0.15	P	
	5.0	2.8	40.1	3	--	--	0.28	P	
	5.0	2.8	39.5	3	--	--	0.12	P	
	90/10 CuNi (UNS C70600)	0.5	2.4	33.3	7	--	--	0.08	P
		0.5	2.2	30.5	7	--	--	0.09	P
1.0		5.0	70.8	8	--	--	0.22	P, CC	
1.0		5.3	75.0	8	--	--	0.16	P, CC	
3.1		14.8	206	8	--	--	0.24	P	
3.1		17.7	246	9	--	--	0.14	P	
5.0		32.8	455	10	--	--	0.45	GC, P, CC, EA	
5.0		27.3	379	9	--	--	0.47	GC, P, CC, EA	
Carbon Steel (UNS K01501)		0.5	28.3	397	103	0.08	0.18	--	GC
		0.5	26.3	369	95	0.13	0.21	--	GC
	1.0	48.6	682	86	0.24	0.35	--	GC	
	1.0	53.2	746	94	0.24	0.43	--	GC	
	3.1	171.9	2414	99	1.11	2.00	--	GC, BP	
	3.1	205.8	2890	119	1.19	1.83	--	GC	
	5.0	284.2	3992	101	1.21	1.88	--	GC	
	5.0	222.2	3121	79	0.99	2.25	--	GC, BP	

N.B. Key to footnotes and abbreviations in Tables 7-20 appears in Table 21.

Table 20 - Corrosion data for specimens exposed in Isle of Wight, England

Alloy	Exposure Duration, year	Mass Loss		Corrosion Rate, ^(e) $\mu\text{m}/\text{year}$	Thickness Loss(b)		Max. Depth of Localized Attack(b) mm	Observations(d)	
		g	g/m^2		Average(c) mm	Maximum mm			
5086 aluminum (UNS A95086)	0.5	0.8	11.4	9	--	--	0.02	P	
	0.5	1.5	20.8	15	--	--	0.02	P	
	1.0	2.3	31.9	12	--	--	0.33	P	
	1.0	2.1	29.1	11	--	--	0.18	P	
	3.1	3.0	42.6	5	--	--	0.10	P	
	3.1	3.3	46.9	6	--	--	0.13	P	
	5.0	3.3	47.4	4	--	--	--	GC	
	5.0	3.5	49.9	4	--	--	--	GC	
	90/10 CuNi (C70600)	0.5	5.4	76.5	17	--	--	0.03	P
		0.5	5.0	70.8	16	--	--	0.08	P
1.0		6.3	89.2	10	--	--	0.10	P	
1.0		6.3	89.2	10	--	--	0.11	P	
3.1		15.9	221	8	--	--	0.40(e)	NUC, CC	
3.1		28.2	392	14	--	--	0.24(e)	NUC, CC	
5.0		43.7	607	14	--	--	0.60(e)	GC, CC	
5.0		57.2	794	18	--	--	0.55(e)	GC, EA, CC	
Carbon Steel (K01501)		0.5	64.0	898	226	0.26	0.36	--	GC
		0.5	44.1	619	156	0.18	0.31	--	GC
	1.0	83.9	1177	148	0.34	0.44	--	GC	
	1.0	201.4	2820	355	0.85	1.06	--	GC	
	3.1	147.0	2065	84	0.78	1.07	--	GC	
	3.1	182.6	2565	104	0.97	1.42	--	GC	
	5.0	242.3	3403	87	0.91	1.19	--	GC	
	5.0	221.7	3114	79	0.99	1.58	--	GC	

N.B. Key to footnotes and abbreviations in Tables 7-20 appears in Table 21.

TABLE 21--Key to footnotes and abbreviations used in Tables 7-20

- (a) Assumes uniform corrosion over entire surface.
- (b) Dash indicates stated parameter not measured.
- (c) Based on 14 measurements.
- (d) - GC General corrosion.
- CC Crevice corrosion beneath mounting washers.
- NUC Nonuniform general corrosion.
- P Bold surface pitting possibly associated with biofouling attachments if present.
- BP Broad pits.
- EA Edge attack.
- (e) Corrosion adjacent to mounting washer.
- (f) Test specimen perforated on boldly exposed surface.
- (g) Erosion of metal beneath mounting washer.
- (h) Only one specimen of each alloy removed and returned after first 6 months of exposure; this eventually resulted in 3 instead of two 5-year panels.
- (i) Second set of specimens returned after 2 instead of 1-year exposure; also, only one specimen of each alloy returned after the 5-year exposure.
- (j) Approximately 0.5" x 1" corner of panel missing (sawed off). Generally similar in appearance to duplicate 3.1-year panel; therefore, assume similar corrosion rate.
- (k) Second set of specimens returned after 1.5 instead of 1-year exposure.
- (*) Reported depth of attack is due to crevice corrosion beneath mounting washer.

Ashok Kumar,¹ Vicki L. Van Blaricum,² Alfred Beitelman,³ and Jeffrey H. Boy⁴

TWENTY YEAR FIELD STUDY OF THE PERFORMANCE OF COATINGS IN SEAWATER

REFERENCE: Kumar, A., Van Blaricum, V. L., Beitelman, A., and Boy, J.H., "Twenty Year Field Study of the Performance of Coatings in Seawater," Corrosion Testing in Natural Waters: Second Volume, ASTM STP 1300, Robert M. Kain, Walter T. Young, Eds., American Society for Testing and Materials, 1997.

ABSTRACT: The objectives of this study were to evaluate the long-term performance of various coatings on steel piles in seawater and to investigate non-destructive electrochemical corrosion testing techniques for coating evaluation in the field. Steel H piles which were 20.3 cm x 20.3 cm and 12.2 m long were installed in Buzzards Bay, Cape Cod, Massachusetts. The piles were coated with various coatings such as coal tar epoxy, polyurethane, flame sprayed zinc and aluminum. Several of the piles were left uncoated for baseline comparison. Sacrificial cathodic protection was provided by anodes to some of the bare and coated steel pilings. Corrosion rate measurements using electrochemical polarization resistance and Tafel plots were conducted periodically in the field during the twenty year study. The results of the Cape Cod, MA, corrosion study were compared with a similar study conducted at the La Costa Island, FL. The long-term coating evaluation showed that flame sprayed aluminum with a topcoat sealer performed best at the cooler temperatures in Massachusetts and polyester glass flake was the best performer in Florida. Coal tar epoxy coatings with zinc-rich primers performed well at both of the locations.

KEYWORDS: coatings, seawater, coatings evaluation, polarization resistance, coal tar epoxy, metallized coatings

The U. S. Army Corps of Engineers and the U. S. Navy use large amounts of steel piles for harbors, docks, and bulkheads in seawater. There are many types of coating systems available to extend the

¹⁻³ Principal Investigator, U.S. Army Construction Engineering Research Laboratories, P.O. Box 9005, Champaign, IL, 61826-9005.

⁴ Materials Engineer, Oak Ridge Institute for Science and Education and U.S. Army Construction Engineering Research Laboratories, P.O. Box 9005, Champaign, IL, 61826-9005.

structural life of the steel piles in seawater. Coal tar epoxy (C-200) with organic zinc-rich primer (E-303) has been used by the Corps with good results for the last 50 years. The coal tar epoxy has water repellent properties and the coating can be applied in one coat which makes it a very cost effective system. However, coal tar is a known carcinogen and safety regulations related to coatings are becoming stricter. Occupational Safety and Health Administration (OSHA) rules regulate the manufacture, application, and field repair of coal tar epoxy coatings. Thus, there is a need to develop and evaluate new coating systems which will comply with the current and anticipated regulations, yet provide high levels of corrosion protection to the structural steel in seawater. Coating manufacturers have claimed better products, and there is a need to objectively evaluate their performance under actual field conditions. For this reason, the U. S. Army Corps of Engineers is performing ongoing field studies for coating and cathodic protection evaluation at two sites: one in the backwaters of the Gulf of Mexico at La Costa Island, Florida, and another in Buzzard's Bay, Cape Cod, Massachusetts.

DESCRIPTION OF BUZZARD'S BAY TEST SITE

The Buzzard's Bay, Cape Cod, MA, test piles were installed in October 1974. The water temperature varies from -1 degree to 19 degree C, with an average temperature of 10 degrees C. The test site consisted of three rows (designated as rows A, B, C) of 22 steel H piles (designated as piles 1 through 22) 20.3 cm x 20.3 cm and 12.2 meters long. The numerical designation of the piles corresponds to a specific combination of substrate material, coating system, and cathodic protection (where applicable). All of the piles were made of ASTM A 36 carbon steel, except for systems 4, 5, and 11 which were made of ASTM A 690 high strength low alloy steel for use in marine environments. Cathodic protection was installed on some of the pilings. The coatings and their compositions for each of the numerical pilings designations at the Buzzard's Bay test site are summarized in Table 1. Row A piles were completely coated. Row B piles were coated except for 2.54 cm by 15.24 cm uncoated areas, or "windows", spaced every 1.22 m along the length of the pile so that undercoating corrosion could be evaluated. Row C piles were coated except for the lower 4.57 m.

Several evaluations of the coatings were conducted between 1975 and the present. The evaluations involved (1) a visual inspection per ASTM Standard D 610-68 to characterize the condition of the coating in the atmospheric zone, splash, tidal, and the immersion zones, and (2) measurement of electrochemical polarization resistance to estimate the coating condition in the immersion zone at high tide.

Row C was pulled out after 5 years and a detailed laboratory evaluation was conducted in accordance with relevant ASTM coating standards. Results of the evaluation have been previously published [1,2,3] and are compared with the "20-Year Results" in Table 2.

The next two sections of this paper will give the results of the most recent visual and electrochemical inspections conducted in August

TABLE 1--Buzzard's Bay test pile preparation details

System No.	Type of Pile*	Type Pile and Protection	No of Coats	Total Dry Coating Thickness** (mm)	Coating Source***
1	H	Bare Carbon Steel			
2	H	Bare Carbon Steel with 2 Zinc Anodes			
3	H	Bare Carbon Steel with 2 Aluminum Anodes			
4	H	Bare ASTM A 690 Steel			
5	H	Bare ASTM A 690 Steel with 2 Zinc Anodes			
6	H	Coal Tar Epoxy, over Zinc-Rich Primer, with 2 Zinc Anodes			
		- Epoxy Zinc-Rich Primer CERL COE Formula No. E-303	1	0.06	Iowa Paint Mfg. CO.
		- Formula C-200, Coal Tar Epoxy	2	0.41-0.51	Koppers
7	H	Coal Tar Epoxy, over Zinc-Rich Primer			
		- Epoxy Zinc-Rich Primer CERL COE Formula No. E-303	1	0.06	Iowa Paint Mfg. CO.
		- Formula C-200, Coal Tar Epoxy	2	0.41-0.51	Koppers
		- Formula C-200, Coal Tar Epoxy	2	0.41-0.51	Koppers

Table 1-- Cond.

System No.	Type of Pile*	Type Pile and Protection	No of Coats	Total Dry Coating Thickness** (mm)	Coating Source***
8	H	Coal Tar Epoxy, over Zinc-Rich Primer - Porter Zinc-Lok No. 352 Primer	1	0.03	Porter Paint Co.
9	H	Coal Tar Epoxy, over Zinc-Rich Primer, Aluminum Oxide Armored at Mud Line - Epoxy Zinc-Rich Primer NCR COE Formula No. E-303 - Formula C-200, Coal Tar Epoxy - Formula C-200, Coal Tar Epoxy + Aluminum Oxide Grit (No. 30) Broadcast into wet final coat.	1 2 1	0.06 0.41-0.51	Iowa Paint Mfg. CO. Koppers
10	H	Coal Tar Epoxy, over Epoxy Resin Primer - Epoxy Resin Primer - Formula C-200, Coal Tar Epoxy	1 2	0.08 0.41-0.51	Porter Paint Co. Koppers
11	H	Coal Tar Epoxy, over Zinc-Rich Primer, on ASTM A 690 Steel Pile - Epoxy Zinc-Rich Primer NCR COE Formula No. E-303 - Formula C-200, Coal Tar Epoxy	1 2	0.06 0.41-0.51	Iowa Paint Mfg. CO. Koppers

Table 1--Cond.

System No.	Type of Pile*	Type Pile and Protection	No of Coats	Total Dry Coating Thickness** (mm)	Coating Source***
12	H	Epoxy over Inorganic Ceramic			
		- Plan-Chem Zinc-ite Primer	1	0.08-0.09	Plas Chem Corp.
		- Plan-Chem Ceram-ite No. 101	1	0.12-0.15	Plas Chem Corp.
13	H	- Plan-Chem 2140Z High Build Epoxy	1	0.18-0.20	Plas Chem Corp.
		Epoxy over Organic Zinc Primer			
		- Zenker No. 11 Primer	1	0.03-0.04	Plas Chem Corp.
		- Chem-Pon 2310X Red	1	0.20-0.23	Plas Chem Corp.
14	H	- Chem-Pon 2310X Gray	1	0.20-0.23	Plas Chem Corp.
		Polyurethane over Organic Zinc-Rich			
14	H	- ChemGlaze Zinc-Rich Primer 9927	1	0.08	Hughson Chem
		- Chemglaze II	2	0.08-0.12	Hughson Chem
15	H	Polyurethane over Organic Zinc-Rich with an Intermediate Elastomer Coat			
		- ChemGlaze Zinc-Rich Primer 9927	1	0.08	Hughson Chem
		- M312 Elastomer	1	0.15-0.20	Hughson Chem
		- ChemGlaze II	2	0.08-0.12	Hughson Chem
16	H	Polyurethane over Flame-Sprayed Zinc, with Intermediate Washcoat Primer			
		- Flame-Sprayed Zinc	1	0.08-0.09	Metalweld or Metco Ureacal Co.
		- Washcoat Primer Formula 117, MIL-P-15328	1	0.12	Seaguard Co.
		- Ureacal 9301 Polyurethane	2	0.09	Metco Ureacal Co.

Table 1--Cond.

System No.	Type of Pile*	Type Pile and Protection	No of Coats	Total Dry Coating Thickness** (mm)	Coating Source***
17	H	Aluminum, Flame Sprayed (Wire)	1	0.15	Metalweld, Metco or equal
18	H	Aluminum, Flame Sprayed with Wash-coat Primer and Aluminum Vinyl Sealer - Flame-Sprayed Aluminum (Wire)	1	0.08-0.09	Metalweld, Metco or equal
		- Washcoat Primer Formula 117, MIL-P-15328	1	0.12	Sea-guard Co
		- Metcoseal AV, Aluminum Vinyl Sealer	2	0.05	Metco
19	H	Zinc, Flame Sprayed, with Coal Tar Emulsion over Coal Tar Solution Top Coats			
		- Flame-Sprayed Zinc (WIRE)	1	0.08-0.09	Metalweld or Metco
		- Wise Chem T-265 Coal Tar Solution	1	0.38	Wise Chem Co.
		- Wise Chem T-264 Coal Tar Evaluation	1	0.18-0.20	Wise Chem Co.
20	H	Vinyl Glass Flake over Vinyl Zinc-Rich			
		- Vinyl Zinc Rich	1	0.05-0.08	CERL Paint Lab
		- Vinyl Glass Flake	3	0.15	CERL Paint Lab

Table 1--Cond.

System No.	Type of Pile*	Type Pile and Protection	No of Coats	Total Dry Coating Thickness** (mm)	Coating Source***
21	H	Vinyl Mastic over Synthetic Resin Topcoat over Washcoat Inorganic Zinc Primer - Dimetcote No. 3 + D3 Curing Solution - No. 54 Topcoat - Vinyl Mastic No. 87	1	0.08	Amercoat Corp.
22	Pipe	Bare Carbon Steel
23	Pipe	Coal Tar Epoxy over Zinc-Rich Primer - Epoxy Zinc-Rich Primer NCR COE Formula No. E-303 - Formula C-200, Coal Tar Epoxy	1	0.06	Iowa Paint Mfg. Co.
24	Pipe	Coal Tar Epoxy, Armored at Mud Line over Zinc-Rich Primer - Epoxy Zinc-Rich Primer NCR COE Formula No. E-303 - Formula C-200, Coal Tar Epoxy - Formula C-200, + Aluminum Oxide (No. 30 Grit) Broadcast into wet final coat (4th coat and Al Oxide applied to between 5.18 and 7.01 mm from bottom of pile).	2	0.41-0.51	Koppers
			1	0.06	Iowa Paint Mfg. Co
			2	0.41-0.51	Koppers
			1	0.25	Koppers

* Steel H-piles are 12.19m lengths of 20.32 cm x 16.33 kg mild carbon steel, except systems 4,5 and 11, which are ASTM A 690 steel H-piles. Systems 22, 23, and 24 are pipe piles, mild carbon steel, 20.32 cm diameter, schedule 40, 0.82 cm wall thickness.

** Film thickness tolerance per cast may be plus or minus 15 percent of given thickness per cm: when no thickness range is given.

*** An approximately equal brand name coating with application and preparation instructions can be furnished by the Government from the same or another source.

TABLE 2--Summary of 5 and 20 year Buzzard's Bay Coating Evaluation Results (ASTM Ratings), CT is coal tar.

Sys. No.	General Coating Description	5 Year Results		20 Year Results		
		Atm	Imm	Atm *	Imm**	Imm
6	CT Epoxy over Zn-Rich w/ Anodes	10	10	5		
7	CT Epoxy over Zn-Rich	9	9	4		
8	CT Epoxy over Zn-Rich	8	9	3	4%	4
9	CT Epoxy over Zn-Rich, Al ₂ O ₃	8	9	4	3%	5
10	CT Epoxy over Epoxy Resin	9	9	5	2%	5
11	CT Epoxy over Zn-Rich on ASTM A 690 Steel	8	9	4	3%	5
12	Epoxy over Inorganic Ceramic	5	0		32%	2
13	Epoxy over Organic Zinc	8	5	2	18%	3
14	Polyurethane over Organic Zinc-Rich	8	6	3	17%	3
15	Polyurethane over Organic Zn-Rich + Elastomeric	8	8	3	5%	4
16	Polyurethane over Inter. Washcoat Primer Zinc, Flame Sprayed	4	0	3		
17	Aluminum, Flame Sprayed	1 / 8***	1 / 8***	6		
18	Vinyl Sealer over Aluminum, Flame Sprayed	8	8	7		
19	CT Emulsion over Zinc, Flame Sprayed	6	0 ****	4		
20	Vinyl Glass Flake over Vinyl Zn-Rich	8	8 ****	5		
21	Vinyl Mastic over Resin	3	4 ****	3		

* = Atmospheric zone, also includes tidal and splash area.

** = Immersion zone, percentages of bare area determined by electrochemical polarization measurements at -0.020 V.

*** = There was a significant difference in the condition of piles 17 A and 17C at Year 5. The rating for pile 17C (removed) is given on the left of the diagonal slash (/). The rating for pile 17 A (not removed) is given on the right of the diagonal slash (/).

**** = Bent by ice.

1995, more than 20 years after the installation of the piles. The results will be compared with results obtained in previous inspections.

RESULTS OF 1995 VISUAL EVALUATION AT BUZZARD'S BAY TEST SITE

The piles at Buzzard's Bay MA were inspected from a boat in October 1992 and August 1995. A total of 22 piles were observed in 2 parallel rows (rows A and B described above). Piles in the 2 rows constituted duplicates of the coating systems. In general, each 12.2 meter length of piling can be divided into the following zones with zero meters referring to the uppermost edge of the piles in their installed (vertical) position: (1) the atmospheric zone (0 to 3 meters), (2) the Splash zone (3 to 3.66 meters), (3) the tidal zone extending from mean low tide to the mean high tide lines (3.66 to 4.0 meters), (4) the immersion zone (4.0 to 6.4 meters), and (5) the embedded zone (6.4 to 12.2 meters). The atmospheric, splash, and tidal zones were examined during the visual inspection.

Many of the coatings had undergone little change between 1992 and 1995, but there are a few exceptions. Detailed observations are given in the following paragraphs. Unless otherwise noted, only a single window, the one immediately above the splash area, was evaluated on row B pilings. Data from the 1995 visual evaluation for the row A pilings are summarized in the "20 Year Results: Atmospheric" column of Table 2.

A number of coatings, especially the metallized coatings, had failures occurring in a regular 0.6 m pattern, perhaps indicating application irregularities. Similarly, many of the piles had failures on about 15.24 cm areas of the edges, perhaps indicating the position of supporting structures during application or shipping. Such irregularities are not considered coating failures and will not be discussed in detail below.

Piles 1, 2, and 3 were bare carbon steel. Pile 2 had zinc anodes and Pile 3 had aluminum anodes. Pile 2 was in the poorest condition of the three, with an appreciable loss of metal on the flanges in the splash area. Some of the failures may have been attributable to the fact that these were the first pile of the row and were subjected to increased physical abuse. Pile 1 was leaning badly because of ice damage. All piles were freely rusting in both the atmospheric and tidal areas and exfoliation was taking place in the splash area. In comparing the corrosion status of the tidal zones of the piles, one could not determine the benefit of the attached anodes. However, flange thickness measurements conducted when Row C was removed in 1979 showed that corrosion damage in the tidal and immersed areas was appreciably reduced on the cathodically protected piles 2C and 3C.

Piles 4 and 5 were bare ASTM A 690 steel. Pile 5 had zinc anodes attached. Both piles were freely rusting in both the atmospheric and tidal areas. Considerable exfoliation had taken place in the splash areas. The amount of exfoliation noted at the splash area of Pile 4 was only exceeded by that on the carbon steel Pile 2. In comparing these

piles with each other visually as well as with the previous carbon steel one could see no benefit from either the anodes or the use of ASTM A 690 steel in the tidal zone or the splash zone. However, detailed measurements of flange thickness which were conducted on the Row C pilings removed in 1979, showed partial corrosion protection in the tidal zone [1, 2]. In 1995, both piles 4 and 5 were corroding in all areas.

Piles 6 and 7 had a Corps of Engineers system consisting of an epoxy zinc primer (E-303) and a coal tar epoxy topcoat (C-200). Zinc anodes were attached to Pile 6. In the 1992 inspection, both piles were approximately 80% bare in the splash areas with extensive exfoliation and 25% bare in the atmospheric areas. In the tidal areas, piles had some bare edges but areas of the flanges and the webs were completely protected. The window on #6 had rust undercutting completely across the pile face, while #7 had a 5 cm undercut on each side of the window. No benefit from the zinc anodes could be noted in the tidal zone and the splash zone. In 1995, the coating system had failed. The edges of all flanges were bare. The coating was curling and peeling on flanges and webs. Most of the coating remaining was adhering to rust scale. The pile was approximately 80% bare in the splash area with extensive exfoliation. Much of this failure took place within the past three years. The only difference between Piles 6 and 7 was the zinc anodes on Pile 6. Coating performances appeared equal in all respects.

Pile 8 had an inorganic zinc primer (Porter Zinc-Lok #352) and a coal tar epoxy topcoat (C-200). In the 1992 inspection the coating had a moderate amount of damage on the edges in the atmospheric areas and was significantly better than 7, 9, and 10 in these areas. Similarly, there was less exfoliation on the edges in the splash area than on 7 and 9. In the tidal areas it was significantly poorer with light corrosion starting on both edges and flanges. There had been little change in the past three years. The coating was still mostly intact. In the atmospheric area there were several 1.2cm to 4 cm diameter areas where rust was creating a blister under the film. There was only minor exfoliation in the splash area. The splash area was approximately 90% protected and the atmospheric area 95% protected. Overall performance was superior to Piles 7 and 9 but slightly poorer than Pile 10.

Pile 9 had a Corps of Engineers system consisting of an epoxy zinc primer (E-303) and a coal tar epoxy topcoat (C-200). Aluminum oxide was added to the final topcoat for added abrasion resistance at the mud line. The mud line area could not be observed. The remainder of the pile was quite similar to Piles 6 and 7. The coating in the splash area was loosely attached with considerable rust under the film. In 1995 the system had failed. Coating which was reported three years ago as being loosely attached in the splash area was now gone. Most of the coating on edges in the atmospheric areas was gone.

Pile 10 had an epoxy primer (Porter Paint Co., product number not available) topcoated with coal tar epoxy (C-200). The atmospheric area edges were 20% corroded and the splash area was less than 10% bare. The tidal area was starting to show some rust on edges but the coating was

providing excellent protection on other areas of the flanges and webs. The window had rust undercutting in an area about 5 cm in each direction. Overall, this coating was very similar to those on Piles 6, 7, and 9, however, its performance was slightly better. In 1995, pile 10 was notably the best of the coal tar epoxy systems. There had been no notable change in the past three years.

Pile 11 was ASTM A 690 steel coated with Corps of Engineers system consisting of an epoxy rich (E-303) primer and a coal tar epoxy (C-200) topcoat. Approximately 50% of the coating was gone in the splash area and 20% of the edges in the tidal area had corrosion. The window allowed rust to progress the full width of the pile face. In comparing this pile visually to piles 6 and 7, one could not note any benefit from the ASTM A 690 steel. Detailed flange thickness measurements were not conducted because of the biofouling which was present on the piles. In the splash area the coating was performing better than on Piles 7 and 9 but worse than Piles 8 and 10. It was equal to 7 in the atmospheric area. Some fouling was removed in the tidal area to reveal substantially intact coating.

Pile 12 had zinc rich primer (Plas Chem Zinc-ite), a ceramic intermediate (Plas Chem Ceram-ite #101), and a high build epoxy topcoat (Plas Chem 2140Z). It was noted during the 1992 inspection that the gray topcoat in the atmospheric area was badly eroded showing red primer in 50% of the area. There was some exfoliation on edges and other corrosion taking place. The coating in the splash area was completely gone and the steel was exfoliating badly. The coating in the tidal area was less than 10% intact. The window allowed rust to progress the full width of the pile. In 1995 this system continued to be significantly poorer than any of the coal tar systems. Pile 12 was equal to Pile 11 in the splash and atmospheric areas but the coating appeared to be completely gone on the tidal and underwater areas.

Pile 13 had an organic zinc rich primer (Plas Chem Zenker #11) and two epoxy topcoats (Plas Chem Chem-Pon 2310X red and gray). In 1992 the coating in the atmospheric area was quite poor on the edges, however, much of this may have been due to application or shipping problems. By 1995 the coating was gone in the splash area and exfoliation was progressing. It was also gone on most edges in the tidal area and the remainder of this area was 30-40% bare. The window allowed rust to progress the full width of the pile face. Although this coating was notably better than pile 12, it was still significantly poorer than any of the coal tar systems.

Piles 14 and 15 had an organic zinc rich primer (Hughson Chemglaze #9927) and a urethane topcoat (Hughson Chemglaze II). Pile 15 also had an intermediate coat of elastomeric urethane (Hughson #M312). The coatings in the atmospheric area were peeling back from the edges and exfoliation was progressing. By 1992, the windows allowed rust to progress across the entire width of the faces of the piles. The coatings were almost gone in the splash areas where more exfoliation was taking place. In the tidal areas, the edges were almost completely bare, however, the coating on other areas on the flanges and webs was

mostly intact and quite flexible. In comparing the two piles it appeared that #14 was slightly poorer due to slightly more rust undercutting 3.81 to 5.08 cm in the tidal area. Both of the piles were significantly poorer than any of the coal tar systems. In 1995, piles 13, 14 and 15 appeared very similar in the upper areas. They had totally failed on atmospheric flanges and edges similar to Piles 7 and 9. They were about equal to Pile 8 in the splash area. In tidal areas that were visible, it was estimated that Pile 13 was 50% bare, Pile 14 was 90% bare and Pile 15 was 10% bare.

Pile 16 had a flame sprayed zinc, a vinyl wash primer (MIL-P-15328) and a polyurethane (Metco Urecal 9301) topcoat. In 1992 the atmospheric area was 80-90% covered with coating, however, the coating was totally blistered with corrosion under the coating. The coating remained very flexible. The window allowed rust to progress the full width of the face of the pile. By 1995 the coating was completely gone in both the splash and tidal areas. Performance of this pile has been significantly poorer than any of the coal tar systems. Pile 16 was equal to or poorer than Pile 7 in the atmospheric areas.

Pile 17 had a flame sprayed aluminum coating. In the 1992 inspection this coating had lines of application-related failure in the atmospheric area. There were also several 25.8 to 77.4 sq. cm areas where dense blistering and delamination had taken place. There were small amounts of bare edges in the splash area. There was no rust undercutting at the window immediately above the splash area nor at the one in the tidal area. Although this coating was providing a high degree of protection in 1992, it appeared that an overall failure was taking place in 1995. Red rust was common on most of the atmospheric and splash areas but no pitting or exfoliation damage was noted. A detailed examination of piling 17C which was removed in 1979 showed extensive surface rusting in the splash zone [1,2].

Pile 18 had a flame sprayed aluminum primer, a vinyl wash primer (MIL-P-15328), and a vinyl aluminum sealer (Metcoseal AV). In 1992 this pile had a few minor bare edges in the tidal area. There were several 6.45 sq. cm bare areas in the splash area as well as dense #5-#6 blistering. There was no rust undercutting at the window. In 1992 the protection to this pile was equal to slightly superior to that on Pile 17. This coating performed better than any other coating at the Buzzard's Bay test site. By 1995 pile 18 had changed little, but it is now far superior to Pile 17. Pile 18B with windows had approximately 30% surface rust in the atmospheric zone including the splash zone.

Pile 19 was primed with a flame sprayed zinc, coated with a coal tar solution (Wise Chem T-265), and topcoated with a coal tar emulsion (Wise Chem T-264). In 1992 the coating was totally gone in both the tidal and splash areas and exfoliation was progressing rapidly in the splash area. In the atmospheric area, some of the topcoat and most of the zinc remained intact. The window allowed rust to progress completely across the face of the pile. This pile was significantly poorer than piles 17 or 18 which were primed with flame sprayed aluminum. In 1995 pile 19 was equal to or poorer than Pile 7 in both the atmospheric and

splash areas.

Pile 20 had a Corps of Engineers vinyl system consisting of a vinyl zinc (VZ-108) primer and a vinyl glass flake (V-110) topcoat. The coating in the tidal area was 90% intact, however, it was completely gone in the splash area. By 1995 the system had completely failed and was in slightly poorer condition than the coal tar systems on piles 6 and 7.

Pile 21 had an inorganic zinc (Dimetcote #3), a synthetic resin (Amercoat #54) topcoat, and a vinyl mastic (Amercoat #87) topcoat. The coating was 75% intact in the tidal area, almost 100% intact in the atmospheric area, and completely gone in the splash area. The window allowed corrosion to progress completely across the face of the pile. Exfoliation was progressing in the splash area. This coating system was superior to the coal tar systems in the atmospheric area, but inferior in the immersion areas.

RESULTS OF 1995 ELECTROCHEMICAL EVALUATION AT BUZZARD'S BAY TEST SITE

Electrochemical polarization measurements were conducted to non-destructively determine the bare steel area in the immersed area of the coated piles. Measurements were conducted from a boat in 1992 and in 1995. Previously, the measurements were conducted from the beach. Stainless steel rods, which were welded to the pilings before installation, provided good electrical connections for performing the measurements. Most of the commercial corrosion testing equipment can not be used for field structures because of the high current requirements and the lack of an AC power source. A portable compact 12 volt battery was used as a power source and a set of resistances were used to adjust the applied current. The initial corrosion potential of each pile was measured with respect to a copper-copper sulfate reference cell before any current was applied. Then, current was passed between each test pile and an auxiliary pile for 5 minutes so that the potential of the test pile was shifted from its initial potential by -0.020 volt. The amount of potential shift was recorded as δV . The amount of current required to achieve the -0.020 volt potential shift at 5 minutes was recorded as δI . This is the polarization resistance, R_p :

$$R_p = \frac{\delta V}{\delta I} \quad (1)$$

The amount of potential shift was increased to -0.150 volt and the required current after 5 minutes was also recorded to compare the data with previous years. When δV is -0.150 volt, the polarization resistance is defined as the Cathodic Protection Index, CPI:

$$CPI = \frac{\delta V}{\delta I} \text{ at } -0.150 \text{ V} \quad (2)$$

The percent bare area was estimated by using bare steel pile as a baseline and assuming that the amount of current per square cm required to shift the potential is linear with respect to bare area. This has been shown previously [2,3]:

$$(\% \text{bare area})_{CN} = 100 \times \frac{A_{BN} \delta I_{CN}}{A_{CN} \delta I_{BN}} \quad (3)$$

where:

$(\% \text{ bare area})_{CN}$ = percent of bare area present on coated pile at year N

A_{BN} = submerged area of bare pile at year N

A_{CN} = submerged area of coated pile at year N

δI_{CN} = current required to shift potential of coated pile at yr. N

δI_{BN} = current required to shift potential of bare pile at yr. N

Electrical polarization measurements were performed on all of the pilings in the 1995 study except for the metallized piles, the cathodically protected piles and piles bent by the ice. The calculated percent bare area in the submerged zone was obtained using the -0.020 volt polarization shift and the corresponding ASTM ratings are presented in Table 2. The calculated bare area using the -0.020 volt polarization shift was within 0.5% of that calculated by -0.150 volt shift. Because of the presence of barnacles in the tidal zone and marine fouling in the submerged areas, the actual coating degradation could be more than the calculated bare area obtained using the -0.020 volt potential shift.

As reported by Brouillette and Hanna [4], steel piles in naval harbors corroded at higher rates above the mud line than below. This was confirmed by inspection and flange thickness measurements on pilings withdrawn after 5 years of service from the Buzzard's Bay test site which showed very little corrosion in the embedded zone [1]. Therefore, the majority of the polarization of the steel would occur in the submerged rather than in the embedded zone.

The corrosion rate of bare steel pilings was measured using the Schwerdtfeger and McDorman technique [5]. The corrosion rate of bare carbon steel was determined to be 0.086 mm (3.4 mils) per year from flange thickness measurements at the Buzzard's Bay test site [1].

COMPARISON WITH LA COSTA ISLAND, FL, TEST SITE

The testing at La Costa Island, FL site was initiated in January 1971. The water temperature varies from 13 degree to 32 degree C, with an average temperature of 24 degrees C. Originally, 23 coatings were applied on pilings and installed for evaluation in a three-row arrangement similar to that at the Buzzard's Bay test site. After 10 years, most of the steel pilings were pulled out for detailed evaluation. The results have been previously published [6,7,8]. The coatings and their composition for the remaining pilings at the La

TABLE 3--La Costa Island test pile preparation details

Sys. No.	Description of Coating System	No. of Coats	Dry Coating Thickness (mm)	Coating Source
28	Coal tar epoxy, garnet -armored at mud line Formula C-200 Formula C-200+ aluminum oxide (#30 grit) broadcast into wet final coat	2 1	0.41-0.51 0.25	U.S.S. Chemicals
29	Polyester glass flake, Carboglas 1601, spray grade	2	1.02	Carboline Co.

Costa Island test site are shown in Table 3. The corrosion rate is higher in the warmer waters at the La Costa Island test site than at the Buzzard's Bay test site. The corrosion rate of bare carbon steel was determined to be 0.18 mm (7.1 mils) per year in the submerged zone at La Costa Island test site [8] compared to 0.086 mm (3.4 mil) per year for bare carbon steel at the Buzzard's Bay test site [1].

The 21-year visual inspection of the polyester glass flake and coal tar epoxy coatings was conducted in 1992. The polyester glass flake (system #29) was the top performing coating with coal tar epoxy (system #28) as a close second. However, the polyester glass flake is a more expensive coating and is more difficult to apply and repair in the field. The coal tar epoxy can be field applied and is easier to repair. The two coatings were left in place for further long-term evaluation.

Polarization measurements to determine the area of bare steel have been conducted for over twenty years. The results have shown that the long term performance of coatings can be predicted from data obtained in the first few years. Therefore, electrical polarization measurements can be used for accelerated testing of new coating systems.

CONCLUSIONS

The following conclusions can be drawn from the results of the Army Corps of Engineers long term (20 years) studies at the Buzzard's Bay, MA, and La Costa Island, FL, test sites:

1. The splash zone was the worst zone at both test site locations.
2. Overall, coal tar epoxy (C-200) with organic zinc-rich primer (E-303) performed well at both locations.

3. At the Buzzard's Bay test site, flame sprayed aluminum with a vinyl sealer (system #18) was the top performer.
4. At the La Costa Island test site, polyester glass flake (system #29) was the top performer.
5. Electrochemical polarization resistance data can be used to determine the bare area of steel and thereby the condition of the coating on submerged areas of steel pilings in the field.

REFERENCES

- [1] Kumar, A., Lampo, R., and Beitelman, A., "Corrosion Control of Pilings in Seawater: Buzzard's Bay", U. S. Army Construction Engineering Research Laboratory, Technical Report M-286, January 1981.
- [2] Kumar, A., Beitelman, A., and Meronyk, E., "Corrosion Control of Pilings in Seawater: Buzzard's Bay, MA," Paper No. 345, National Association of Corrosion Engineers International Annual Conference, CORROSION 84, 1984.
- [3] Beitelman, A., Van Blaricum, V., and Kumar, A., "Performance of Coatings in Seawater: A Field Study", Paper No 439, National Association of Corrosion Engineers (NACE) International Annual Conference, CORROSION 93, 1993.
- [4] Brouillette, C.V., and Hanna, A.E., Corrosion Survey of Steel Sheet Piling, Tech Report 097, U.S. Naval Civil Engineering Laboratory, Port Hueneme, CA, (Dec 1960)
- [5] Schwerdtfeger, W.J. and McDorman, O.N., "Measurement of Corrosion Rate of Metal from its Polarization Characteristics" Journal of the Electrochemical Society, Vol 99, p. 407, 1952.
- [6] Kumar, A., and Wittier, D., "Coatings and Cathodic Protection of Pilings in Seawater: Results of 5-Year Exposure", Materials Performance 18, 12 (1979), p. 9-19.
- [7] Bukowski, J., and Kumar, A., "Coatings and Cathodic Protection of Piling in Seawater: Results of 10-Year Exposure at La Costa Island, FL", U. S. Army Construction Engineering Research Laboratory, Technical Report M-321, August 1982.
- [8] Van Blaricum, V., and Kumar, A., "Field Evaluation of Cathodic Protection Index for Bare and Coated Steel in Seawater", Paper No 528, National Association of Corrosion Engineers (NACE) International Annual Conference, CORROSION 93, 1993.

ACKNOWLEDGMENTS

Jeffrey H. Boy would like to acknowledge that this research was supported in part by an appointment to the Research Participation Program at the U.S. Army Construction Engineering Research Laboratories (USACERL) administered by Oak Ridge Institute for Science and Education through an interagency agreement between the U.S. Department of Energy and USACERL.

Albert W. Zeuthen¹ and Robert M. Kain²

CREVICE CORROSION TESTING OF AUSTENITIC, SUPERAUSTENITIC, SUPERFERRITIC, AND SUPERDUPLEX STAINLESS TYPE ALLOYS IN SEAWATER

REFERENCE: Zeuthen, A. W. and Kain, R. M., “Crevice Corrosion Testing of Austenitic Superaustenitic, Superferritic, and Superduplex Stainless Type Alloys in Seawater,” Corrosion Testing in Natural Waters: Second Volume, ASTM STP 1300, Robert M. Kain, Walter T. Young, Eds., American Society for Testing and Materials, 1997.

ABSTRACT: In industry, many problems from corrosion occurring in crevices have been experienced and reported. These include the refining industry, offshore drilling platforms, fossil and nuclear power plants, chemical plants and the public utilities. The services are highly variable. Corrosion mechanisms and the results experienced are influenced by severe environments which cannot always be avoided.

Corrosion testing is considered useful not only in comparing materials, but also in selecting materials from the design standpoint. The ultimate goal is to use materials which are superior to those currently in use. This will result in fewer outages, reduce repairs and significantly lower costs.

This paper provides the results from four seawater test programs addressing crevice corrosion resistance of a number of “superferritic,” “superaustenitic,” and “superduplex” alloys, along with conventional “300 Series” stainless steel. These programs included exposure to natural fouling organisms which can produce crevices, and testing which comprised several different manmade crevice configurations. Alloys found to be resistant under some test conditions were prone to attack under others. All of the “super stainless” steels were found to be more resistant to crevice corrosion than conventional austenitic grades, but some were susceptible to some degree.

KEYWORDS: crevice corrosion, bi-metallic crevice corrosion, superferritic, austenitic, superaustenitic, superduplex, stainless steel, seawater.

¹Albert W. Zeuthen, Section Head Mat. Eng., Long Island Lighting Co., Melville, NY 11747.

²Robert M. Kain, Senior Corrosion Scientist, LaQue Center for Corrosion Technology, Inc., Wrightsville Beach, NC 28480.

INTRODUCTION

Crevice corrosion testing of stainless alloys in natural waters first came to the attention of the Long Island Lighting Company (LILCO) in 1978 when the process was considered as potentially useful for distinguishing the difference in corrosion resistance between materials. Earlier (unpublished) seawater crevice corrosion testing, for example, distinguished differences in one alloy's resistance due to variations in chemistry or microstructure. Those crevice corrosion tests were deemed successful and others have been performed from time to time. Service experience has also demonstrated and confirmed the value and importance of corrosion testing.

Because service conditions can vary as a function of environment and design, these variables must be considered in the selection of the most appropriate material. This is particularly true for stainless grades as their crevice corrosion resistance may be influenced by a number of interrelated metallurgical, geometrical and environmental factors [1]. Accordingly, it is beneficial to examine data from different types of tests which consider these variables. In this respect, ASTM G-78 can provide useful guidance in test design and interpretation of results obtained [2].

This paper describes four test programs involving the crevice corrosion testing of a number of "super stainless alloys" which may be used in coastal power plants or other facilities which handle seawater for cooling. The first test (Program I) discussed considers the behavior of two superferritic and two superaustenitic alloys exposed at various locations on Long Island Sound, N.Y. Two separate, but related tests (Programs II and III), expanded the scope of work to include a broader range of alloys ranging from 300-series stainless steels to the family of 6 percent molybdenum-nitrogen containing superaustenitic stainless alloys, and several new super-duplex materials. These tests, conducted in seawater from Banks Channel, Wrightsville Beach, N.C., were considered to be more severe - principally because of the vinyl sleeve type crevice conditions provided. The fourth test program (IV) to be discussed examines stainless alloy resistance to crevice corrosion when metal-to-metal type crevices are created by like or dissimilar metals. Such conditions could exist at tube-to-tube support plate sites in condensers and heat exchangers. These tests were also conducted at the North Carolina site noted above. All materials tested are identified in Table 1 by their Unified Numbering System designations [3] and their nominal compositions. Material from different heats was utilized for test specimens in the various programs, but these conformed to UNS specifications.

TEST PROGRAM I

Experimental

During the summer of 1990, single tube specimens of four different stainless materials were suspended in Long Island Sound seawater at three LILCO power plant sites for a period of 41 days. As identified in Table 1, the materials investigated were S44735, S31254, N08367 and

**TABLE 1—Identification of Alloys and Product Forms Tested in
Various Seawater Environments**

UNS Designation	Common Trade Name	Test Program	Nominal Composition (wt.%)					
			Cr	Ni	Mo	N	Cu	Other
S44735	29-4C	I ¹	92	0.03	3.9	0.03		
S44660	Sea Cure	I ¹	26	2.5	3.0	0.02		
S31254	254SMO	I ¹ , II ¹	20	18	6.0	0.18	0.70	
N08367	AL-6XN	I ¹ , II ¹ , IV ¹	21	24	6.3	0.22		
N08925	25-6Mo	II ¹	20	25	6.6	0.15	0.85	
N08926	1925hMo	II ¹	20	25	6.4	0.20	0.86	
S32750	SAF2507	II ¹ , IV ²	25	4.0	3.85	0.26	0.82	
S30400	Type 304	IV ^{1,2}	19	10.0				
S31603	Type 316L	III ¹ , IV ²	16.7	10.3	2.1		0.33	
S31703	Type 317L	III ¹	18.4	12.8	3.2			
S32550	Ferralum 255	III ¹	25.0	5.9	3.1	0.18	1.7	
S32760 ³	Zeron 100	III ¹	25.4	7.1	3.6	0.26	0.7	0.7W
S39274	DP-3W	III ¹	25.1	2.6	3.2	0.26	0.5	2W
K*****	Carbon Steel	IV ²	----- Not determined -----					

¹ Tube specimens

² Plate specimens

³ Previously designated S39276

S44660 (A, B, C and D respectively). Two nylon serrated hose clamps were fitted tightly on each tube to provide crevices. The tubes, which ranged in OD sizes of 0.19 mm to 25.4 mm (0.75 in. to 1.00 in.), were suspended one above the other with nylon line so that their axis were vertical. The uppermost tube (D) was located five feet from the bottom and the lowest tube (A) one foot from the bottom in water approximately 16 feet deep. In time, macrofoulers developed and created additional (natural) crevice sites. Seawater hydrology data was not obtained for the above tests.

Test Results

Figure 1 identifies the geographical location of the test sites on Long Island Sound along with photographs showing the extent of fouling incurred. Note that the severity of the fouling deposits varied with the power plant location and also with the depth of the water, particularly at the Port Jefferson and Northport sites. Inspection of the tubes revealed no evidence of attack at barnacle attachment sites. Except for a light etch at one of the clamp sites on one of the alloy S44735 tubes (Figure 2), all materials were resistant to crevice corrosion in these tests. Due to the prolific amount of fouling which encapsulated the tubes in the Glenwood tests, it is believed that crevice corrosion, if initiated, would be stifled by the lack of any effective cathodic surface area.

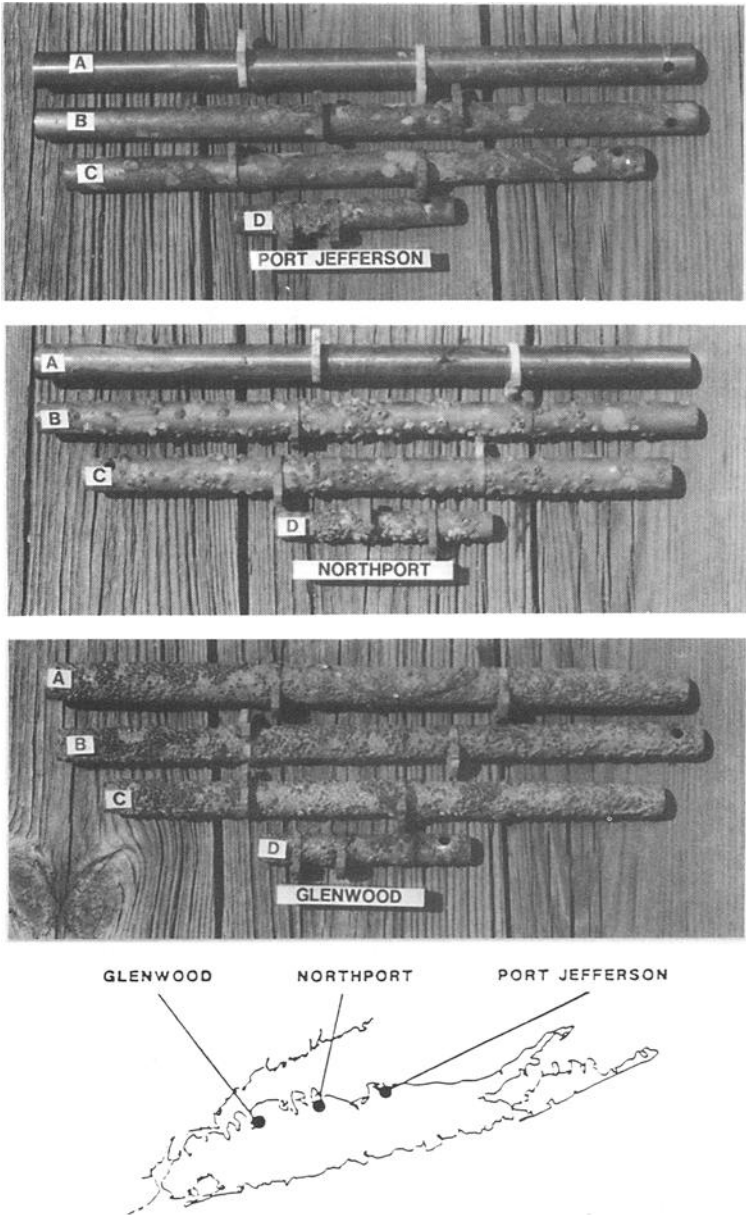


FIG. 1--Location of Program I exposure sites and appearance of test specimens after 41 days in Long Island Sound seawater.

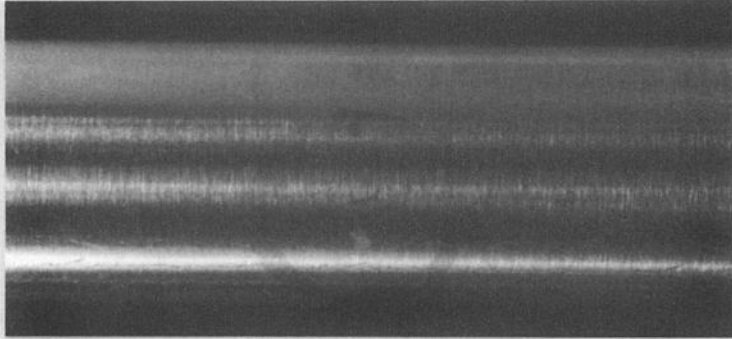


FIG. 2—Area of superficial attack found beneath clamp on S44735 tube exposed in Long Island Sound at the Port Jefferson site.

TEST PROGRAMS II AND III (Vinyl Sleeve Testing)

Two separate but related test programs were conducted to investigate the crevice corrosion resistance of 10 stainless tubing alloys in seawater at Wrightsville Beach, N.C. As indicated in Table 1, two of the alloys selected, NO8367 and S31254, had been included in the Long Island Sound tests described previously in Program I. Also included were two other “superaustenitic” alloys (N08925 and N08926) and four “superduplex” alloys (S32550, S32750, S32760 and S39274).

Experimental Considerations

Table 2 identifies the materials tested in Program II and III, respectively. All tubular specimens were tested in triplicate in their respective mill finishes. The length of each specimen was 150 mm (6 inches). Table 2 gives the dimensions for each tube/pipe material. As discussed below, differences in specimen OD and ID dimensions created some variability in test conditions provided or achieved. As also shown in Table 2, these included the seawater velocity through the tubes and the severity of the crevice created on the OD of the tubes.

In each series of tests, replicate specimens were connected together with sections of vinyl tubing (Tygon®). This tubing, referred to henceforth as vinyl sleeves, was positioned to cover approximately 25 mm (~1 inch) at each end of the specimen. Accordingly, two crevice sites were created on each specimen for a total of 6 sites per alloy. The sleeves were secured with serrated nylon hose clamps positioned about 6.5 mm (¼ inch) back from the crevice mouth created on the alloy tubing OD. Figure 3 shows a typical alloy tube/vinyl sleeve crevice assembly.

TABLE 2--Summary of Tube/Pipe Dimensions and Other Test Conditions for Indicated Program

Program No.	Alloy/UNS Designations	Dimensions (mm)		Seawater Velocity (m/s)	Assumed Crevice Severity**
		O.D.	I.D.		
II	N08926	33.5	26.5	1.6	S
II	N08367*	25.4	24.2	2.0	MS
II	S32750	25.5	22.1	2.4	MS
II	N08925*	26.8	18.8	3.3	S
II	S31254	19.1	15.9	4.0	MS
III	S31603*	19.1	15.7	2.4	MS
III	S31703*	25.4	21.2	2.4	MS
III	S39274	25.4	21.2	2.4	MS
III	S32760	19.1	15.9	2.4	MS
III	S32550*	25.4	21.0	2.4	MS

* Denotes units converted from original mill provided dimensions in English units for indicated alloy.

** Severe (s) or moderately severe (MS) interference fit.

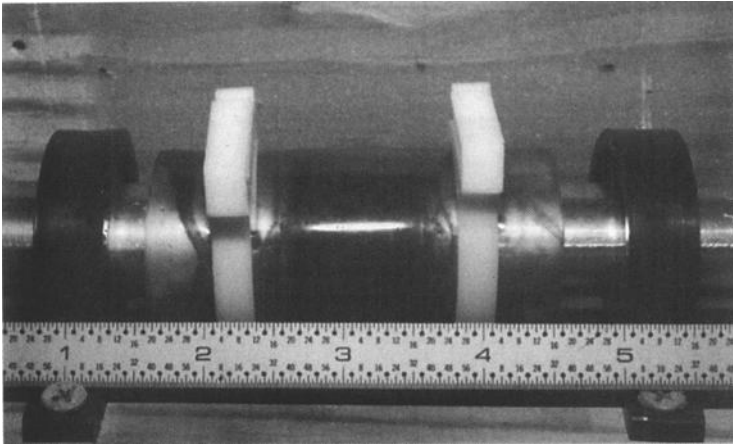


FIG. 3--Typical alloy tube/vinyl sleeve assembly.

Because of differences in the tube ID dimension and operation of Test II at a fixed bulk flow rate, different velocities ranging from 1.6 to 4.8 m/s (5.4 to 15.6 ft/s) were created. In Test III, two separate test lines were assembled and operated at different bulk flows to provide a consistent velocity of 2.4 m/s through all tubes in that series. Test velocities approximated or

exceeded the minimum practical design velocity for seawater condensers and heat exchangers - about 1.5 m/s (5 ft/s) and preferably 1.8 m/s (6 ft/s) [5]. While maintenance of this velocity appears to minimize the attachment of marine macrofoulers, microfouling is possible at these and at even higher velocities. Microfouling on the surface of stainless type alloys contributes to ennoblement of the corrosion potential and increased risk of crevice corrosion if a critical crevice geometry is present for a given material [6,7].

Vinyl sleeves have been used elsewhere to investigate the crevice corrosion resistance of several stainless and nickel-base alloys [3,4]. One of the first published tests involved the "20 Cr-6 Mo" alloy N08366 [4]. Because the vinyl sleeve configuration is capable of creating deep-tight crevices, they are considered severe and conducive to promoting crevice corrosion. The severity of the crevice appears to be dependent on the interference fit between the tube OD being tested and the ID of the available vinyl sleeve material. In the present series of tests, the ID (~19.1 mm and 25.4 mm) of vinyl sleeves utilized were either approximately equal to, or somewhat smaller than, the alloy tube being tested. Thus, materials tested in the latter situation may have been exposed with more severe crevices (S) than those in the former situation (MS). Presumably, alloys N08925 and N08926 were tested with tighter crevices than the other alloys.

Seawater Hydrology and Test Temperatures

Program II and III tests were conducted during the summer months of 1992 and 1993, respectively, and with raw (strained only) natural seawater, having the characteristics shown by the hydrology data provided in Table 3. The mean seawater temperature for the two tests, each 60 days in duration, was 28.2°C and 28.6°C, respectively.

TABLE 3--Seawater Hydrology Data Covering Indicated 60-Day Test Programs

Parameter	Program II Summer 1992	Program III Summer 1993	Program IV Summer 1994
Temp. Range °	27.0 - 29.0	26.9 - 30.4	24.5 - 28.6
Dissolved Oxygen (mg/L)	5.84 - 6.36	5.30 - 6.49	5.41 - 6.97
% Saturation	87.6 - 101.3	88.3 - 100.9	87.8 - 103.1
pH	7.8 - 8.0	7.9 - 8.0	7.9 - 8.0
Salinity (g/L)	31.96 - 35.71	35.12 - 36.62	34.14 - 35.99
Chlorinity (g/L)	17.69 - 19.97	19.44 - 20.85	18.62 - 19.92
Sulfate (g/L)	2.47 - 2.83	2.77 - 2.86	2.63 - 2.81
Conductivity (mS)	51.8 - 58.0	49.3 - 57.8	54.1 - 54.9

Results and Discussion

Crevice Corrosion Initiation--The translucent nature of the vinyl sleeves enables *in-situ* inspections of the crevice sites. Table 4 gives the earliest times for the visible detection of crevice corrosion. Because the frequency of inspections was intentionally reduced as testing progressed, and possible differences in alloy crevice corrosion propagation rates, these times may or may not be accurate indicators of the absolute times to initiation. Nonetheless, a substantial difference in the apparent initiation times between the traditional 300 series and the newer more highly alloyed materials was detected. Also shown in Table 4 is the corresponding number of available crevice sites that were attacked within 60 days. Two alloys, S32760 and S39274, were completely resistant and three alloys, S31603, S31703 and S31254, incurred attack at all 6 crevice sites. The remaining 4 alloys showed more variable behavior, with 2 to 4 sites being resistant. In the earlier Long Island Sound tests, both N08367 and S31254 were found to be resistant to crevice corrosion under conditions described for Program I. Environmental differences between Long Island Sound seawater and Atlantic Ocean water in Banks Channel at Wrightsville Beach, N.C., and crevice geometry differences, could account for the differences in alloy resistance to crevice corrosion initiation noted between these two test programs (i.e., I and II).

TABLE 4--Summary of Crevice Corrosion Resistance Data for 10 Tubing Alloys Exposed to Flowing Seawater in Test Program II and III

Alloy Tubing UNS Designation	Test Velocity (m/s)	Crevice Severity	<u>Initiation Resistance</u>		<u>Propagation Resistance</u>	
			Earliest Detection Time (Days)	Number of Sites Attacked	Affected Crevice Area (mm ²)	Maximum Depth of Attack (mm)
S31603	2.4	MS	4	6	<10-137	0.2-0.22
S31703	2.4	MS	4	6	<10-595	<0.01-0.57
S31254	4.0	MS	7	6	<10-20	<0.01-0.03
S32750	2.4	MS	14	3	<10-10	0.01-0.13
N08925	3.3	S	14	3	20-180	<0.01-0.13
N08367	2.0	MS	14	3	<10-30	<0.01-0.15
S32550	2.4	MS	43	4	<10-29	0.01-0.05
N08926	1.6	S	53	2	<10	0.02-0.08
S32760	2.4	MS	OK-60	0	None	0.00
S39274	2.4	MS	OK-60	0	None	0.00

Propagation Resistance--Table 4 also provides data on the area and depth of crevice corrosion incurred by the affected specimens. The two 300-series austenitic stainless steels, S31703 and S31603, incurred the greatest amount of crevice corrosion, respectively. Except for one site each, on the N08925 and S32550 tubes, the attack on these and the other susceptible alloys was minimal with respect to affected area. With the exception of two

affected crevice sites on one N08925 (0.13 mm deep) and one NO8367 (0.15 mm deep) specimen, the overall ranges of maximum depth of attack exhibited by the superaustenitic and superduplex stainless alloy tubes were comparable.

Overview

As with most tests of this nature, there is a temptation to rank materials on their “go” or “no-go” resistance to initiation or to their overall susceptibility to attack, including propagation. In lieu of the variables indicated above, the following critique is offered:

300-Series Stainless Steel—Alloys S31603 and S31703 were tested at the same velocity (2.4 m/s) and with nominally the same crevice geometry, which we have identified as being moderately severe. Despite the fact that S31703 contains higher levels of chromium, nickel and molybdenum, in this test S31703 exhibited the same susceptibility to initiation as did S31603. Figure 4 documents some of the affected crevice sites for these two alloys. Based on previous seawater test experience and mathematical modeling by others [8,9], this behavior is not totally unexpected. One possible explanation for the somewhat shallower penetration measured for the S31603 is provided at the end of this critique.

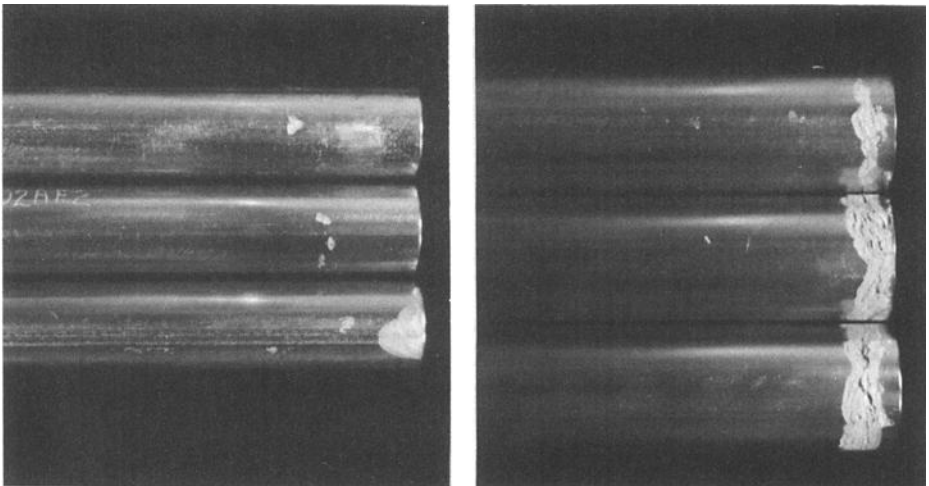


FIG. 4--Examples of crevice corrosion found at vinyl sleeve sites (left) S31603 and (right) S31703 tube specimens after 60 days exposure to seawater.

"Superaustenitics" (S31254, N08367, N08925, N08926)—Except for a lower nickel content in S31254 and somewhat lower copper in N08367, the chemistries for the four superaustenitics are quite similar and all were found to be susceptible to crevice corrosion, albeit generally mild in comparison to the above 300-series grades. Initiation data for this class of materials suggests some influence of test velocity and crevice severity on behavior observed. For example, as shown in Table 4, the number of affected sites was greatest for those alloys tested at the higher velocities. This effect is more apparent for the materials tested with “moderately severe” crevice geometries than with “severe” ones. Overall, there were no substantial differences in the propagation behavior of these alloys. However, the above velocity and geometry factors may have accounted for the relatively minor differences noted. For example, S31254, which was tested with moderately severe crevice and at the highest velocity, exhibited the least penetration.

"Superduplex alloys" (S32550, S32760, S32750, S39274)—All testing of these materials was conducted at the same nominal velocity of 2.4 m/s. The susceptibility/resistance of two alloys (S32550 and S32750) was similar to above superaustenitics. It is presently uncertain if the full resistance exhibited by the remaining two alloys, S32760 and S39274, is due to their alloy content (including tungsten) duplex-microstructure, the nature of the moderately severe crevices, or to some combination of the above.

Influence of Biofouling

It was mentioned earlier that velocity can impact biofouling in condenser tubes. Since biofilms assist in the crevice corrosion process, a reduction in these films would be beneficial, particularly from the standpoint of propagation. This has been demonstrated in other crevice corrosion tests employing biocidal treatment of seawater [4]. In the present series of tests, the I.D.'s of S31603, S31254 and S32760 were smaller than those of the other tubes tested. Reduced tube size (ID) may have contributed to somewhat higher fluid shear stresses, which could conceivably help minimize microfouling and its influence of crevice corrosion propagation. This scenario may explain, in part, the greater resistance to propagation exhibited by S31603 over S31703 tubes as well as that for S31254 tubes over others in the "20Cr-6Mo" family. It may also account for the observed differences identified between S32760 and the susceptible duplex alloys S32750 and S32550.

Some of the alloys tested herein were included in other programs comprising exposure of sheet material fitted with other type crevice formers, producing a range of crevice conditions [10]. Those tests were conducted under quiescent seawater conditions when microfouling was abundant and ennoblement of potentials quantified. Some of the same susceptible materials in those tests exhibited appreciably greater rates of propagation within the same time frame described in the present tests.

Summary

All superduplex and superaustenitic alloys tested exhibited greater resistance to seawater than lower alloyed grades of 300-series stainless steel, S31603 and S31703.

Differences in behavior among alloys within a given class can be related to experimental variables as well as to alloy composition. Of the six alloys tested under similar seawater flow conditions (2.4 m/s) and similar crevice conditions (MS), alloys S39274 and S32760 were found to be fully resistant.

TEST PROGRAM IV (Galvanic/Crevice Corrosion Investigations)

Previously described research programs covered crevice corrosion testing of different stainless alloys fitted with non-metallic crevice formers. Heat exchanger constructions, whether of entirely new materials or of retubing existing heat exchangers, usually will entail the use of dissimilar materials for tubesheets and tube supports. Operating experience has shown that serious failures can occur in crevices at these locations. These can be evidenced by wall thinning of the tubes, enlargement of tube support plate holes, or a combination of both. This program, conducted in late summer of 1994, was performed in seawater to simulate worst case conditions. However, other natural or chloride contaminated freshwater under certain adverse conditions, may also contribute to localized corrosion of materials of construction.

Experimental

Figure 5 illustrates a typical test assembly comprising three tubes and three tube support plate specimens. A total of four such assemblies were fabricated. One of these was of all S30400 construction and served as the test control, since S30400 resistance to crevice corrosion in seawater is known to be poor. The other three assemblies all consisted of three alloy N08367 tubes and three tube support plates of either carbon steel, S31600 or the duplex stainless steel S37250. All tubes were 15.99 mm (5/8-inch) OD by 205 mm (12 inches) long. Support plates measured 75 mm x 80 mm with thickness ranging from 9.5 mm to 12.7 mm. Holes were drilled and reamed to a dimension providing about a 0.13 mm (0.005 inch) clearance for insertion of the tubes. The composition of the materials tested are shown in Table 1. These tests were conducted in a 400 liter trough filled with ambient temperature filtered (5 micron) seawater with continuous refreshment at a rate of approximately 1 L/min., or 4 changes daily. The mean daily seawater temperature was 25.9°C and the test duration was 60 days. The seawater hydrology was within the range shown in Table 3.

Results and Discussion

Mixed-metal corrosion potentials were measured initially and after 24 hours. These are shown in Table 5. Note that the potential of the all-stainless assemblies became more noble after 24 hours while the couple potential of the N08367 carbon steel assembly shifted in the active direction. After 24 hours, the N08367/S37250 assembly exhibited the most noble potential. The more active couple potential exhibited by the S30400 tube/plate assembly is likely due to the onset of localized corrosion as described below.

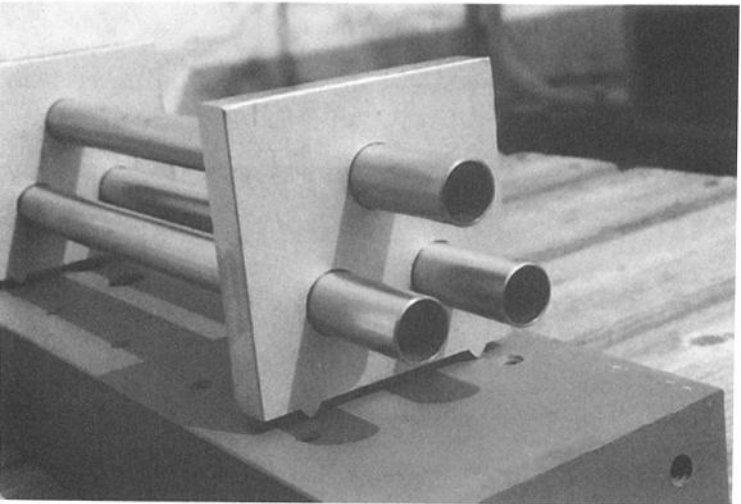
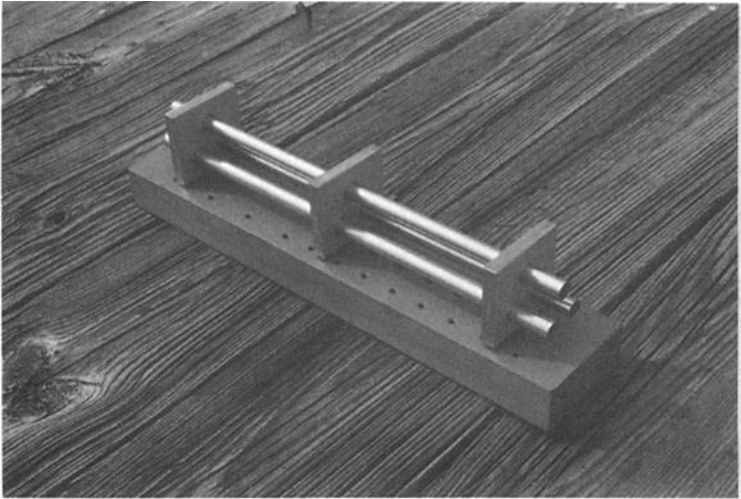


FIG. 5--Overall view (top) and close-up view (bottom) of galvanic/crevice corrosion test assembly comprising 3 tubes and 3 tube support plates.

TABLE 5--Corrosion Potentials for Dissimilar Metal Tube and Plate Assemblies

Coupled Materials		Volts vs. Ag/AgCl/Seawater Reference	
Tube	Plate	Initial	24 Hours
N08367	Carbon Steel	-0.665	-0.749
N08367	S31603	-0.199	-0.045
N08367	S37250	-0.181	-0.002
S30400	S30400	-0.232	-0.150

S30400 Control Assembly--Crevice corrosion was detected, *in-situ*, at the three sites created at the center support plate within 4 days. Post-test inspection revealed significant attack of the tubes (Figure 6-left) as well as the support plate (Figure 7). In contrast, and as shown in Figure 6-right attack found at 4 of the 6 other crevice locations was very light. In all cases, the attack incurred by the support plate mirrored that of the tubes, and vice-versa. Table 6 gives depth of attack data for the affected tube sites. It is conceivable that a small amount of misalignment produced tighter crevices between the tubes and center plate than at either end plate, thus accounting for the greatest amount of attack at the former sites. The deepest penetration was approximately 50 percent of the tube wall thickness. The site-to-site variations in depth of attack are consistent with those exhibited by some of the tubing specimens in the previously discussed vinyl sleeve tests (Table 5). Penetrations, due to crevice corrosion, at the center support plate holes (Figure 7) were on the order of 0.050 to 0.60 mm deep.

TABLE 6--Depth of Crevice Corrosion Incurred by S30400 Tube Specimens (mm)

Tube No.	Support Plate Location		
	Left	Center	Right
1	<0.01	0.46	<0.01
2	0.01	0.40	0.00
3	0.01	0.50	0.00

Mixed Stainless Alloy Assemblies--All N08367 tubes and corresponding S31600 and S32750 support plates were resistant to galvanic/crevice corrosion at the sites provided. Considering that the crevices were not particularly severe in terms of tightness, the resistance exhibited by even S31600 is not so surprising. Although S31600 was resistant to crevice corrosion at the intended sites, some severe localized corrosion developed on the exposed plate edges. As documented in Figure 7, the same type attack was incurred by some of the S30400 plates. This attack may have been influenced by micro-crevices resulting from machining and

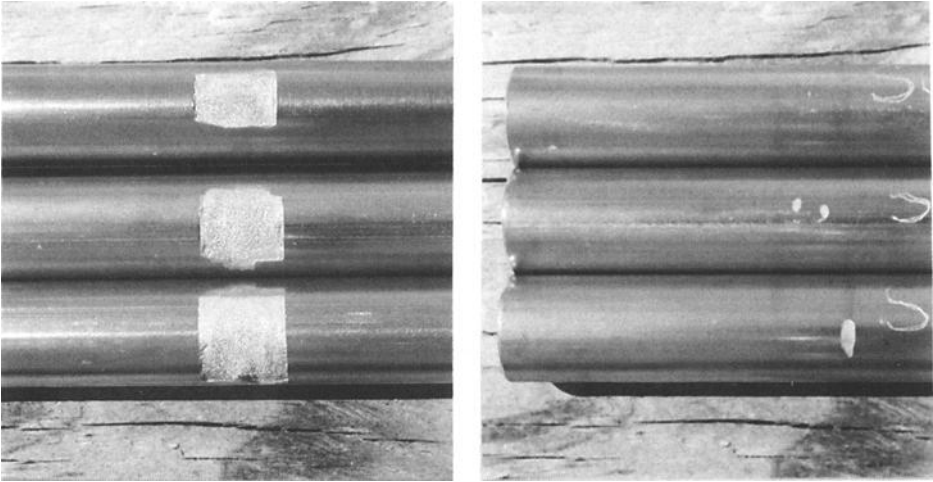


FIG. 6--Crevice corrosion incurred by S30403 tubes at tube support plate locations (left - center support sites, right - end support sites)



FIG. 7--Crevice corrosion at S30400 center support plate sites.

possible related exposure of metal sulfides in the cross-sectional microstructure. The duplex alloy S37250 plates were resistant to this form of localized corrosion. Table 7 gives mass loss data for each of the support plate members of the four different alloys. As indicated, the localized corrosion incurred by some of the S30400 and S31600 plates resulted in total mass loss which exceeded that of the carbon steel resulting from self- or galvanic corrosion.

TABLE 7--Mass Loss Results for Support Plate Specimens

Plate Material	Plate No.	Mass Loss (g)
Carbon Steel	-1	3.08
	-2	3.09
	-3	2.81
S30400	-1	0.00
	-2	5.08
	-3	0.18
S31603	-1	0.09
	-2	5.25
	-3	0.00
S37250	-1	0.00
	-2	0.02
	-3	0.00

N08367/Carbon-Steel Assembly--No evidence of crevice corrosion was found at any of the N08367 tubes in this assembly configuration. This can be attributed to the alloy's inherent resistance to crevice corrosion as well as to any galvanic protection afforded by the carbon steel plate members. While the support plate thickness was reduced by about 0.06 mm, the hole diameters increased by an average of 0.14 mm or only 1 percent of the original. This is substantially less than the crevice related enlargement in the S30400 plates described above. Overall, N08367 did not appear to promote accelerated galvanic corrosion at the carbon steel contact sites. This behavior is consistent with galvanic corrosion trends in a highly conductive electrolyte, such as seawater. In less conductive waters, galvanic corrosion would be more localized nearest the contact sites.

Based on the mass loss data (Table 7), carbon steel plates exhibited a short-term (60-day), uniform corrosion rate of 170 $\mu\text{m}/\text{y}$ (6.6 mpy). These rates approximate that reported for freely corroding K01501 carbon specimens exposed for 6 months at the same seawater test site in the ASTM Worldwide Seawater Corrosivity Study [11]. Corrosion rate data for the steel plates, together with the corrosive potential data shown previously in Table 6 suggests that the N08367 tubes involved were readily polarized toward the potential of steel, thereby minimizing

the galvanic influence in this case. In the present test, conducted under nominal quiescent conditions, the accumulation of corrosion products may have retarded any accelerating corrosion due to galvanic coupling with N08367. Galvanic corrosion of carbon steel may be greater in power plant service where expected turbulence could remove or minimize the build-up of corrosion products and where a larger, and consequently more adverse, stainless steel to carbon steel area ratios may exist.

Calcareous Deposits--Varying amounts of calcareous deposits were found on all tubes except the N08367 tubes assembled with S37250 plates. These deposits frequently form on the cathodic member of galvanic couples as well as on the cathode areas of some materials incurring localized corrosion. In the present tests, N08367 tubes assembled with carbon steel plates developed the thickest deposits, to the extent that this impeded removal of the tubes from the support plates. The development of thick calcareous scale on stainless steel tubes could be problematic if service units were drained and not subsequently rinsed with fresh water. Under such conditions, chlorides trapped in the moist deposits may promote pitting of some (lower) grades of stainless steel. In such cases, galvanic protection from, say, carbon steel would not be available during outages (with the system drained). In this regard, however, the 600 series superaustenitic alloy (N08367) and the superduplex alloy (S37250) are expected to exhibit greater resistance to localized corrosion than either of the 300-series stainless steels in the present study.

SUMMARY

- S30400 tubes incurred varying degrees of crevice corrosion.
- S30400 plates incurred both localized edge attack and crevice corrosion at tube support plate hole sites.
- The above combinations clearly demonstrated that with appropriate conditions rapid and extensive crevice corrosion can occur.
- N08367 tubes in carbon steel and in stainless steel support plates were resistant to corrosion. Corrosion of carbon steel plates could be greater in heat exchangers where turbulence could remove or minimize the build up of corrosion products.
- S31603 support plates incurred extensive corrosion on exposed edges. Under normal circumstances, support plates would be seal-welded to the shell and, therefore, these surfaces would not be exposed.
- The duplex stainless alloy S37250 plate, coupled with N08367 tubes, was fully resistant to corrosion.
- The development of calcareous deposits on cathodic surfaces could be problematic in some plant scenarios.

CONCLUSIONS

Crevice corrosion is an important factor that should be considered in the materials selection process. This not only applies to a seawater environment, but also to fresh water installations which could be contaminated with seawater or brackish waters.

As demonstrated by the research/testing program described, many factors can influence the localized corrosion resistance of stainless steels, and these must be considered when evaluating the performance of candidate alloys. These include, for example, the severity of the crevices present and the actual environmental conditions.

Corrosion testing in natural seawater has identified differences in the behavior of different classes of stainless type materials and among alloys within these classes. In the present series of tests, the newer superaustenitic and superduplex alloys out-performed conventional 300 series stainless steels. Although two superduplex alloys (UNS S32760 and S39274) were fully resistant under the conditions identified, this resistance may be challenged by the presence of more severe crevices such as those which may have influenced the superaustenitic alloys, N08925 and N08926.

New materials are available which can be utilized in construction to mitigate corrosion problems that have received relatively little attention in industry.

REFERENCES

- [1] Oldfield, J. W. and Sutton, W. H., "Crevice Corrosion of Stainless Steels. I. A Mathematical Model", British Corrosion Journal, Vol.13, No 1, January 1978, p.13.
- [2] 1995 Annual Book of ASTM Standards, Vol. 03.02 Wear and Erosion; Metal Corrosion. Section 3 Metal Test Methods and Analytical Procedures, American Society for Testing and Materials, West Conshohocken, PA, 1995.
- [3] Tipton, D. G. "Effects of Mechanical Cleaning on Seawater Corrosion of Candidate Heat Exchange Materials - Part I", 7th Ocean Energy Conference, Argonne National Laboratories ANL/OTEC-BCM-013, Washington, DC, 1980.
- [4] Klein, P. A., Ferrara, R. J., and Kain, R. M. "Crevice Corrosion of Nickel-Chromium-Molybdenum Alloys in Natural and Chlorinated Seawater", NACE CORROSION/89, paper no. 112, NACE International, Inc., Houston, TX, 1989.
- [5] Guidelines for Selection of Nickel Stainless Steel for Marine Environments, Natural Waters and Brine, Reference Book Series, Vol. 2, Nickel Development Institute, Toronto, Canada, 1987, p. 17.

- [6] Zhang, H. S. and Dexter, S.C., "Effect of Marine Biofilms on Crevice Corrosion of Stainless Alloys", NACE CORROSION/92, paper no. 400, NACE International, Inc., Houston, TX, 1992.
- [7] Kain, R. M., "Effects of Surface Finish on the Crevice Corrosion Resistance of Stainless Steel in Seawater and Related Environments", NACE CORROSION/91, paper no. 508, NACE International, Inc., Houston, TX, 1991.
- [8] Kain, R. M., "Crevice Corrosion Resistance of Austenitic Stainless Steel in Ambient and Elevated Temperature Seawater", NACE CORROSION/79, paper no. 230, NACE International, Inc., Houston, TX, 1979.
- [9] Oldfield, J. W., Kain, R. M., and Lee, T. S., Proceedings of Stainless Steel '84 Symposium, Goteberg, Sweden, 1984.
- [10] Kain, R. M., Proceedings of the 12th International Corrosion Congress, Vol. 3A, NACE International, Inc., Houston, TX, 1993, p. 347.
- [11] Kirk, W. W. and Pikul, S. J., "Seawater Corrosivity Around the World: Results from Three Years of Testing" ASTM STP 1086 Corrosion in Material Waters, American Society for Testing and Materials, West Conshohocken, PA, 1990, p. 2.

J. Peter Ault¹ and George A. Gehring, Jr.¹

STATISTICAL ANALYSIS OF PITTING CORROSION IN CONDENSER TUBES

REFERENCE: Ault, J. Peter, and Gehring, George A., Jr., "Statistical Analysis of Pitting Corrosion in Condenser Tubes," *Corrosion Testing in Natural Waters: Second Volume*, ASTM STP 1300, Robert M. Kain, Walter T. Young, Eds., American Society for Testing and Materials, 1997.

ABSTRACT: Condenser tube failure via wall penetration allows cooling water to contaminate the working fluid (steam). Contamination, especially from brackish or saltwater, will lower steam quality and thus lower overall plant efficiency. Because of the importance of minimizing leakages, power plant engineers are primarily concerned with the maximum localized corrosion in a unit rather than average corrosion values or rates. Extreme value analysis is a useful tool for evaluating the condition of condenser tubing. Extreme value statistical techniques allow the prediction of the most probable deepest pit in a given surface area based upon data acquired from a smaller surface area. Data is gathered from a physical examination of actual tubes (either in-service or from a sidestream unit) rather than small sample coupons. Three distinct applications of extreme value statistics to condenser tube evaluation are presented in this paper: (1) condition assessment of an operating condenser, (2) design data for material selection, and (3) research tool for assessing impact of various factors on condenser tube corrosion.

The projections for operating units based on extreme value analysis are shown to be more useful than those made on the basis of other techniques such as eddy current or electrochemical measurements. Extreme value analysis would benefit from advances in two key areas: (1) development of an accurate and economical method for the measurement of maximum pit depths of condenser tubes in-situ would enhance the application of extreme value statistical analysis to the assessment of condenser tubing corrosion pitting and (2) development of methodologies to predict pit depth-time relationship in addition to pit depth-area relationship would be useful for modeling purposes.

KEYWORDS: pitting corrosion, statistics of extremes, condition assessment

¹ Ocean City Research Corporation, Ocean City, New Jersey 08226.

BACKGROUND

Consideration of corrosion performance is often the key to proper selection of tube alloy for steam surface condensers, particularly for those cooled by seawater and brackish water. Contamination of the working fluid will lower the steam quality, thus decreasing overall power generation efficiency.

One or more types of corrosion can cause condenser tube failures in seawater service. These corrosion types include turbulence/velocity-stimulated corrosion at inlet ends or at partial tube blockages, galvanic-induced corrosion caused by a mismatch between tube and tubesheet/waterbox alloys, and selective corrosion attack caused by microstructural differences resulting from improper welding or fabrication techniques. An accurate knowledge of operating conditions, condenser configuration, and metallurgical factors enables reasonable assessment of the probability for these types of corrosion and for resulting failures. Such failures can then be avoided by corrective design changes.

Another type of corrosion that must be considered is pitting-type corrosion. Pitting-type corrosion frequently causes condenser tube failures. Prediction of a particular alloy's propensity for pitting corrosion can involve some special problems. Experience has taught that certain stainless steel alloys, such as 316 and 304, have a particular susceptibility to pitting corrosion. Laboratory testing of new alloys is often used to determine pitting susceptibility. Electrochemical measurement techniques have demonstrated their value in this application. Sometimes, however, pitting corrosion becomes a problem in real-life service conditions even when laboratory studies indicate pitting immunity. An alloy may suffer pitting failures in what seems to be the same environment in which it previously performed satisfactorily.

Frequently, pitting seems random both in distribution and depth. Rather subtle environmental changes may stimulate rapid pitting of some alloys. As-produced surface films, surface contamination, and heat treatment can all influence corrosion pitting. These factors increase the difficulty of assessing corrosion pitting propensity and of selecting an appropriate tube alloy. An erroneous assessment can lead, in its extremes, to either expensive premature condenser retubing or the selection of an unnecessarily expensive alloy.

This paper discusses the use of a statistical technique known as extreme value analysis for assessing pitting corrosion in condenser tubing. The technique is broadly applicable to condition assessment, design problems, and applied research. Extreme value analysis is discussed in detail and examples of its practical application are discussed.

ANALYSIS USING STATISTICS OF EXTREMES

The normal probability relationship and its familiar bell-shaped curve represent a totality of data—all of the scores on a test, average soil resistivities, or all pit depths form the basis for the curve. Extreme value probability theory requires consideration of an extreme group of data—the highest (or lowest) score of each group of students, the lowest measured soil resistivity in each area, or the maximum pit depth of each unit area

of exposed material [1]. The cumulative probability function, $\Phi(Y)$, for an exponential extreme value distribution of a standard variate Y is

$$\Phi(Y) = \exp(-\exp(-Y)). \quad (1)$$

Application of the equation to practical situations requires statistically valid collection of data. A practical and consistent sample size must be selected and enough samples must be taken to attain reliable results. For the present analysis, the deepest pit in each sample area is measured as accurately as possible. These maximum pit depths (X_i) form the data base. The desired probability plot is obtained by finding a plotting position (X_i, P_i) for each pit. Each pit depth (X_i) is associated with a probability coordinate, $P_i = i/(n+1)$; where i is the rank of the pit depth, counting from the smallest, and n is the total number of maximum pit depths. These data are graphed using a uniform scale along the vertical axis for the observed pit depths and an extreme value probability scale along the horizontal axis. The best fit straight line determined by regression analysis will be of the form:

$$X_i = u + A(-\ln(-\ln(P_i))) \quad (2)$$

where,

u = mode, the most probable value for X , and

A = constant.

In a given system, examination of a larger percentage of the system will reveal greater maximum pit depths. However, pit depths systematically measured on less than the entire system can predict the maximum pit depth that exists on the entire system. As an example, assume the total inspected surface area is divided into 100 equal statistical subareas, each representing 1 meter of condenser tube. The maximum pit depth is measured on each subarea. The parameters of equation (2) are found as described above. Now assume that there are 100 000 meters of tube in the condenser, 1 000 times the inspected surface area. One hundred thousand statistical subareas comprise the total structure surface. We define return period as the number of observations required to find an observation equal to or exceeding a given value. Mathematically, the return period is equal to the reciprocal of the probability.

The above-described structure has a return of 100 000 (number of statistical subareas) corresponding to an assumed probability (P) of 0.99999. To predict the maximum pit depth existing on the entire structure, equation (2) is solved with P equal to 0.99999. If this value exceeds the wall thickness, substituting the wall thickness value for X in equation (2) and solving for cumulative probability will yield the probable number of statistical subareas with wall penetrations. In general, the probable number of statistical subareas with a pit exceeding any depth X can be predicted.

The effect of sample size is, perhaps, one of the least understood factors regarding corrosion pitting. The most important pit in piping systems where leakage is a concern is the deepest pit. This pit causes the first tubing wall penetration and the first leak. Corrosion engineers have known for a long time that the larger the sample, the deeper the deepest pit. They have not, however, generally been able to find a way to deal with this knowledge. Almost all corrosion testing data presented in the literature concerns average corrosion rates and average pit depths. Sometimes the depth of the deepest pit for a period of time is noted. Often the depth of this deepest pit is used for estimating the maximum pitting rate, even when the equipment to which it will be applied has a surface area orders of magnitude greater than that from which the test data was accumulated. A greater pit depth will be associated with the larger equipment area (versus the test coupon area). Alloy selection based upon such pitting rate estimates from small areas may result in pitting failures far sooner than expected.

The most important pit in a condenser tube is its deepest pit. The most important tube in a condenser is the single tube with the deepest pit of all tubes. It will leak first. The next most important pits are those nearly as deep as the deepest pit. The time between the first tube failure and subsequent failures depends upon the statistical distribution of these pits and the rate at which corrosion continues.

EVALUATION OF CONDENSER TUBE CONDITION

A power plant drawing its cooling water from an estuarial seawater source has 70/30 copper-nickel (CuNi) alloy condenser tubing that lasted about 14 years before corrosion necessitated its replacement. This life was within expectations. Management confidently selected the same alloy for the replacement tubes with no doubts that the new tubes would last as long as the tubes which were replaced. Shortly after installation of the new tubes, some concern developed regarding possible corrosion of the longitudinal tube weld [2].

This concern led to the installation of a test facility for evaluation of longitudinal tube weld corrosion. The test facility comprised an array of tubes installed as a bypass to the operating condensers. The primary components consisted of a 15 cm tube used for weight loss determinations, a 1.4 m tube used for pit depth measurements and a proprietary segmented tube used for electrochemical polarization measurements [3].

The 15 cm tube and the segmented tube were used to determine the average corrosion rates during the test period. The 15 cm length was weighed prior to and at the conclusion of the test. The difference between the two weights gave the total weight loss caused by corrosion. This weight loss was then used as a basis for calculating what the total wall thickness loss would have been if the corrosion was distributed evenly over the internal surface of the tube.

The segmented tube was used for the real-time determination of corrosion rates based on the measurement of the value of polarization resistance of the middle tube segment. This technique has been widely discussed in the literature [4,5,6]. The unique value of the segmented tube lies in the fact that the polarization resistance is measured on a tube segment that is subjected to the identical flow conditions as experienced by a tube in actual service. Since the segment is cut from a tube of the same lot as used in the

condenser, its metallurgical properties and surface films are also identical to those of the actual condenser tubes. This overcomes some major errors that can be introduced by the use of corrosion probes. Such probes see neither the same flow conditions as the condenser tubes nor do they necessarily have the same metallurgical and surface film characteristics as the condenser tubes. Water velocity varied from zero to full flow depending on operating conditions. Condenser cooling water passed through the unit for most of the one-year operating period.

The periodic electrochemical polarization measurements were made with flow at its design value. The corrosion rates calculated from the polarization resistance values were always within the lower range expected of the 70/30 CuNi alloy in unpolluted seawater. The total corrosion loss over the entire test period was calculated by integrating the corrosion rate with time. The calculated value agreed closely with the corrosion rate determined from the weight loss measurements. No major changes in corrosion rates were detected from measurements on the segmented tube during the course of the test. The corrosion rates decreased with time over the early part of the test, then became relatively stable.

Physical inspection of tube sections removed periodically throughout the test period showed no unusual corrosion. Microscopic examination showed no significant selective corrosion at, or adjacent to, the longitudinal weld.

A total of about 9.45 m (31 ft) of tubing was inspected for pitting at the conclusion of the test period. This tubing had been in the bypass unit for the entire test duration. Superficial data analysis would have indicated no alarming conditions. If it had been assumed the tubes of the operating condenser would have the same maximum pitting rate as that seen on the inspected test sections, there would have been no reason to expect early corrosion failures.

Five 1.4 m long tube sections were examined for pitting. The deepest pit in each section was identified and its depth measured microscopically. The pit depth values, multiplied by a constant, gave a projected value of depth after one year's exposure to design water flow velocity. Figure 1 shows these data plotted on extreme value probability coordinates.

Considering a condenser with a total of 1 371.6 m (4 500 ft) of tubing, the line of most probable extremes determined by regression analysis determines the depth of the most probable deepest pit as 411 μm (16.2 mils). The two-thirds probability band shows that, with two chances out of three, the depth of the most probable deepest pit falls between 358 and 465 μm (14.1 and 18.3 mils). If pitting continued at a constant rate, with a tube wall thickness of 1.3 mm (0.05 in), the first tube failure would occur in about 3 years. If the total length of tubing in the condenser was 13 716 m (45 000 feet), the most probable maximum pitting rate would be 523 μm (20.59 mils) per year, giving a time to the most probable first failure of 2 years.

The data upon which the projections were based was extremely limited. Even so, this method of data analysis indicated the possibility of a severe problem. After less than three years' service, eddy current inspection indicated pitting of the condenser tubes. Nearly 0.5 percent of the tubes in one unit showed pitting in excess of 40 percent of wall thickness. The second unit showed pit depths in excess of 80 percent of the wall for 0.8 percent of the tubes inspected. Tubes in one unit showed pitting in excess of 40 percent

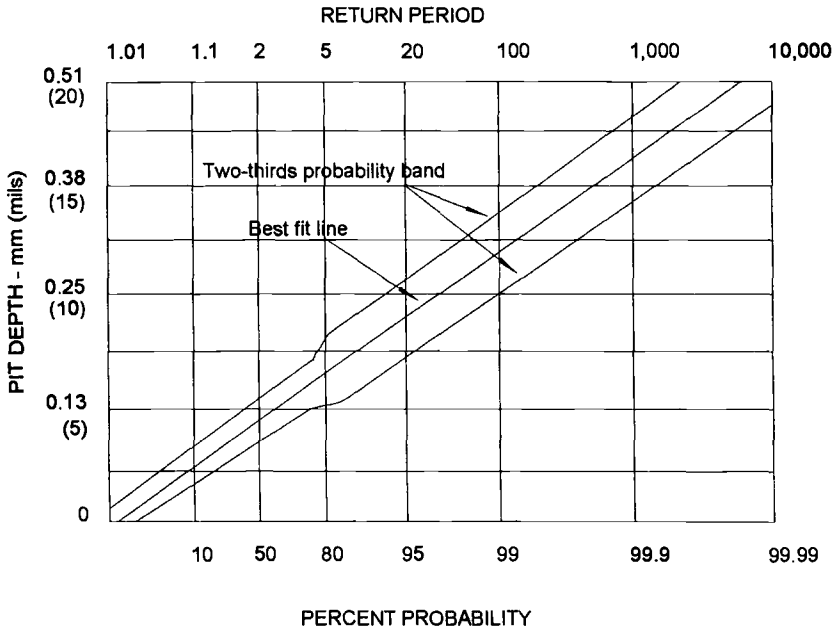


FIG 1--Extreme value distribution of pit depths.

of wall thickness. Tubes in one unit leaked about nine months after the inspection. By the end of the fourth year of service 12 tubes had leaked.

One weakness of the extreme value analysis presented is the limited data upon which it was based. Removal of tubes from a condenser is difficult and expensive. Microscopic determination of the depth of the maximum pit in each statistical unit is time consuming. The usefulness of extreme value statistical analysis would be enhanced if maximum pit depth data could be obtained economically and accurately from a higher percentage of the condenser tubes. Nondestructive eddy current measurements are widely used to assess corrosion damage in condenser tubes. Figure 2 shows a comparison of pit depths, as physically measured, to pit depths as determined by eddy current measurements.

The lack of agreement between the data from the two sources is disappointing. It suggests that eddy current measurements do not form a useful basis for extreme value probability analysis. Perhaps eddy current measurement accuracy could, without excessive cost, be increased to a level of usefulness for extreme value analysis. If so, the electric power industry would have an even more economical method for applying the powerful tool of extreme value statistical analysis to the evaluation of condenser tube corrosion.

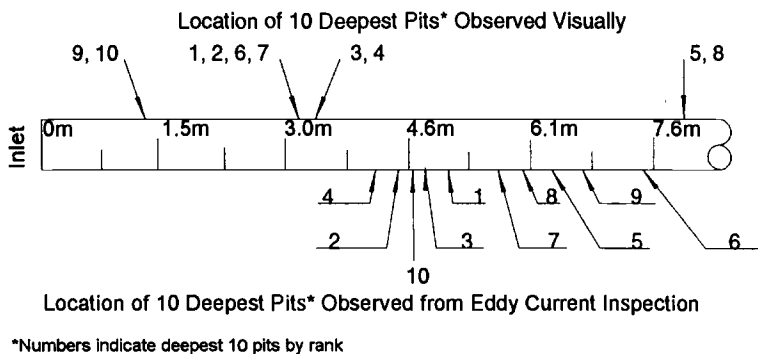


FIG 2--Pit depths, eddy current vs. physical measurement.

MATERIAL SELECTION DATA FOR RETUBING AN OPERATING CONDENSER

A condenser at an east coast power station originally consisted of approximately 22 000, 22 mm (0.88 in) diameter, 21.3 (70 ft) long tubes. All tubes were 90/10 CuNi except for the air removal section which were 70/30 CuNi. Tube wall thickness was 0.81 mm (0.032 in). The nominal cooling water velocity was 2.4 m per second (8 fps). Two induced-draft cooling towers provided cooling in an open recirculating system using brackish make-up water. The recirculating water conductivity was limited to 55 000 micromhos/cm (18 ohm-cm) [7].

Within several months after start-up, a number of condenser tube failures occurred. Over the next two years, approximately 5 percent of the 21 000 90/10 CuNi tubes in the condenser suffered full-wall penetrations due to pitting corrosion.

To eliminate future failures, it was necessary to identify the causes of the premature failure. A condenser test unit with the following attributes was constructed and operated under various conditions:

- cooling water conditions including heat transfer, flow velocity, tube cleaning, and water chemistry were maintained similarly to those in the full-scale condenser;
- data was obtained from sufficiently long lengths of tube to meaningfully characterize pitting behavior;
- alternative tube materials were exposed under identical conditions;
- on-line, real-time corrosion rates and heat transfer information were obtained;

- the effectiveness of alternative water treatments, plant operating parameters, and microbiologically-induced corrosion were evaluated.

The test unit was constructed on a site adjacent to the plant intake pump house along a discharge canal. Water to the unit was fed from the canal. The unit included:

- evaporators for concentrating the water to achieve a resistivity level similar to the actual operating environment,
- water heaters and heat exchangers to achieve heat transfer conditions similar to those in the condenser,
- chemical holding tanks and metering pumps to achieve desired water chemistries,
- instrumentation for measuring and recording pertinent operating data.

An array of flow loops permitted nine separate tests to be conducted simultaneously.

Over the year-long period the test unit was operated, tests were carried out in three separate 3-month phases. The test program included a number of experimental variables, some of which were dictated by early test results. Experimental variables included the following:

- temperature (ambient, 49° C, 60° C)
- water resistivity (18, 35 Ω -cm)
- velocity (2.4, 3.7 m/s)
- corrosion inhibitor treatment
 - tolyltriazole (TTA)
 - ferrous sulfate (FeSO_4)
 - TTA + zinc
 - proprietary inhibitor
- anti-fouling treatment
- dispersant treatment
- alternative tube materials
- periodic cleaning

Figure 3 shows all pitting data for 90/10 CuNi tubes plotted as a function of extreme value probability. The plotted pit depths are actual data corrected to a 1-year exposure time assuming the pitting rate to be constant with time. Eight data points associated with the eight deepest pit values deviate widely from the trend defined by the remaining points and obviously skew the line of expected extremes so that many points fall outside of the two-thirds confidence band. All of the eight deepest pit values were of pits in tubes with TTA inhibitor treatment.

Figure 4 shows the extreme value probability plot of pit depths from all 90/10 CuNi tubes except those that received TTA treatment. The dramatic difference between the plots of figure 3 and figure 4 is evident.

Figure 5 shows the extreme value probability plot of pit depths from only those 90/10 CuNi tubes receiving the TTA treatment. The dissimilarity of this plot to that shown in figure 4 is evident.

The above results were unsuspected in that they showed the TTA treatment increased significantly the pitting propensity of the 90/10 CuNi tubes. Unfortunately, this treatment is the one used in the failed condenser for the majority of its life. There seems little question that this treatment increased the pitting rate which led to the premature failure of an excessive number of tubes in this condenser. No experimental variable had as significant an effect on projected service life as the TTA treatment.

Figure 6 shows corrosion rates determined from maximum pit depth measurements versus corrosion rates calculated from polarization resistance measurements. The maximum pit depths and polarization resistance data were obtained from the same tubes. The corrosion rates determined from pit depth measurements vary an order of magnitude from the corrosion rate calculations based on polarization resistance measurements. More importantly, there is no obvious trend line that relates the two sets of data. These data suggest that where pitting is the dominant form of corrosion (typical in steam surface condenser tubes), general corrosion rates determined by polarization resistance measurements or weight loss will be of little value.

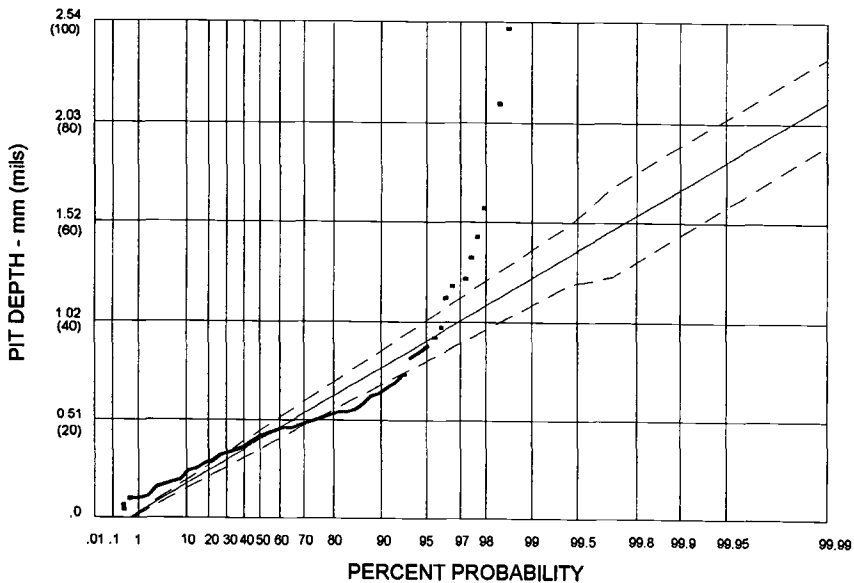


FIG 3-- Maximum pit depth vs. extreme value probability for all 90/10 CuNi tubes.

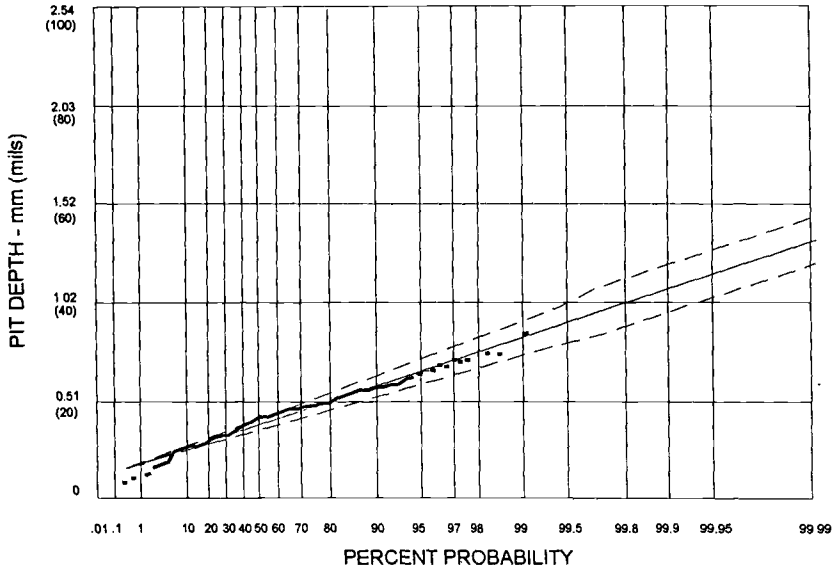


FIG 4--Maximum pit depth vs. extreme value probability for all 90/10 CuNi tubes excluding those exposed to TTA-treated water.

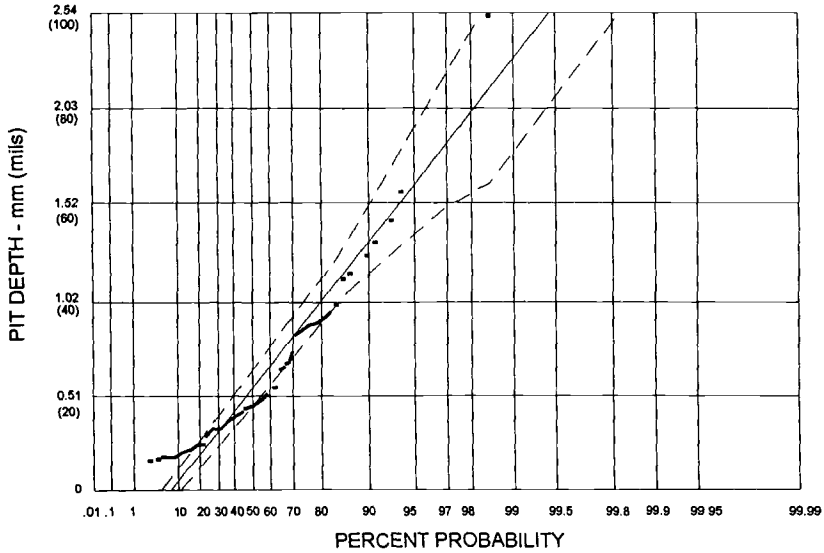


FIG 5--Maximum pit depth vs. extreme value probability for 90/10 CuNi tubes exposed to TTA-treated water.

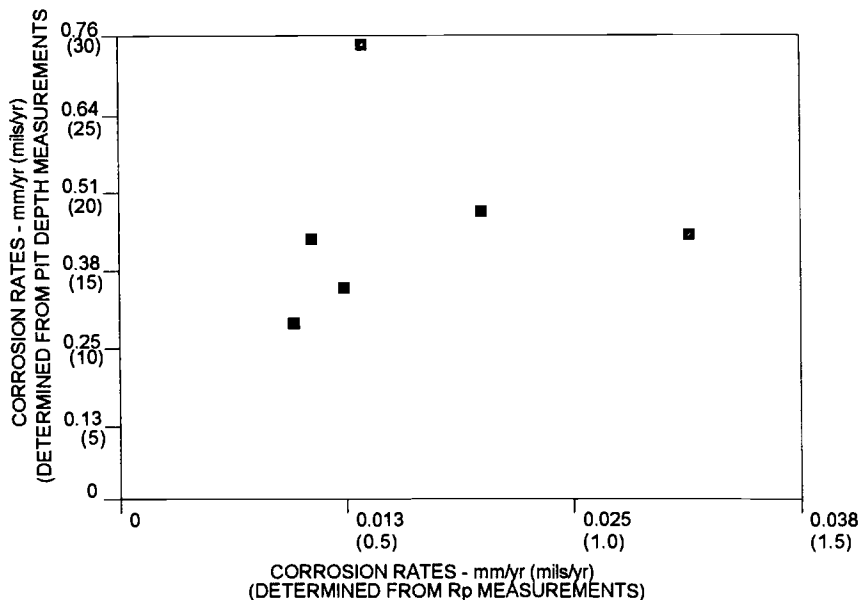


FIG 6--Comparison of corrosion rates by different methods.

LABORATORY EVALUATION OF CONDENSER OPERATING CONDITIONS

Extreme value analysis of pit depths has been used extensively by the authors to gather experimental data for the evaluation of the effects of various parameters on the corrosion of condenser tubes. In the second example from this paper, multiple variables were evaluated in order to determine the conditions that caused premature failure. Key aspects of experimental design to make the results meaningful include:

- use realistic test section geometry (use actual condenser tubes)
- use natural cooling water
- divide test sections into an appropriate number of statistical areas (large enough to be representative, small enough to be easily evaluated)
- to accurately identify and measure the deepest pit in each statistical area.

The Electric Power Research Institute (EPRI) has sponsored laboratory studies where extreme value analysis was central to data evaluation. Two of these studies evaluated the effect of intermittent, high dosage chlorine on the corrosion of stainless steel and copper-nickel condenser tubes [8,9]. The studies showed that specific high dosages of chlorine should not adversely affect the performance of the materials tested.

Another study evaluated the effects of sand, sulfide, temperature, and cathodic protection on corrosion of condenser tubing [10]. The study showed:

- The presence of sulfide accelerates dealloying and galvanic attack of copper alloy tube sheets.
- Sulfide decreases the effectiveness and increases cathodic protection current requirements in the condenser waterbox.
- Depending on specific conditions, suspended sand can increase the corrosion of condenser tubes. However, the effects are less than those of sulfides.
- Cathodic protection as usually applied in a condenser water box provides adequate protection to tubesheets and provides limited protection to the ends of the tubes.
- Increasing water temperature can either increase or decrease corrosion rate depending on the specific conditions (alloy, presence of sulfide, etc.).

CONCLUSIONS

1. A method of statistical analysis has been presented that is useful for projecting data gathered on a few representative condenser tubes to larger, operating condensers. For the method to be successful, data must be gathered in a systematic manner. This means dividing the sample into meaningful statistical subareas and accurately determining the single deepest pit in each subarea.
2. The authors have found microscopic examination of representative tubes to be the only accurate way to gather useful data for analysis. Eddy current data proved inadequate for the analysis technique. As figure 2 demonstrates, eddy current does not necessarily identify the locations of deepest pits for analysis. The development of an accurate, in-situ measurement technique would enhance the usefulness of the extreme value analysis technique.
3. Development of a pit depth-time relationship that complements the pit depth-area relationship presented would be useful for modeling purposes.

REFERENCES

- [1] Gumbel, E.J., *Statistics of Extremes*, Columbia University Press, 1968.
- [2] Gehring, G.A., Jr., Meany, J.J., Jr., Buffa, J.A., "Prediction and Assessment of Condenser Tube Pitting Corrosion," ASME/IEEE Power Generation Conference, Milwaukee, WI, Oct. 20-24, 1985.
- [3] Meany, J.J., U.S. Patent No. 5,504,324; a method and apparatus for the real-time determination of corrosion rates on the internal surfaces of condenser tubing.

- [4] Stern, M. and Geary, A.L., "Electrochemical Polarization - Part 1, A Theoretical Analysis of the Shape of Polarization Curves," *J. Electrochemical Society*, Vol. 104, 1957.
- [5] Mansfeld, F., "Electrochemical Background of the Polarization Resistance Technique," *CORROSION '73*, National Association of Corrosion Engineers 1973.
- [6] Jones, D.A., "The Advantages of Galvanostatic Polarization Resistance Measurements," *Corrosion*, Vol. 39, No. 11, 1983, p.444.
- [7] Gehring, G.A., Jr., Pond, R., Cramblitt, K.L., and Shulder, S.J., "Accelerated Failure of Copper-Nickel Condenser Tubing," EPRI Condenser Technology Conference, 1990.
- [8] Gehring, G.A., Jr., Mussalli, Y., Syrett, B. and Chow, W., "Effects of Targeted Chlorination on Corrosion of AL-6X Stainless Steel Tubes in Seawater," paper presented at ASME/IEEE Power Generation Conference, Oct. 4-8, 1987.
- [9] "Effect of Targeted Chlorination on the Corrosion Behavior of Copper-Nickel Condenser Tubing," EPRI Project 2300-17, Final Report, October, 1992.
- [10] "Effects of Sulfide, Sand, Temperature, and Cathodic Protection on Corrosion of Condensers," EPRI Project 1689-3, Interim Report, May, 1986.

Robert M. Kain,¹ Wayne L. Adamson,² and Brian Weber³

CORROSION COUPON TESTING IN NATURAL WATERS: A CASE HISTORY DEALING WITH REVERSE OSMOSIS DESALINATION OF SEAWATER

REFERENCE: Kain, R.M., Adamson, W.L., and Weber, B., "Corrosion Coupon Testing in Natural Waters: A Case History Dealing with Reverse Osmosis Desalination of Seawater," *Corrosion Testing in Natural Waters: Second Volume*, ASTM STP 1300, Robert M. Kain and Walter T. Young, Eds., American Society for Testing and Materials, 1997.

ABSTRACT: Corrosion testing in natural waters has generally focused on assessing either resistance of materials to corrosion in a given environment or characterizing environmental corrosivity. Sometimes both can be accomplished simultaneously. For example, while the objective of another test program reported in this symposium was to determine the corrosivity of seawater world-wide, the corrosion resistance of three very diverse materials was also identified. In those tests, relatively large specimens (100 mm x 300 mm) were exposed in accordance with ASTM G52: Standard Practice for Exposing and Evaluating Metals and Alloys in Surface Seawater.

This paper describes a series of corrosion tests performed to determine the general and localized corrosion behavior of two stainless alloys (UNS S31603 and UNS NO8367) and 70/30 CuNi (UNS C71500) in three aqueous environments associated with advanced reverse osmosis (RO) desalination of natural seawater. In addition to seawater (the RO feed stock), the other environments included a 2nd-pass RO brine with lower chloride content and total dissolved solids than raw seawater, and an ultrapure 3rd-pass permeate.

Two ASTM standards were reviewed for guidance in the design of the experiment. Since testing could be conducted in an operating prototype RO system, the test program followed the general procedures for an in-plant corrosion tests described by ASTM G4-95: Standard Guide for Conducting Corrosion Coupon Tests in Field Applications. This standard, along with G78-95: Standard Guide for Crevice Corrosion Testing of Iron-Base and Nickel-Base Alloys in Seawater and Other Chloride-Containing Environments, provided guidance in the selection of test specimens and mounting fixtures as well as crevice formers utilized. The G78-95 standard guide also provided considerations associated with the interpretation of the crevice corrosion test results.

Keywords: general corrosion, localized corrosion, seawater, brine, ultra pure water, stainless steels, 70/30 CuNi, crevice geometry, in-plant testing, sheet material, tube material.

¹Senior Corrosion Scientist, LaQue Center for Corrosion Technology, Inc., Wrightsville Beach, NC 28480; ²Consultant, Annapolis, MD 21403; ³Supervisory, Mechanical Engineer, Naval Surface Warfare Center, Annapolis, MD 21402

INTRODUCTION

Reverse osmosis (RO) desalination technology has become established over a number of years for producing potable water from various natural waters, including seawater. While some RO systems utilize non-metallic construction materials for the pressure vessels to contain the membrane cartridges, metallic materials are desired where higher pressures and/or enhanced fire resistance are required. Already there is extensive use of stainless alloy piping in high volume RO plants in the Middle Eastern countries, and in Malta which rely heavily on this technology [1,2].

In the past 10 years, RO desalination has been used as an alternative technology to traditional distillation plants aboard ships for producing potable water [3]. More recently the emphasis has shifted to the development of multi-pass RO water systems that are capable of providing both potable water for general use and ultrapure water for boilers, electronic cooling, turbine washdowns and other special shipboard needs.

Corrosion resistance is essential to the operation of RO systems constructed of metallic materials. This is because localized corrosion cannot be tolerated at the critical pressure seals which separate feedwater, brine, and the product water (permeate). Secondly, there is little tolerance for the generation of corrosion products which can affect RO membrane performance.

A U. S. Navy sponsored corrosion test program was undertaken to help establish materials selection criteria for pressure vessels. This investigation examined the general and localized corrosion resistance of two stainless alloys, and a copper-nickel alloy. Because of the extensive use of copper-nickel in shipboard piping, the potential corrosivity of RO ultrapure water on these systems was also considered important [4].

Since an operating prototype RO unit was available, the present investigation essentially became an in-plant corrosion test. It was performed in accord with ASTM G4-95: "Standard Guide for Conducting Corrosion Coupon Tests in Field Application" [5].

Because crevice corrosion of the stainless steels was of particular concern, ASTM G78 "Standard Guide for Crevice Corrosion Testing of Iron-Base and Nickel-Base Stainless Alloys in Seawater and Other Chloride-Containing Waters" was reviewed when developing the test matrix [5].

This paper focuses mainly on the experimental design of the tests in relation to the above-mentioned ASTM standards. Test results generated by exposure of the materials to filtered seawater (RO feed stock), an intermediate-pass brine by-product, and ultrapure product water are also presented and discussed. Additional discussion of these results has been presented elsewhere [6]. Results from these tests may be applicable to users of RO systems not only on ships, but also for offshore platforms, and other applications for desalting seawater or other waters.

EXPERIMENTAL

General Consideration

ASTM G4-95 covers in-plant corrosion testing of metals and alloys without regard to alloy type, family or class. It does, however, caution the user that, in some cases, corrosion products from other plant equipment could affect the corrosion resistance of corrosion coupons being tested. Similarly, the placement of certain dissimilar metal coupons in close proximity to each other could influence their behavior.

ASTM G78-95 is specifically for crevice corrosion testing of iron-base and nickel-base type alloys. If susceptible, these materials exhibit attack within the crevice area. In contrast, some other “non-stainless-type” alloys, such as copper-nickels, often tend to suffer localized corrosion just outside the crevice rather than within it. Despite this distinction, traditional crevice corrosion tests are routinely performed on Cu-Ni alloys and Ni-Cu alloys [7].

Both ASTM G4 and G78 provide guidance in the design of test specimens, selection of crevice formers and ancillary hardware utilized for fasteners, and test racks. These aspects of testing are described below.

Test Materials

Selection--70/30 CuNi (UNS C71500), Type 316L stainless steel (UNS S31603), and a 6% Mo “super austenitic” stainless steel (UNS N08367) were tested. Alloy N08367 is one of a number of commercially available “20Cr-6Mo alloys” that contain nitrogen to prevent the formation of sigma phase and to enhance localized corrosion resistance. Although alloy N08367 has exhibited crevice corrosion in some previous seawater tests [8], its resistance in other tests [9] justified its selection for the present investigation.

Because of its susceptibility to crevice corrosion in seawater, S31603 was selected as the control material.

Product Form--Although most in-plant corrosion tests and crevice corrosion tests, in general, involve exposure of test coupons prepared from flat sheet or plate materials, testing cylindrical shapes (rod, bar, and tubular) is also covered by the above ASTM standards. Fabrication of metallic RO pressure vessels would involve both tubular materials (shells) and plate materials (end caps). Accordingly, both product forms were included in the present investigation. Table 1 gives the chemical composition of the alloy sheet and tube products tested.

Specific Design--With respect to flat specimens, ASTM G4 describes the advantages and disadvantages of preparing square or rectangular specimens versus circular shapes. The selection of one form over another may be dictated by the amount of test material available and/or the facilities for machining. Neither of these were constraints in

the present test program. However, the size of the specimens was dictated by the ID of the fiber reinforced plastic (FRP) RO pressure vessels utilized for these in-plant corrosion tests. For the two stainless alloys, 76 x 76 x 3 mm sheet specimens were machined. In the case of the CuNi, 58 mm diameter disc specimens that were already available were utilized.

Tubular specimens for the three alloys were cut from 25.4 mm (1-inch) OD tubing and machined to a final length of 152 mm.

TABLE 1--Chemical composition of materials tested (weight percent)

Alloy/Product Forms	C	Cr	Ni	Mo	N	Cu	Mn	Si	S	P
<u>S31603</u> -Sheet	0.019	16.31	10.14	2.10	0.038	0.24	1.71	0.54	0.010	0.028
-Tube	0.018	16.56	10.21	2.19	0.030	0.34	1.76	0.44	0.016	0.030
<u>N08367</u> -Sheet	0.021	20.52	23.90	6.22	0.20	0.21	0.34	0.44	0.001	0.026
-Tube	0.017	20.39	24.01	6.23	0.23	0.22	0.22	0.36	0.005	0.024
	Cu	Ni	Fe	Mn	Zn	C	P	Pb		
<u>C71500</u> -Sheet	68.68	30.12	0.52	0.40	0.25	0.017	0.003	0.005		
-Tube	68.9	30.1	0.59	0.47	0.14	0.04	0.007	0.02		

Surface Finish--Surface finish can influence the crevice corrosion resistance of stainless steels in seawater and other saline waters [10,11]. Stainless steel sheet specimens were prepared with ground surface finishes at the intended crevice sites. This preparation which entailed circular grinding with wet SiC abrasive papers (50 mm diameter disks), has been used previously in other crevice corrosion programs [10,11], as well as the round robin testing that was used in developing ASTM G78.[5] In practice, pressure vessel end caps would be machined, while the shells are likely to be in the produced mill finish common to pipe material selected. Accordingly, stainless alloy tubes were tested in their respective mill finishes.

Previously reported crevice corrosion test results for S31603 have shown the benefits of electropolishing [10]. Additional ground sheet specimens and as-produced tube specimens of S31603 were electropolished in order to investigate the resistance to RO waters, particularly in the 2nd-pass brine. In the present investigation, the 70/30 CuNi specimens, both sheet coupons and tubes, were tested in their respective as-produced mill finishes.

Replication--Nine specimens were prepared for each of the above alloy/product-form/surface-condition combinations. Thus, triplicate specimens of these were exposed to each of three in-plant RO environments described in detail later.

Cleaning--All coupon and tube specimens were degreased with acetone and then detergent scrubbed with a bristle brush (including the ID's and OD's of the tubes), rinsed with water, rinsed in fresh acetone and dried.

Weighing--The test specimens were weighed on an electronic balance to an accuracy to 0.001 g.

Crevice Formers--Several configurations of nonmetal-to-metal type crevice formers were utilized. In the case of the coupon specimens, Perspex Crevice Assemblies (PCAs) were used [9,10]. These were 30 mm OD x 20 mm ID annular-shaped washers, machined from acrylic plastic sheet. Each washer had six holes which provided test environment access to the ID crevice mouth; the nominal crevice depth was 2.5 mm (one-half the annulus). These crevice formers are depicted in ASTM G78-95 [5]. The PCA contact surfaces were ground flat with 600 grit SiC and subsequently polished with 0.3 μm and 0.05 μm Al_2O_3 slurry, respectively. PCA washers were affixed on both sides of each specimen, using an insulated titanium 1/4-20 fastener, and consistently tightened to an initial torque of 8.5 Nm (75 in-lbs).

The tube specimens were fitted with PVC pipe couplings that had internal rubber compression (gland) fittings. The glands were 19 mm wide. In order to ensure a tight, consistent fit, the glands were slit longitudinally so that the ID would conform more closely to the alloy tube OD. O-rings (Buna-N) were also used as crevice formers. Different size O-rings were used to vary the severity of the resulting crevice. For each of the three tube materials, one specimen of each was fitted with two 23.8 mm ID (15/16-inch) O-rings and another with two 20.6 mm ID (13/16-inch) O-rings; the latter was expected to provide a more severe crevice geometry. The O-rings were each 3.5 mm thick. The third tube specimen in each group was exposed with only the previously described compression fittings.

Several tubes were connected in series with the PVC fitting caps tightened to the same degree --- as determined by the termination of the threads on the male portion of the coupling. The PVC fittings served a dual role -- that of a "test rack". This arrangement prevented contact of the alloy tubing with the RO pressure vessel, thus avoiding the creation of any unwanted or uncontrolled crevice sites. Utilizing the extended ends of the fasteners, the PCA specimens were mounted on PVC test racks, similar in design to that illustrated in ASTM G4-95 [5] for exposure of coupons in pipes in in-plant corrosion tests.

Apparatus--A total of six 100 mm diameter FRP-type RO pressure vessels (without membranes) were used to expose the test specimens. Two vessels in series were designated for each of the three selected environments: filtered seawater control, 2nd-pass brine, and 3rd-pass permeate. The nine coupons with the PCAs were exposed in one vessel, and the nine tube specimens, with the O-rings and compression fittings, in the other. Figures 1 and 2 show completed assemblies being inserted in the test vessels. In the stainless steel tests, the vessel with the tube specimens was upstream of that containing

the coupons. Being fewer in number, all CuNi specimens were exposed in the same test vessel.

The test vessels were placed on wooden test racks constructed on a 10° incline to ensure that all test specimens were fully immersed in the test environment at all times. Figure 3 shows an overall view of the prototype RO equipment utilized. As shown in Figure 4, the vessels containing the control specimens were exposed in a sidestream from multi-media filters. The other vessels were in series with respect to the 2nd-pass brine discharge and 3rd-pass permeate (product waters).

Environmental Conditions

In-plant corrosion testing subjects the materials being tested to the normal environment as well as excursions in environmental conditions. During the course of the two 90-day test runs, seawater, brine and permeate flowed through the corresponding test vessels approximately 10 to 15 percent of the time (~8 hrs/day for 30 of the 90 days). Non-flowing (i.e., nonrefreshed) conditions ranged in duration from overnight to as long as 16 days. When the RO system operated, flow through the vessels containing the seawater test specimens, and the 3rd-pass permeate test specimens was maintained at about 0.02 m/s. Flow-through to the 2nd-pass brine test vessel was <0.01 m/s. For the stainless steel test specimens, the average temperature of the filtered seawater (when flowing) was 12.1°C for the first 30 days and 9.9°C over the total 90-day period. The temperature of the brine and permeate water ranged from about 10° to 30°C. When the RO system was not operating, the non-refreshed environments were nearly at room temperature (22C ± 2°C).

Testing of the CuNi specimens commenced about mid-way through the 90-day test on the stainless steels (i.e., the CuNi specimens were exposed at the downstream locations “vacated” by removal of the PCA test specimens). Flowing conditions for the CuNi were maintained for about 15 percent of the total exposure time, as described above for the stainless steel specimens. When the RO system operated, the filtered seawater mean temperature for the CuNi test was 14.9°C. The 2nd-pass brine and 3rd-pass permeate water temperatures approximated those noted above for the stainless steel exposure. The longest non-refreshed period for the CuNi specimens was also 16 days.

During the conduct of these tests the salinity of the filtered seawater ranged from 33.5 g/L to 36.9 g/L.

Total dissolved solids in the 2nd-pass brine ranged from 0.2 g/L to 3.3 g/L, while conductivity ranged from about 500 to 5000 μSiemens.

The 3rd-pass permeate water typically contained ≤0.2 mg/L Cl⁻. A single, 4-hour excursion resulted in a maximum chloride level of 1.8 mg/L. The conductivity of the permeate was typically about 2 μSiemens or less.

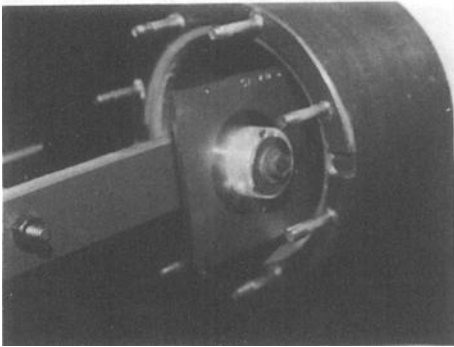


FIG. 1--View of sheet material specimens with PCAs being installed in an empty RO membrane vessel.

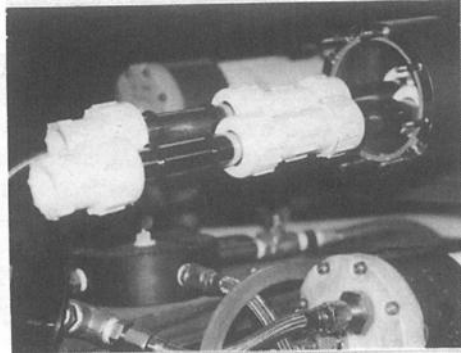


FIG. 2--View of tube specimens with compression fittings and O-ring type crevice formers.

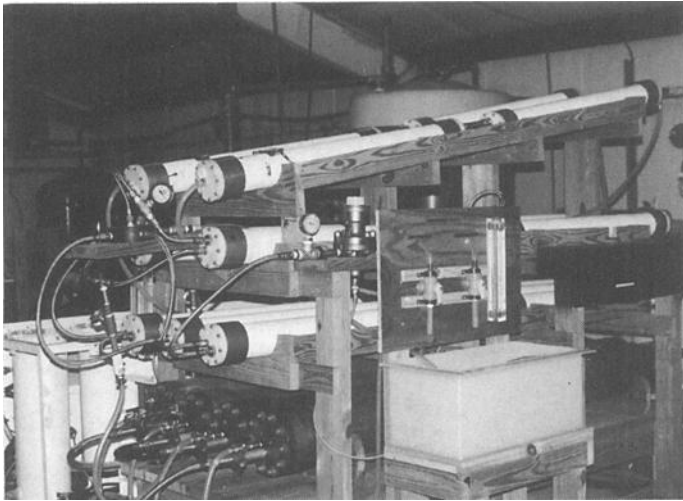


FIG. 3--Overall view of operating RO unit utilized for in-plant corrosion testing of stainless steel and CuNi test specimens.

While the seawater and 3rd-pass permeate tests were conducted at atmospheric pressure, the 2nd-pass brine recycle line (Figure 4) operated at about 3 atmospheres.

RESULTS AND DISCUSSION

Stainless Steel Crevice Corrosion Initiation Resistance

Evaluation Techniques--Since these tests were conducted in FRP-type pressure vessels, there was no opportunity to inspect the specimens in-situ for early signs of crevice corrosion initiation. This is one limitation of in-plant corrosion testing. In contrast, other types of corrosion tests that are conducted, for example, in open tanks and troughs, enable the investigator to observe staining and/or the accumulation of corrosion products at the crevice-former locations. In many cases, it has been demonstrated that these in-situ inspections can reveal very early times to crevice-corrosion initiation for susceptible materials [9-11]. In-plant tests, on the other hand, reveal only that crevice corrosion has or has not occurred, and to what extent, after the specimens are removed, dismantled, and examined. This is an important point because documenting the time to initiation can be extremely valuable when interpreting test results with regard to propagation, particularly if only one test period is involved.

In the present evaluation, the test specimens were examined for any evidence of corrosion at the various crevice sites created on the sheet coupons and tube specimens after exposure and cleaning. Any degree of attack found, regardless of area or depth, represented an affected crevice site.

Material Performance--Times to initiation can be described broadly as less than 30 days and less than 90 days for the sheet coupon and the tube specimen tests, respectively. Table 2 summarizes the incidence of crevice corrosion for the various material/crevice-former combinations tested in the three types of waters. The number of affected sites is shown along with the total number of each type available on the replicate specimens.

In the case of the PCA tests, all three materials were fully resistant in the ultrapure (3rd-pass) permeate, as well as in the 2nd pass brine tests, but incurred attack in seawater within 30 days. As shown in Table 2, all six PCA sites on the ground N08367 specimen and the ground and electropolished S31603 were attacked, whereas half the number on the controls (ground S31603) were affected. In the latter case, one site on each of three specimens was attacked.

As-produced tubes of three materials exposed to the ultrapure water were again found to be fully resistant. While the N08367 and electropolished S31603 tubes were also resistant to crevice corrosion at the rubber gland and O-ring crevice sites in the 2nd-pass brine test, the S31603 controls were found to be susceptible. In this case, the attack was limited to one rubber gland site on each tube. As shown in Table 2, N08367 tubes exposed to seawater exhibited attack at all of the rubber gland sites, but none of the O-

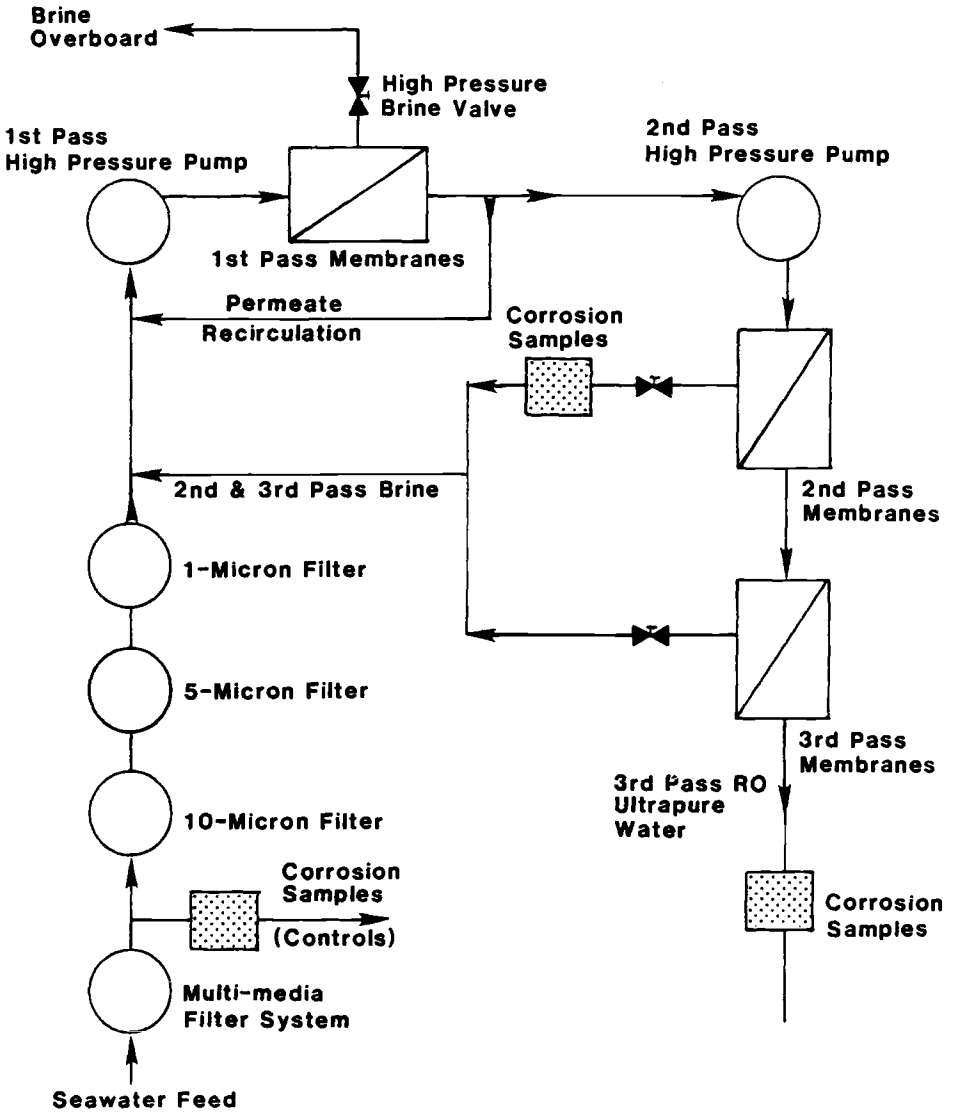


FIG. 4--Schematic of three pass reverse osmosis water treatment system.

ring sites. In contrast, the electropolished S31603 tubes were fully resistant. On the other hand, S31603 tubes exposed to seawater without electropolishing incurred attack at five rubber gland sites and one of the O-ring sites in 90 days. This affected site was associated with one of the two larger ID O-rings. While the small diameter O-rings could have conceivably produced tighter crevices, stretching (to fit over tube) could also have reduced the effective crevice depth. Therefore, it appears that the affected site (under one of the 23.88 mm ID O-rings) had some critical combination of crevice depth and crevice tightness (gap dimension).

TABLE 2--Incidence of crevice corrosion for indicated test
(number of sites attacked/number available)

	Stainless Steel	Stainless Steel	
	<u>Sheet Materials*</u>	<u>Tube Materials</u>	
	30-Day Tests	90-Day Tests	
	PCAs	Glands**	O-Rings
<u>Natural Seawater</u>			
As-Produced S31603	3/6	5/6	1/4
Electropolished S31603	6/6	0/6	0/4
As-Produced N08367	6/6	6/6	0/4
<u>2nd-Pass Brine</u>			
As-Produced S31603	0/6	3/6	0/4
Electropolished S31603	0/6	0/6	0/4
As-Produced N08367	0/6	0/6	0/4
<u>3rd-Pass Permeate</u>			
As-Produced S31603	0/6	0/6	0/4
Electropolished S31603	0/6	0/6	0/4
As-Produced N08367	0/6	0/6	0/4

* 120-grit finish at crevice areas
** Rubber gland compression fitting

Stainless Steel Crevice Corrosion Propagation Resistance

Evaluation Techniques--In certain applications, some degree of crevice corrosion may be tolerated. However, at critical seals in RO equipment this may not be the case. Maximum depth of attack is frequently used as a criterion for evaluating alloy resistance to crevice corrosion propagation. Total damage assessments in laboratory and in-plant investigations may also use other criteria such as mass loss, affected area, penetration range and average depth of attack. In the present investigation, a needlepoint depth gauge, and in some cases a focusing microscope, were used to measure depth of attack. These techniques are accurate to ± 0.01 mm. Visible, but not measurable depths at affected sites were recorded as < 0.01 mm. The deepest measurements taken at 30°

intervals around the annular crevice sites on the PCA specimens and around the circumference of the tube specimen were recorded. In all cases, the maximum depth at any affected site was recorded. For the PCA tests, affected area estimates were also made; in this case, as a percentage of the total contact surface of the 30 mm OD x 20 mm ID crevice former. Affected crevice areas can be readily measured on flat and cylindrical specimens with the aid of a transparent grid divided into 1 mm² segments.

PCA Specimens—Table 3 gives the 30-day crevice corrosion propagation results for PCA specimens exposed to filtered seawater. In terms of affected area, the surface-ground N08367 and S31603 specimens, respectively, exhibited the least and greatest side-to-side variability. The affected area range for the electropolished S31603 was similar to that for the N08367 specimens, but with somewhat greater side-to-side variability. Figure 5 shows a representative view of affected sites on the S31603 and N08367 PCA fitted specimens. As shown in Table 3, comparable depths of attack were measured for the two series of S31603 specimens. The overall range of penetration is within the range reported elsewhere for other PCA tests in continuously refreshed seawater [9,10]. While N08367 exhibited crevice corrosion at all six crevice sites, the depth of attack was consistently ≤ 0.01 mm. In a previous PCA test conducted in open tanks, other N08367 specimens from a different heat of sheet material were fully resistant after 60 days' exposure to filtered (5 μ m) seawater at 25°C. However, certain other "20Cr-6Mo" alloys incurred attack and to a greater depth than that shown in Table 3 [9].

TABLE 3—30-day propagation results for stainless steel PCA specimens exposed to filtered seawater*

Material	Surface Preparation	Specimen Number	Percent Crevice Area Attacked		Penetration Range (mm)	
			Side A	Side B	Side A	Side B
S31603	(120 SiC)	1	0	80	0.00	<0.01-0.79
		2	80	0	<0.01-0.57	0.00
		3	0	60	0.00	<0.01-0.76
S31603	(120 SiC + electropolished)	1	10	40	<0.01-0.12	<0.01-0.13
		2	25	20	<0.01-0.38	<0.01-0.34
		3	<10	30	<0.01	<0.01-0.82
N08367	(120 SiC)	1	20	10-20	<0.01-0.01	<0.01
		2	60	40	<0.01-0.01	<0.01
		3	50	50	<0.01	<0.01

* Corresponding specimens exposed to 2nd-pass brine and 3rd-pass permeate were fully resistant.

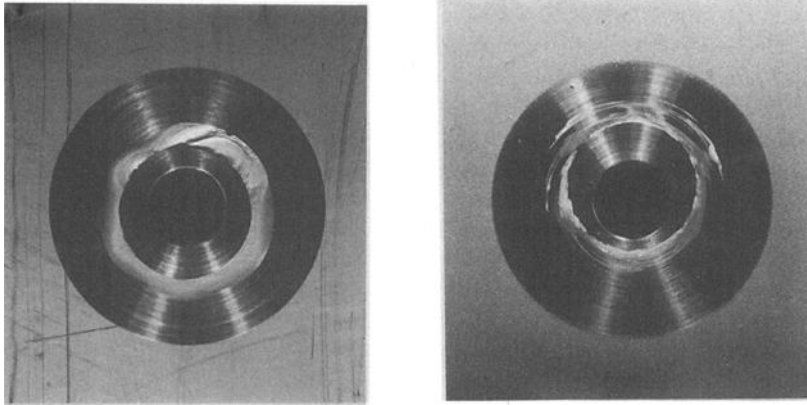


FIG. 5--Typical appearance of S31603 (left) and N08367 (right) PCA test specimens after 30 days exposure to filtered seawater.

Tube Specimens

The photographs in Figure 6 compare the resistance of the as-produced S31603 tubes exposed to the seawater and 2nd-pass environments, respectively. For the latter, attack occurred at fewer rubber gland sites, and the overall affected area was considerably less. Table 4 gives the 90-day crevice corrosion depth of attack results for the above specimens. Specimens exposed to seawater again exhibited a broad range of penetrations, in this case covering from <0.01 to 0.76 mm, 3 orders of magnitude. As can be seen from Table 4, and also in Figure 6 (left), the intensity of attack at the one affected O-ring site was comparable to that at the rubber gland sites and vice-versa. Table 4 shows that the maximum depth of crevice corrosion incurred in the 2nd-pass brine test was less than half that in full strength seawater. The photographs in Figure 7 show the appearance of the electropolished S31603 and the as-produced N08367 tubes from the seawater exposure, respectively. Crevice corrosion incurred by the N08367 was again found to be considerably less than that for the S31603 controls. In the case of N08367 (Figure 7 right), it can be seen that the attack incurred followed a similar pattern at each site. These correspond to raised sections on the ID's of the rubber glands, which create the primary seals for this type of fitting. In all cases, crevice corrosion incurred by the N08367 tubes within 90 days was 0.01 mm or less. This is the same order of penetration incurred in the 30-day PCA tests.

Corrosion Resistance of C71500 to Various RO Waters

Corrosion Characterization--Both the sheet material specimens with PCAs and the tube specimens with rubber glands and O-rings were exposed for 90 days. However, these were removed briefly for a cursory inspection after 45 days. This coincided with the interruption of testing to remove the stainless steel tubes which had already accumulated their 90 days of exposure. Since the crevice formers and specimen surfaces were not

disturbed in any way, this interruption is analogous to draining of an RO system to replace some, but not all, membrane elements.

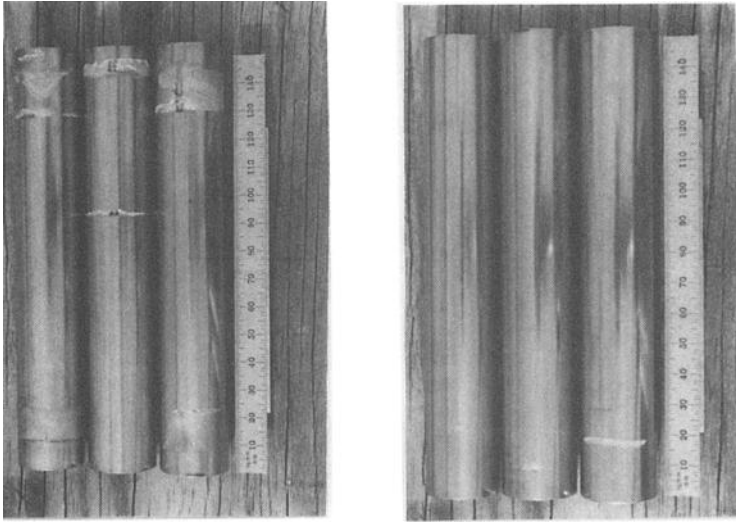


FIG. 6--Appearance of as-produced S31603 tubes after 90 days exposure to multi-media filtered seawater (left) and lower chloride-containing RO 2nd-pass brine.

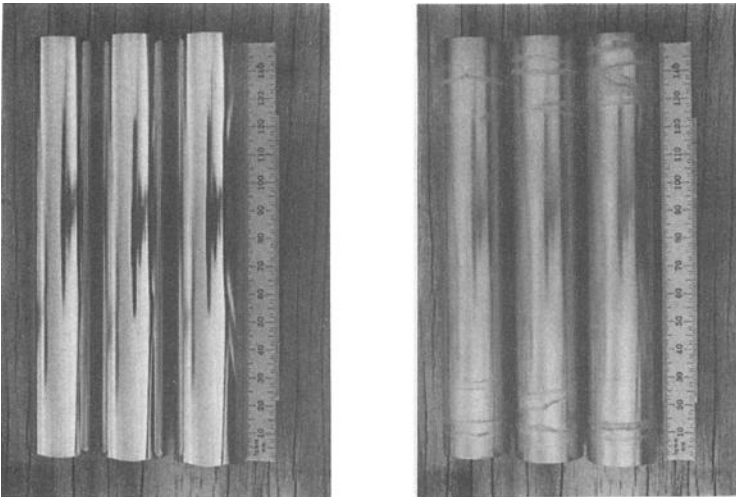


FIG. 7--Appearance of electropolished S31603 (left) and as-produced N08367 (right) tube specimens after 90 days exposure to multi-media filtered seawater.

TABLE 4—90-day results for stainless steel tube specimens

RO-Water Environment/ Alloy Identification	Specimen No.	Depth of Crevice Corrosion Incurred (mm)		
		Rubber Gland	O-Ring Crevice Sites	
		Compression Fitting Crevice Sites	28.8 mm ID	20.6 mm ID
Seawater Control				
As-Produced S31603	1	<0.01 to 1.05	--	--
	2	<0.01 to 0.73	<0.01 to 0.76	--
	3	0.02 to 1.16	--	Resistant
Electropolished S31603	1	Resistant	--	--
	2	Resistant	Resistant	--
	3	Resistant	--	--
As-Produced N08367	1	<0.01	--	--
	2	<0.01	Resistant	--
	3	<0.01	--	--
2nd-Pass Brine				
As-produced S31603	1	0.02	--	--
	2	0.30	Resistant	--
	3	<0.01 to 0.01	--	Resistant
Electropolished S31603	1	Resistant	--	--
	2	Resistant	Resistant	--
	3	Resistant	--	Resistant
As-Produced N08367	1	Resistant	--	--
	2	Resistant	Resistant	--
	3	Resistant	--	Resistant

This 45-day inspection revealed different film forming behavior for the C71500 specimens in each of the three RO media. Specimens exposed to seawater exhibited a typical pale green coloration and little evidence of crevice-related attack. Those exposed to the 2nd-pass brine had developed some reddish copper coloration, while those exposed to the ultrapure permeate exhibited spotty blue-black areas.

Final inspection after 90 days revealed an increase in the thickness of the green film on the seawater specimens, and more area of blue-black staining on those in the ultrapure water tests. Specimens exposed to the 2nd-pass brine exhibited more of the reddish copper coloration and also with accumulations of blue-green corrosion products at areas of localized attack. The latter was most pronounced at the O-ring sites on the tube specimens and adjacent to PCA washers. Energy dispersive X-ray (EDX) analysis of the red film indicated that it was predominately copper. In the case of the 2nd-pass brine test, both sheet and tube specimens exhibited bright, shallow areas of attack at discontinuities in the reddish film, see for example, Figure 8.

The propensity for crevice-related corrosion of 70/30, and other CuNi alloys, differs from that of stainless steels. Crevice corrosion on stainless steels occurs beneath the crevice former, whereas that on CuNi occurs just outside the crevice. The latter has been attributed to the creation of metal-ion concentration cells which produce anodic sites adjacent to the crevice [12].

Figure 9 shows the crevice-related attack incurred by one of the C71500 tube specimens in the 2nd-pass brine test. In contrast to the above, crevice-related attack on specimens in the seawater portion of the test was minimal. Figure 10, for example, compares the typical appearance of C71500 and NO8367 tubes after 90 days of testing in seawater.

Extent of Propagation--Mass loss results, reflecting general and localized corrosion, for sheet material and tube specimens are given in Table 5. Because of their larger size and consequently larger crevice areas, the total mass loss for the tube specimens was greater than that for corresponding sheet material specimens. For both product forms, the highest and lowest mass loss values were associated with the 2nd-pass brine and 3rd-pass permeate, respectively. Mass loss incurred by the sheet material with PCAs exposed to the 2nd-pass brine was about twice that incurred in filtered seawater and about 13 times that in the 3rd-pass permeate.

When mass-loss data are normalized on a per unit-area basis, comparable values are obtained for sheet and tube specimens in the 2nd-pass brine tests. For the other two environments, the tube specimens exhibited 2 to 3 times more mass-loss/unit-area than the sheet specimens.

Regardless of the above differences, corrosion rates (based on total mass loss), shown in Table 5 in all cases were ≤ 0.01 mm/yr. The general corrosion rate for C71500 in quiet seawater is frequently cited as < 1 mpy (< 0.025 mm/yr). The short-term corrosion rates in the foregoing tests are lower than the long-term rates for C71500 in non-filtered, quiescent and slowly moving seawater as reported by others [13].

As previously indicated, crevice-related attack was most pronounced in the 2nd-pass brine tests. Thus, use of a general corrosion rate could be misleading in that particular case. Table 6 provides information on the depths of attack incurred at various sites on the sheet material specimens with PCA's and the tube specimen fitted with glands and O-rings.

The greatest depth of attack after 90 days was found at an area somewhat removed from the PCA (0.12 mm) on one sheet specimen and adjacent to one of the 23.8 mm O-ring sites (0.08 mm) exposed to the 2nd-pass brine.

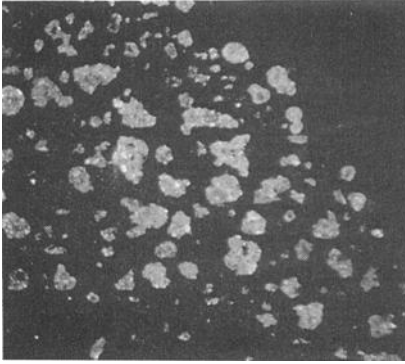


FIG. 8--Photomicrograph showing superficial pitting incurred by C71500 sheet material and tube specimens during 90-day exposure to 2nd-pass brine. (Original magnification 22X)

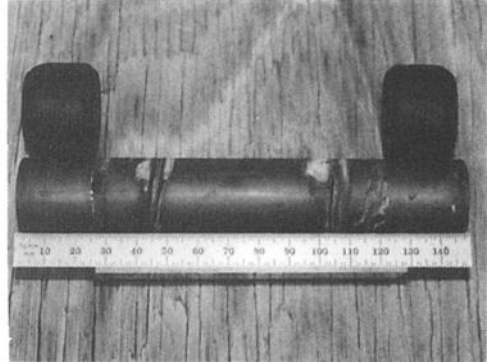


FIG. 9--Appearance of C71500 tube specimen after 90 days' exposure to 2nd-pass brine; rubber glands (shown) and O-rings removed.

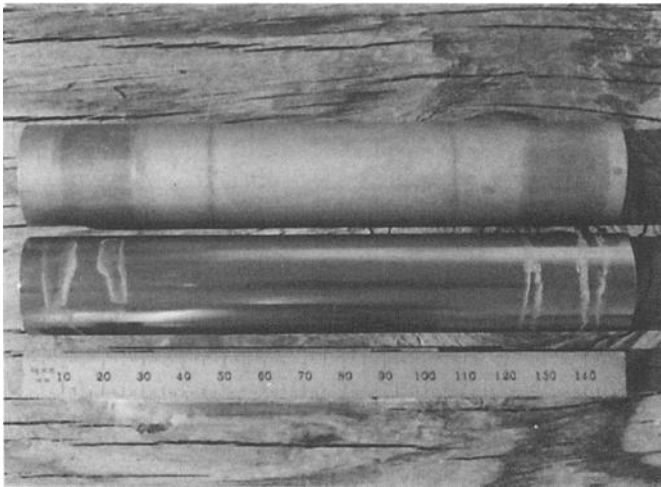


FIG. 10--Post-test appearance of tube specimens showing crevice corrosion behavior of 70/30 CuNi (top) and 20Cr-6Mo austenitic stainless steel (bottom).

TABLE 5--Summary of average mass loss and corrosion rate data for C71500

Material/Specimens	Filtered Seawater		2nd-Pass Brine		3rd-Pass Peameate	
	Mass Loss (mg)	Corr. Rate (mm/y)	Mass Loss (mg)	Corr. Rate (mm/y)	Mass Loss (mg)	Corr. Rate (mm/y)
Sheet Material Triplicate PCA specimens (avg)	52.9	1.2	96.0	2.2	7.6	0.2
Tube Materials 3 tubes with and w/o O-rings	400	2.0	484	2.4	116	0.6

TABLE 6--Penetration data for C71500 in 90-day tests*

Filtered Seawater	-	Negligible crevice-related attack at PCA, rubber gland and O-ring sites
2nd-pass Brine	-	Maximum depth of attack adjacent to PCA = 0.04 mm
	-	Maximum depth of attack elsewhere on sheet specimens = 0.12 mm
	-	Maximum depth of localized pitting at discontinuities in copper colored film on sheet and tube <0.01 mm
	-	Maximum depth of attack adjacent to rubber gland = 0.04 mm
	-	Maximum depth of attack adjacent to 20.6 mm O-ring <0.01 mm
	-	Maximum depth of attack adjacent to 23.8 mm O-ring = 0.08 mm
3rd-Pass Peameate	-	Visible but negligible (<0.01 mm) attack within PCA area and adjacent to 23.8 mm O-ring site

* measured with a focusing depth microscope

SUMMARY AND CONCLUSIONS

A full-scale, 3-pass RO system was utilized to conduct in-plant corrosion tests aimed at characterizing the performance of candidate pressure vessel materials. UNS S31603 stainless steel represented the control material and use of filtered natural seawater provided the baseline test conditions. Other environments included RO 2nd-pass brine and ultrapure RO 3rd-pass permeate. Testing involved exposure of sheet and tube specimens of S31603, electropolished S31603, and the "20Cr-6Mo" (N-containing) alloy UNS N08367. Perspex Crevice Assemblies (PCA, annular plastic washers), rubber O-rings and rubber compression glands provided a range of crevice conditions. Because of its historical use as a corrosion resistant marine alloy, CuNi C71500 was included in these investigations.

30-day testing of surface-ground sheet material fitted with PCA's resulted in crevice corrosion of all three stainless materials exposed to natural seawater. All specimens in the PCA test were fully resistant to the 2nd pass brine and 3rd pass permeate water.

Stainless Steels

In the 90-day seawater tests on tube specimens, as-produced S31603 and N08367 incurred attack at the rubber compression-gland sites. In addition, there was some susceptibility of the S31603 control material fitted with O-rings. While N08367 was fully resistant to the 2nd-pass brine and 3rd-pass permeate environments, the S31603 control tube exhibited some attack at the rubber compression-gland sites in the 2nd-pass brine tests.

S31603 tube specimens electropolished in the as-produced condition were found to be fully resistant to crevice corrosion in all three environments.

In those cases where both the S31603 control material and the 6% molybdenum-containing alloy N08367 incurred crevice corrosion initiation, the latter exhibited significantly greater resistance to propagation of attack.

Both electropolished S31603 and as-produced N08367 exhibited resistance to crevice corrosion over a range of "severe" crevice geometries and appear suitable candidate materials for construction of 2nd-pass and 3rd-pass RO pressure vessels. In addition, as-produced S31603 can be considered a suitable candidate material for the high purity 3rd-pass permeate (boiler quality water) environment, but not the 2nd-pass brine or seawater, from a crevice corrosion standpoint. As reported elsewhere, electropolished S31603 stainless steel and another "20Cr-6Mo" (N-containing) alloy, S31254, exhibited crevice corrosion resistance in waters of varying TDS and Cl⁻ levels [10,11]. The present test results support these earlier findings.

70/30 CuNi

Visual examination clearly showed that the areas directly beneath the crevice formers (e.g., gland-seal gaskets, and O-rings), on the exposed CuNi specimens, were resistant to corrosion. This behavior is significant in regard to the intended use of such materials for RO pressure vessels -- which depend heavily on leak-tight seals to separate supply waters, brine and permeate for efficient operation.

Regardless of product form, i.e., sheet or tube, C71500 incurred the greatest degree of corrosion in the 2nd-pass brine environment. This environment promoted both crevice-related attack and general surface dissolution.

Despite the attack incurred in the 2nd-pass brine, general corrosion rates of C71500, computed from mass loss, were within the range typical for this alloy in natural seawater in the absence of excessive velocity (e.g., >10 ft/s) or turbulence.

It is uncertain if continuous flow at the current or somewhat higher rates would exacerbate the degree of attack observed for C71500 in 2nd-pass brine. Moreover, the effects of dissolved oxygen levels in low TDS waters require additional study.

Corrosion incurred by C71500 in the ultrapure, 3rd-pass permeate was superficial.

While C71500 incurred some crevice-related attack, the location (outside of the crevice) and the degree of attack incurred -- relative to, say, crevice corrosion of S31603 in seawater -- indicates that C71500 remains a candidate material for this application. Based on a review of the present pressure vessel designs, it appears that this behavior may effectively serve to "relocate" the most susceptible areas away from the critical seals. These areas also appear to be of sufficient thickness and, hence, should "tolerate" the degree of crevice-related attack indicated by the present test results.

General

The present in-plant corrosion tests provided an opportunity to evaluate materials performance under actual and realistic operating conditions. For example, specimens were exposed to three different waters associated with RO desalination, with variations in water temperature and flow interruptions likely to be encountered in service. Since the above seawater tests were conducted in a side-stream, the high pressure conditions associated with 1st-pass RO were not duplicated. Others have reported that increasing hydrostatic pressure in seawater decreases the molybdenum concentration in the passive layer of stainless alloys.[14] Such observations may raise additional interest in further in-plant testing of high molybdenum-containing stainless alloys in RO systems. Future reports on the performance of stainless alloys in existing full-scale RO treatment plants will provide opportunities for comparison with data generated in test programs of the type described in this paper.

Overall, the two ASTM Standard Guides (G04 and G78) cited provided valuable information applicable to the design and interpretation of these natural water corrosion tests.

ACKNOWLEDGMENT

Appreciation is offered to our co-workers who participated in the conduct of tests, preparation and reviews of this manuscript, and to the management of both organizations for their support and encouragement to present this work.

REFERENCES

- [1] Todd, B., "Nickel-Containing Materials in Marine and Related Environments", Technical Series No. 10011, Nickel Development Institute, Toronto, Canada.
- [2] Lamendola, M.F. and Tua, A., Desalination & Water Reuse, Vol. 5, No. 1, 1995, p. 18.
- [3] Pizzino, J.F., Adamson, W.L., and Smith, W.L., Naval Engineers Journal, Vol. 130, No. 3, 1991, p.126.
- [4] Harfst, W.F., Ultra Pure Water, Vol. 3, 1993, p. 57.
- [5] 1995 Annual Book of ASTM Standards, Vol. 03.02 Wear and Erosion; Metal Corrosion Sect. 3 Metal Test Methods and Analytical Procedures, ASTM, West Conshohocken, PA.
- [6] Kain, R.M., Weber B., and Adamson, W.L., "Localized and General Corrosion Resistance of Candidate Metallic Materials for RO-Membrane Cartridges," Paper No. 208, CORROSION/95, NACE International, Inc., Houston, TX, March 1995.
- [7] Kain, R.M., Klein, P.A., Hays, R.A., and Ferrara, R.J., "The Effect of Electrolytic Chlorination on the Crevice Corrosion Behavior of 70/30 Copper-Nickel and Nickel-Copper Alloy 400", Paper No. 509, CORROSION/91, NACE International, Inc., Houston, TX, March 1991.
- [8] Klein, P.A., Krause, C.D., Frait, C.L., and Kain, R.M., "A Localized Corrosion Assessment of 6% Molybdenum Stainless Steel Condenser Tubing at the Calvert Cliffs Nuclear Power Plant", Paper No. 490, CORROSION/94, NACE International, Inc., Houston, TX, March 1994.
- [9] Kain, R.M., Proceedings of the 12th International Corrosion Congress, NACE International, Inc., Houston, TX, September 1993, Vol. 3A, p. 1889.
- [10] Kain, R.M., "Effects of Surface Finish on the Crevice Corrosion Resistance of Stainless Steels in Seawater and Related Environments", Paper No. 508, CORROSION/91, NACE International, Inc., Houston, TX, March 1991.
- [11] Kain, R.M. and Oldfield, J.W., "Crevice Corrosion Behavior of Stainless Steels in Chloride and Sulfate Containing Waters", Paper No. 384, CORROSION/90, NACE International, Inc., Houston, TX, April 1990.
- [12] LaQue, F.L., Marine Corrosion Causes and Prevention, John Wiley & Sons, New York, NY, 1975, p. 35.

- [13] Efrid, K.D. and Anderson, D.B., Materials Performance, Vol. 14, No. 11, 1975, p. 37.
- [14] Beccaria, A.M. and Puggi, G., "The Influence of Passive Film Composition on the Resistance to Localized Corrosion of Some Stainless Steels in Seawater", International Symposium on Localized Dissolution and Corrosion: Passivity and Its Breakdown, ASM International, Materials Park, OH, 1994.

Mahmoud R. Reda,¹ Jamal N. Alhajji²

COMPARISON OF CURRENT REVERSAL CHRONOPOTENTIOMETRY (CRC) AND SMALL AMPLITUDE CYCLIC VOLTAMMETRY (SACV) METHOD TO DETERMINE THE LONG-TERM CORROSION TENDENCY OF COPPER-NICKEL ALLOYS IN POLLUTED AND UNPOLLUTED SEAWATER UNDER JET-IMPINGEMENT CONDITIONS

REFERENCE: Reda, M. R., and Alhajji, J. N., "Comparison of Current Reversal Chronopotentiometry (CRC) and Small Amplitude Cyclic Voltammetry (SACV) Method to Determine the Long-Term Corrosion Tendency of Copper-Nickel Alloys in Polluted and Unpolluted Seawater Under Jet-Impingement Conditions," *Corrosion Testing in Natural Waters: Second Volume*, ASTM STP 1300, Robert M. Kain, Walter T. Young, Eds., American Society for Testing and Materials, 1997.

ABSTRACT: The cyclic current reversal chronopotentiometry (CRC) technique is utilized to determine the long-term corrosion tendency of UNS C70600 and UNS C71500 copper-nickel alloys in sulfide polluted and unpolluted seawater. The CRC results were compared with the corrosion tendency obtained by the modified linear polarization method Small Amplitude Cyclic Voltammetry (SACV) over a long exposure time and the results are in agreement for both C70600 and C71500 alloys. This contradicts the conclusions on the effects of sulfide on copper-nickel alloys by many previous investigators who misinterpreted the sharp active shift in potential as an indication of increase in corrosion rate. For an active/passive alloy such as C71500 a higher amplitude current per cycle is required (e.g. 100 $\mu\text{A}/20$ seconds) in the CRC method and under jet-impingement conditions, while a lower amplitude current per cycle (e.g. 1 $\mu\text{A}/20$ seconds) is required for an alloy that does not exhibit active/passive behavior. The CRC technique was found to be unsuccessful in screening out the long-term corrosion tendency of copper alloys in polluted and unpolluted sea water and under stagnant or stirred conditions (i. e. non-jet-impingement conditions).

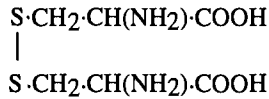
KEYWORDS: Current Reversal Chronopotentiometry (CRC), sea water, jet-impingement, Small Amplitude Cyclic Voltammetry (SACV)

Nickel alloys and particularly copper–nickel alloys are commonly used in seawater applications. A great deal of research has concentrated on studying the performance of these alloys in this environment [1-7]. The corrosion performance of these alloys has been shown to be very suitable in marine service. Although these alloys have been shown to be highly suitable in unpolluted seawater, enhanced corrosion in seawater has been shown to be

¹ Corrosion and Environmental Control Consultant, 5014 New St. Suite 119, Burlington, Ontario, L7L 6E8, Canada

² Department of Mechanical engineering, Corrosion and Materials Laboratory, College of Engineering and Petroleum, Kuwait University, PO Box 5969, Safat, 13060 - Kuwait.

associated with sulfide contamination [1-7]. These alloys have also shown to be susceptible to impingement attack even in unpolluted seawater [8-10]. As indicated by Evans [9] even with the best materials (e.g. pure nickel) there is still risk of corrosion to condenser tubes if the water used contains hydrogen sulfide or *cystine*



a substance derived from seaweed. It was concluded [9] that this trouble has not been entirely overcome. In this investigation the corrosion behavior of copper-nickel alloys C70600 and C71500, respectively under aerated static, aerated stirred, and under impingement attack in sulfide polluted seawater (0 to 100 ppm S⁼) has been studied by Cyclic Current Reversal Chronopotentiometry (CRC) [11]. Akkaya and Ambrose [12] confirmed that CRC can be utilized to predict long-term corrosion behavior of copper alloys in water. To study the application of this technique for evaluating the corrosion behavior of copper-nickel alloys in sulfide-polluted seawater, an intentional, abrupt change of current between anodic and cathodic values was also used. In order to separate Faradaic and non-Faradaic processes the effect of the current amplitude was investigated. To check the validity of the technique, results of the CRC were compared with conventional methods for corrosion rate measurement, such as the linear polarization resistance, over a long exposure time. Thus, the purpose of the investigation was to determine the feasibility of using the CRC method as a tool to evaluate the long-term corrosion behavior of copper/nickel alloys in polluted and unpolluted seawater.

EXPERIMENTAL METHOD

Test Specimens

Copper-nickel specimens were supplied in the form of pipes which were cut and flattened into sheets. The copper-nickel alloys were 90/10 and 70/30 Cu/Ni (C70600 and C71500). The chemical analysis of the alloys investigated are shown in Table 1.

TABLE 1--The composition of the alloys investigated.

Alloy	Composition (Wt %)					
	Cu	Ni	Fe	Mn	Zn	Al
C70600	88	10	1.4	0.4	—	—
C71500	69	30	0.6	0.5	—	—
Copper	99.9	—	—	—	—	—
Al-Brass	77.5	—	—	—	20.5	2.0

The samples were prepared by punching out of 5/8-inch disks from the "flattened sheets". Annealing was carried out to remove the effects of cold working induced by flattening and punching processes. This was followed by surface grinding of each specimen according to ASTM standards [13]. This was followed by a grinding process of the surface of each specimen according to ASTM standards (G 61-86 & G 59-78) [13]. The specimen were then degreased thoroughly using acetone and rinsed with double distilled water and dried.

Test Conditions

Experiments on corrosion measurement were conducted in "standard" seawater. This was prepared with double distilled water and "standard" sea salt. The standard sea salt (Marinemix + Bio-Elements from: Wiegandt GMBH & Co. F. R. Germany) was used to eliminate the day-to-day variations of natural seawater. The samples were pre-conditioned for four hours in the seawater prior to the experiments. Experiments were then conducted in plain seawater or in sulfide polluted seawater. The sulfide was introduced in the recirculated seawater system at the onset of the experiments using research grade sodium sulfide (Na_2S). The level of sulfide in the seawater was checked by the iodimetric method [14] of analysis throughout the tests .

Testing Equipment and Procedure

Electrochemical corrosion measurements were made at 20 °C for all the previously mentioned conditions, using a computer-controlled Potentiostat / Galvanostat (EG&G Model 273A). A modified electrochemical corrosion testing cell was used where a combination of a circulating pump and a jet nozzle (diameter = 0.001 m) was set up to simulate jet-impingement attack as shown in Fig. 1. The average stream velocity at the tip of the nozzle was calculated from volume flow and orifice size and found to be 6.1 m/s. The distance between the tip of the nozzle and the working electrode was fixed at 3 mm. The reference electrode was saturated calomel (SCE). The stability of the SCE was checked, against a fresh SCE following each experiment. Four current amplitudes were investigated $\pm 1 \mu\text{A}$, $\pm 10 \mu\text{A}$, $\pm 50 \mu\text{A}$ and $\pm 100 \mu\text{A}$. In the polluted seawater the sulfide concentration were 0, 2, 10 and 100 ppm. The principle of the CRC technique is illustrated in Fig. 2.

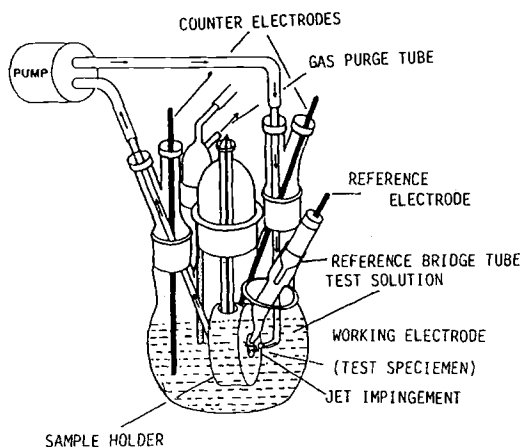


FIG. 1--The electrochemical cell utilized to simulate impingement attack.

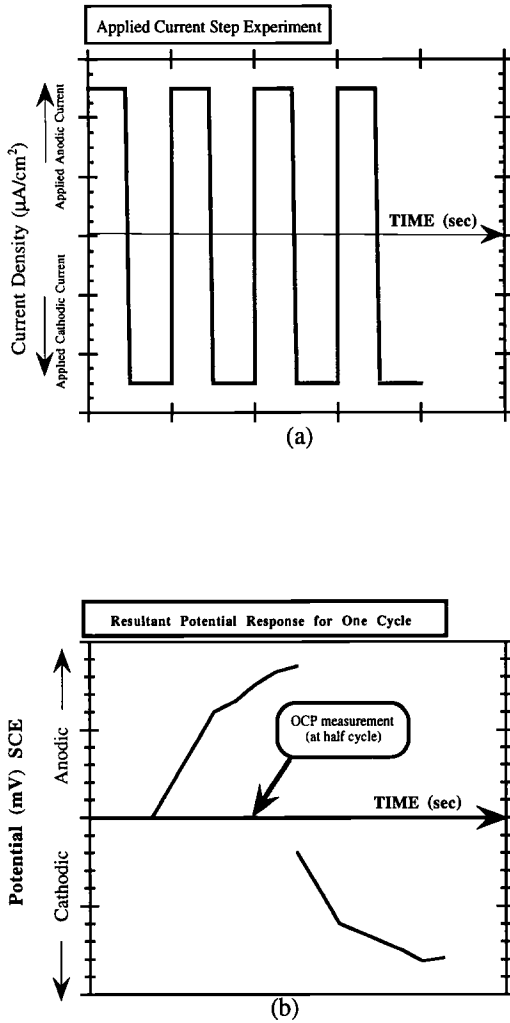


FIG. 2--A schematic diagram showing (a) the input applied current steps and (b) the resultant potential response from a single current cycle for the cyclic current reversal chronopotentiometric experiment.

Corrosion tendency was measured by Small Amplitude Cyclic Voltammetry (SACV) [10], and polarization resistance values (R_p) determined. The scan rate of the experiments was 0.05 mV/sec. This slow scan rate was selected to ensure minimal hysteresis of the SACV loop [10]. The scan range for the SACV was from $-5 \text{ mV}_{\text{SCE}}$ to $+5 \text{ mV}_{\text{SCE}}$.

RESULTS AND ANALYSIS

Corrosion Rate By Linear Polarization Method or SACV

Long-term exposure corrosion rate data (inverse of polarization resistance, i.e. $1/R_p$) obtained from the linear polarization method are given in Figs. 3 and 4 for C70600 and C71500 respectively. Furthermore, Fig. 5 shows the open circuit potential during long-term exposure periods of C70600 determined by SACV. Generally, the corrosion tendency of the C70600 and C71500 in sulfide polluted seawater decreases with increasing sulfide concentration. This contradicts the typically expected corrosion tendency in a sulfide environment which has been reported by many investigators.^{5-7,15} From Fig. 5 it can be concluded that, in the presence of sulfide, the open circuit potential, $E_{i=0}$, becomes nearly constant after long exposure periods and is noble in unpolluted seawater. From Figs. 3 and 4 for the corrosion tendency ($1/R_p$) obtained by modified linear polarization method, two conclusions are evident. First, sulfide can arrest the corrosion rate especially at concentrations higher than 2 ppm which is in agreement with the results for both alloys. Second, there is a correlation between OCP shift with $1/R_p$ behavior under these conditions.

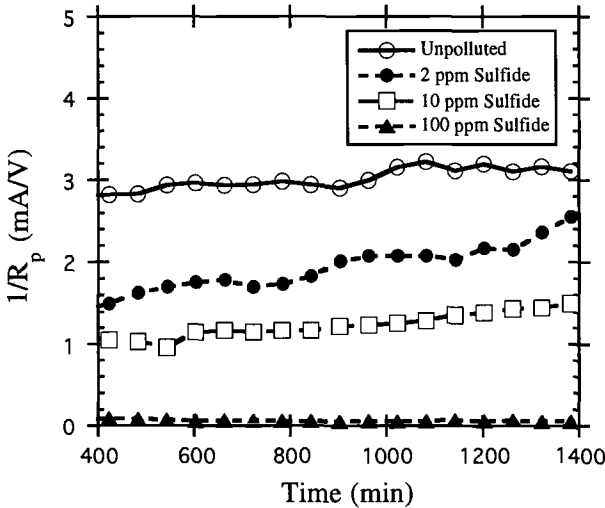


FIG. 3--The corrosion tendency of the C70600 in aerated, sulfide-polluted seawater as a function of exposure time at 6.1 m/s jet velocity.

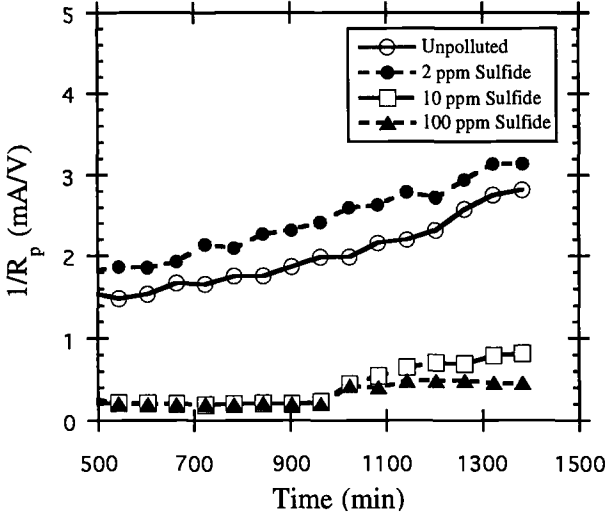


FIG. 4--The corrosion tendency of the C71500 in aerated, sulfide-polluted seawater as a function of exposure time at 6.1 m/s jet velocity.

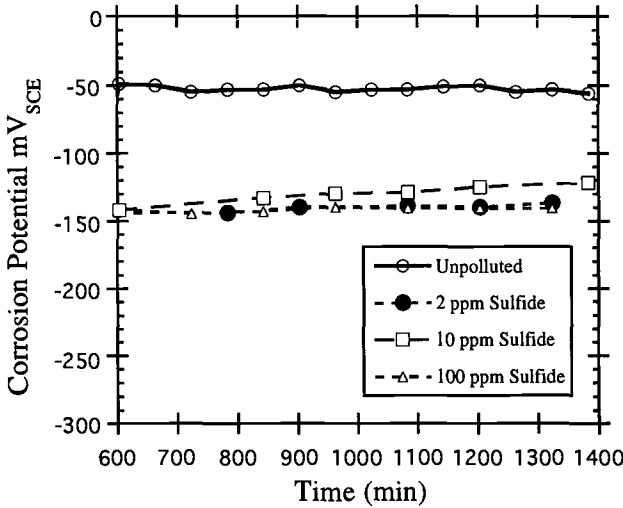


FIG. 5--The corrosion potential of the C70600 alloy in aerated, sulfide-polluted seawater as a function of exposure time at 6.1 m/s jet velocity.

The CRC method for stagnant and stirred aerated conditions :

Fig. 6 compares the resultant open circuit potential, $E_{i=0}$, versus cycle number for four different alloys in aerated, stagnant, unpolluted seawater. These alloys were tested by applying a fluctuating currents steps of $\pm 50 \mu\text{A}/\text{cm}^2/40 \text{ sec}$ per cycle (an anodic step of $50 \mu\text{A}$ for 20 sec and a cathodic step of $-50 \mu\text{A}$ for 20 sec). The results indicate that both C70600 and C71500 establish nearly constant noble potentials of about 10 and $-30 \text{ mV}_{\text{SCE}}$, respectively; while Al-brass and copper have a nearly constant active potential of around $-170 \text{ mV}_{\text{SCE}}$. It is well documented that Cu/Ni alloys are superior to copper or aluminum brass [8-9] for seawater applications. CRC should have resulted in a more positive potential response for the Cu/Ni alloys similar to that obtained by Akkaya and Ambrose [12]. According to Akkaya and Ambrose [12] a positive potential response to the cyclic current reversal voltammetry (CCRV) is an indication of more stability and the formation of protective surface barrier. It is attempted to extend the findings of Akkaya and Ambrose [12] in evaluating the validity of CRC test for screening out the corrosion tendency of the alloys in other environments such as seawater under various conditions. Electrochemical tests of these alloys were conducted in aerated, stirred, unpolluted seawater. The results of these tests are given in Fig. 7 which shows that the potential of copper-nickel alloys are shifted in the noble directions indicating lower corrosive tendency. While the potential response of aluminum-brass and copper shifts toward more active values indicating a higher corrosion tendency.

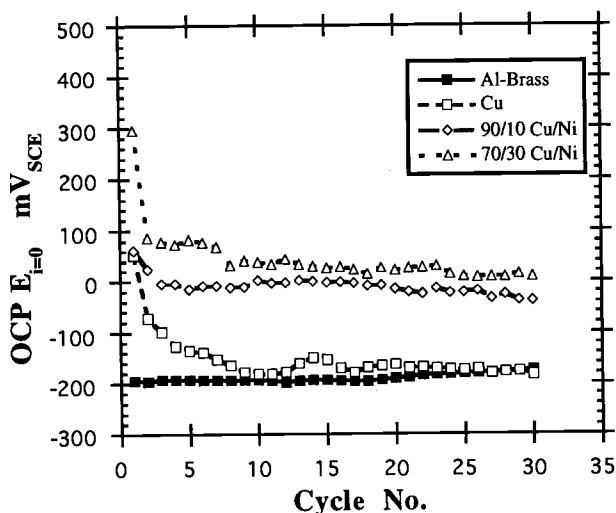


FIG. 6--Observed open circuit potential (OCP) for various alloys in unpolluted seawater under stagnant, aerated conditions. [One Cycle = $\pm 50 \mu\text{A}/\text{cm}^2/40 \text{ sec}$]

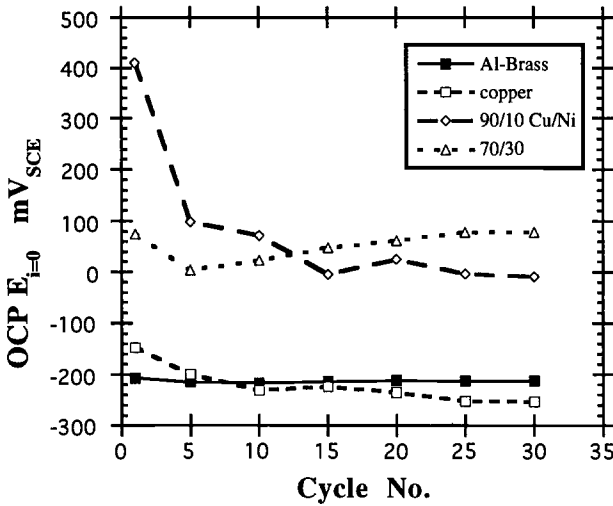


FIG. 7--Observed open circuit potential (OCP) for various alloys in unpolluted seawater under stirred, aerated conditions. [One Cycle = $\pm 50 \mu\text{A}/\text{cm}^2/40 \text{ sec}$]

The CRC method under jet-impingement conditions :

Figs. 8 and 9 show results of the CRC technique [$\pm 1 \mu\text{A}/\text{cm}^2/20 \text{ sec}$] in aerated, sulfide-polluted seawater under jet-impingement conditions for C70600 and C71500, respectively. This environments simulates conditions frequently encountered in seawater service (e.g. heat exchangers [16]). The results confirm the previously known fact that as the sulfide concentration increases, the potential shifts progressively to more active values which was explained by many investigator [5-7] as an indication of increase in corrosion rate [5-7, 15]. This is also supported by the CCRV method proposed by Ambrose and Akkaya [12]. Corrosion tendency measurements ($1/R_p$) of these alloys in sulfide polluted seawater for long term exposure given in Figs. 3 and 4 show that lower corrosion rates were obtained with increasing sulfide concentration. This is due to the formation of copper sulfide layer that act as a physical barrier to further corrosion. This trend disagrees with the previously reported corrosion rates under these conditions [5-7]. However, our results agree with the results of Wood et al [17] that sulfide concentration as high as 100 ppm can impart protection to these alloys under these conditions. It is clear that in the presence of 100 ppm sulfide, the potential shifts to very active values, while the shift in the open circuit potential, $E_{i=0}$, for low concentrations of sulfide is small. This trend is more clear for C71500 alloy than for C70600 because of the differences in the corrosion mechanisms for the two alloys [8-10]. According to Uhlig [8], C70600 alloy protects itself in seawater by corroding uniformly at a low rate and thus avoiding biofouling and pitting. For the C71500 alloy, which depends on its passive film for protection.

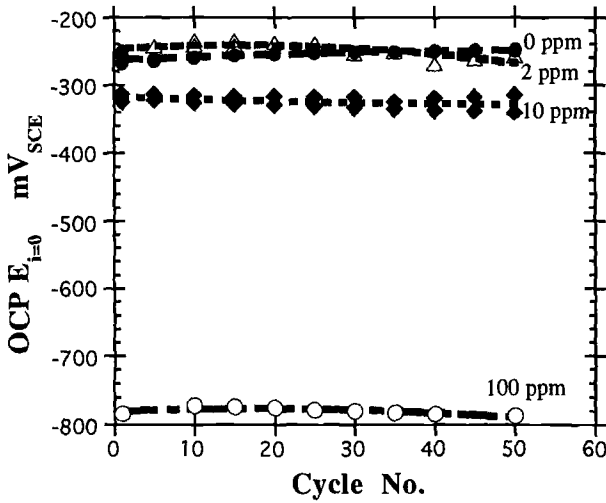


FIG. 8--A comparison of the observed open circuit potential (OCP) for C70600 in sulfide-polluted, aerated seawater under jet-impingement conditions.
 [One Cycle = $\pm 1 \mu\text{A}/\text{cm}^2/20 \text{ sec}$]

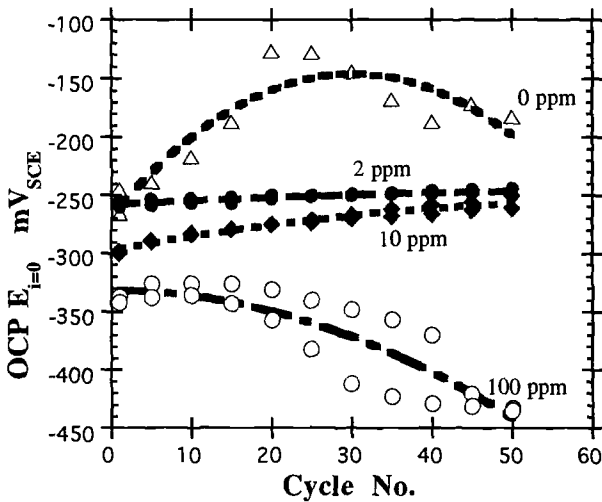


FIG. 9--A comparison of the observed open circuit potential (OCP) for C71500 in sulfide-polluted, aerated seawater under jet-impingement conditions.
 [One Cycle = $\pm 1 \mu\text{A}/\text{cm}^2/20 \text{ sec}$]

Figs. 10 and 11 show the effects of increased CRC applied current [$\pm 10 \mu\text{A}/\text{cm}^2/20 \text{ sec}$] for C70600 and C71500, respectively in sulfide-polluted, aerated seawater under jet-impingement conditions. Based on Ambrose and Akkaya [12] it can be incorrectly concluded that increasing the sulfide level increases the corrosion tendency of these alloys. This is again inconsistent with the corrosion rate measurements obtained from long term exposure of these alloys in sulfide polluted seawater given in Figs. 3 and 4. The decrease in corrosion tendency with increasing sulfide concentration is manifested here as a shift in the observed open circuit potential in the active direction. Figs. 12 and 13 show the effects of increasing applied current signal to $\pm 100 \mu\text{A}/\text{cm}^2/20 \text{ sec}$. It is clear that a different response is shown for Cu-Ni alloys especially for low sulfide concentrations. However, for 100 ppm sulfide the open circuit potential, $E_{i=0}$, response is a large shift in potential in the active direction, which is similar to the previously observed trend for smaller current signal. The different OCP behavior observed for the lower sulfide concentrations in Figs. 12 and 13 as compared to higher sulfide concentration (100 ppm) is due to the higher applied current amplitude (i.e. $\pm 100 \mu\text{A}/\text{cm}^2/20 \text{ sec}$) which give rise to alternate electrochemical reactions to be active. Essentially, low applied current steps will activate non Faradaic processes while high applied current will induce Faradaic processes [11]. The details of these Faradaic and non Faradaic processes will be explained shortly.

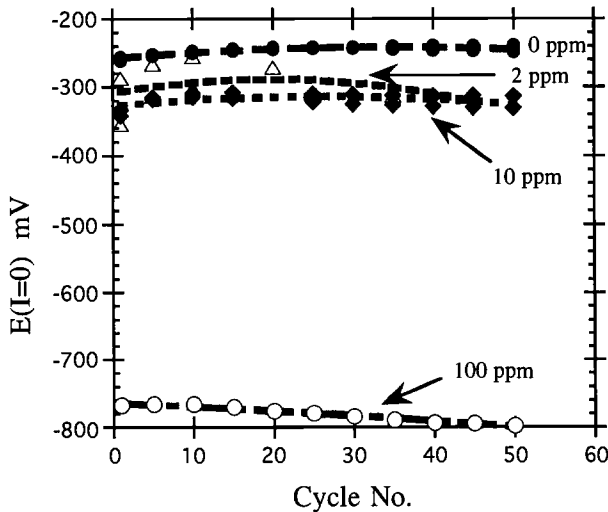


FIG. 10--Observed open circuit potential (OCP) for C70600 in sulfide-polluted, aerated seawater under jet-impingement conditions. [$\pm 10 \mu\text{A}/\text{cm}^2/20 \text{ sec}$]

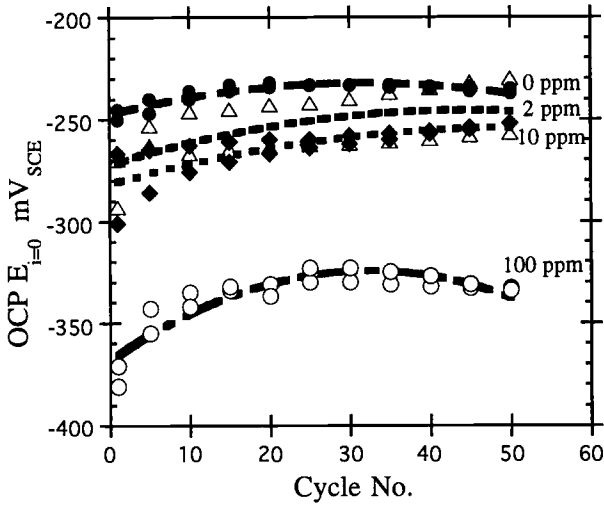


FIG. 11--Observed open circuit potential (OCP) for C71500 in sulfide-polluted, aerated seawater under jet-impingement conditions. [$\pm 10 \mu\text{A}/\text{cm}^2/20 \text{ sec}$]

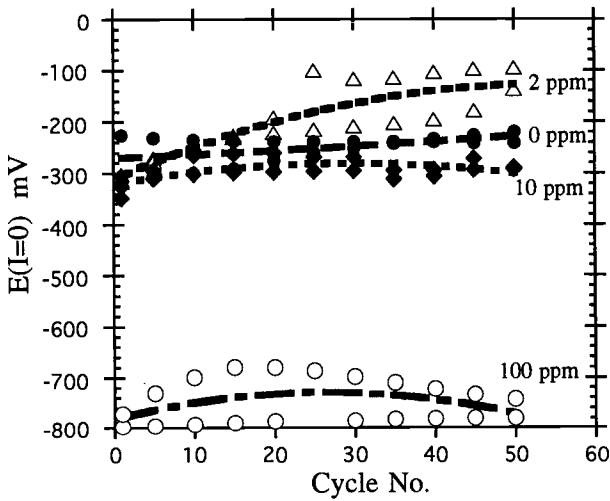


FIG. 12--Observed open circuit potential (OCP) for C70600 in sulfide-polluted, aerated seawater under jet-impingement conditions. [$\pm 100 \mu\text{A}/\text{cm}^2/20 \text{ sec}$]

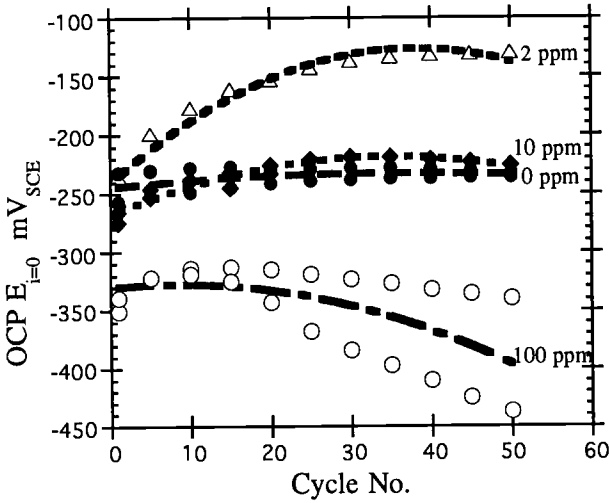


FIG. 13--Observed open circuit potential (OCP) for C71500 alloy in sulfide-polluted, aerated seawater under jet-impingement conditions. [$\pm 100 \mu\text{A}/\text{cm}^2/20 \text{ sec}$]

Fig. 14, compares the response of C71500 and C70600 in sulfide-polluted seawater at a CRC current signal of $\pm 50 \mu\text{A}/\text{cm}^2/20 \text{ sec}$ for a total of 50 cycles. It can be seen that as the sulfide concentration is increased, the open circuit potential shifts progressively toward more active values which indicate that corrosion product layer formed offers a protective effect. It is also clear that C70600 is superior to C71500 in sulfide polluted seawater under jet-impingement conditions. This is in agreement with the earlier conclusions of Anderson and Badia [16] in which it was concluded that C70600 alloys can be more resistant to corrosion than C71500 alloy under erosion-corrosion (impingement attack) conditions with jet velocity above 6 m/s.

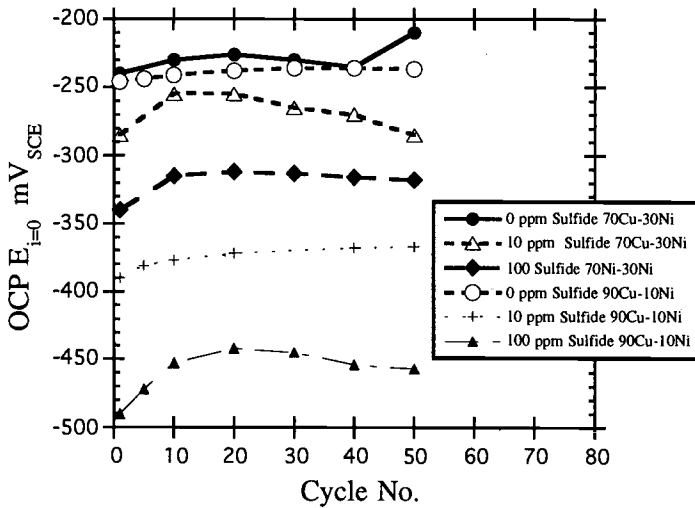


FIG. 14--Observed open circuit potential (OCP) for the Cu-Ni alloys in sulfide-polluted, aerated seawater under jet-impingement conditions. [$\pm 50 \mu\text{A}/\text{cm}^2/20 \text{ sec}$]

CRC versus modified Linear Polarization method or SACV

It is attempted here to rationalize the reason for the observed response of copper-nickel alloys in sulfide-polluted seawater. First, it is observed that increasing the sulfide concentration will shift the open circuit potential, $E_{i=0}$, toward more negative values which indicates an a decreasing tendency to corrode with increasing sulfide concentrations as shown in Figs. 3-5. In fact for C70600, a comparison between Figs. 8, 10 and 12 obtained by the CRC method with the long exposure time corrosion rate data (inverse of polarization resistance, i.e. $1/R_p$) obtained from the linear polarization method given in Fig. 3 supports the earlier conclusion that increasing sulfide concentration results in a decrease in corrosion rate. This contradicts with many published research results that indicate increasing sulfide concentration leads to an active shift in the corrosion potential and a subsequent increase in corrosion rate. However, our results are in agreement with the conclusions of Wood et al [17] that sulfide can inhibit corrosion of copper/nickel alloys. Furthermore, Fig. 5 shows the open circuit potential during long-term exposure periods determined by SACV. The results supports the above conclusions that, in the presence of sulfide, the open circuit potential, $E_{i=0}$, becomes nearly constant after long exposure periods and is more noble in unpolluted seawater. Moreover, it can be seen that lower amplitude current per cycle (e.g. $\pm 1 \mu\text{A}/\text{cm}^2/20 \text{ sec}$ and $\pm 10 \mu\text{A}/\text{cm}^2/20 \text{ sec}$, as is shown in Figs. 8 and 10) gives a very realistic prediction of the long term effect. Thus for C71500, comparing Figs. 9, 11 and 13 representing the CRC results with Fig. 4 for the corrosion tendency ($1/R_p$) obtained by modified linear polarization method, two conclusions are evident. First, sulfide can arrest the corrosion rate especially at concentrations higher than 2 ppm which is in agreement with the

results for C70600 alloy. Second, for an active/passive alloy such as C71500 higher amplitude current per cycle gives more realistic prediction of corrosion behavior. Thus, in Fig. 13, at a current density of $100 \mu\text{A}/\text{cm}^2/20 \text{ sec}$, there is a correlation between OCP shift with $1/R_p$ behavior in Fig. 4 for 0, 2 and 100 ppm, but not for 10 ppm sulfide. This is so, since C70600 is not an active/passive metal which is according to Uhlig [8] protect itself by corroding uniformly at a very low rate avoiding biofouling and localized attack.

The Effects of Applied Current Magnitude

Low applied current density (less than $10 \mu\text{A}/\text{cm}^2$) is usually associated with non-Faradaic processes [11] such as adsorption and desorption. In such processes the structure of the electrode-solution interface can change with changing potential or solution composition. Figs. 8-11 illustrate the effects of adsorption of sulfide in which there is a gradual shift in the open circuit potential with increasing sulfide concentration. Sulfur adsorption results in a layer composed of CuS_2 and CuS which affects the potential behavior of the surface. These sulfur-containing layers on metals and alloys are brittle, non-protective and poorly adhering to the surface and favors the occurrence of localized attack. This is clear in Figs. 9 and 11 for C71500. This trend is not so obvious for C70600. This is due to the difference in the corrosion mechanism of the two copper-nickel alloy. It is known that [6] the protective mechanism for C71500 is the formation of a strong, adherent, protective, passive layer. On the other hand, C70600 corrodes uniformly at a low rate, and resists localized attack and biofouling to a greater extent. The effect of current is discussed below. It is observed that at low current amplitude, the open circuit potential, $E_{i=0}$, shifts toward more active values with increasing adsorption of sulfide at the surface. This trend is very systematic for C71500 since as the non-active and passive (semiconductor) layer receives the negatively charged sulfide ions, the substrate layer potential responds accordingly toward more negative values. For C70600, because of its different protective mechanism which results in low, uniform corrosion rate, the trend is not so clear due to simultaneous occurrence of both surface adsorption (similar to C71500) and sulfide reacting with dissolved metal ions in the solution.

At high current density and low sulfide concentration the Pourbaix diagram can be used to infer that formation of sulfate occurs through the oxidation of sulfide. At high current density amplitude and low sulfide concentration, the current is utilized mainly for the oxidation of the low concentrations of sulfide available and thus the alloy surface exhibits inert behavior which catalyzes the oxidation of sulfide as inferred from the Pourbaix diagram. Nickel and its alloys are known to be an excellent catalysts for oxidation reactions in aqueous solutions [18].

The mechanism is entirely different at high current density amplitude and high sulfide concentrations, where the abundant sulfide ions available at the surface play a dual role. First, they consume the electrons supplied by the applied current and thus get oxidized to sulfate. Secondly, sulfide ions also undergo regular oxidation reactions with the surface. The dominating mechanisms are summarized in Table 2.

TABLE 2--The dominating corrosion processes as a function of sulfide concentration and current amplitude.

Conc.	Low Current	High Current
Low Sulfide	◆ Non-Faradaic Adsorption of Sulfide	◆ Oxidation of Sulfide to Sulfate
High Sulfide	◆ Faradaic	◆ Oxidation of Sulfide to Sulfate Consumes the Current

CONCLUSIONS

- The CRC results under jet-impingement conditions were compared with the corrosion tendency obtained under similar conditions by the modified linear polarization method over a long exposure time and the results are in agreement for both C70600 and C71500 alloys.
- The sharp active shift in potential from the open circuit potential for C70600 and C71500 alloys in sulfide environment can be misinterpreted as an indication of increased corrosion rate.
- The CRC method should not be used to determine the long-term corrosion tendency in seawater as reported previously.
- The observed open-circuit potential (OCP) following each current cycle depends on the magnitude of the amplitude current per cycle. The OCP becomes more active with increasing sulfide concentration. This is more evident for higher amplitude current per cycle for C71500, and at lower amplitude current per cycle for C70600.
- Under jet-impingement conditions, C70600 can be more resistant to corrosion in sulfide-polluted seawater than C71500. This is in agreement with results reported by others previously.

ACKNOWLEDGMENT

This work was financially supported by Kuwait University Research Unit under grant No. EM-067 . This support is gratefully acknowledged.

REFERENCES

- [1] Reda, M. R. and Alhajji, J. N., "The Effect of Trace Organic Compounds on the Corrosion of Copper-Nickel Alloys in Sulfide-Polluted Seawater," Industrial & Engineering Chemistry Research, Vol. 32, No. 6, 1993.
- [2] Reda, M. R. and Alhajji, J. N., "The Effect of Complexing Agents on the Corrosion of Copper/Nickel Alloys in Sulfide-Polluted Seawater Under Impingement Attack", 12th International Corrosion Congress, Houston, Texas, Sep., 19-24, 1993, Sponsored by NACE.
- [3] Alhajji, J. N. and Reda, M. R., Corrosion Science, Vol. 34, 1992, p. 163.
- [4] Alhajji, J. N. and Reda, M. R., Journal of Electrochemical Society, Vol. 141, No. 6, 1994, p. 1432.
- [5] Syrett, B.C., Macdonald, D. D. and Wing, S. S., Corrosion, Vol. 35, 1979, p. 409.
- [6] Syrett, B.C., Macdonald, D. D., Corrosion, Vol. 35, 1979, p. 505.
- [7] Syrett, B.C. Corrosion Science, Vol. 21, No. 3, 1981, p. 187.
- [8] Uhlig, H. H. and Revie, R. W., Corrosion and Corrosion Control, Third Edition, John Wiley and Sons, New York, NY, 1991.
- [9] Evans, U. R., An Introduction to Metallic Corrosion, 3rd Edition, Edward Arnold Publishers Limited, Scotland, 1981.
- [10] Fontana, M. G. and Greene, N. D., Corrosion Engineering, 2nd Edition, Chapter 9, McGraw Hill, New York 1987.
- [11] Bard, A. J., and Faulkner, L. R., Electrochemical Methods, John Wiley, Canada, 1980, p. 250.
- [12] Akkaya, M. and Ambrose, J. R., Materials Performance, Vol. 3, 1987, p. 9.
- [13] ASTM 1990, Annual Book of ASTM Standards, Section 3, Vol. 3.02, 1990, G1-90.
- [14] Standard Methods for the Examination of Water and Wastewater, 14th ed. American Public Health Association, Washington DC, 1976, Part 428, pp 504-505.
- [15] Gudas, J. P. and Hack, H. P. Corrosion, Vol. 35, No. 6, 1979, pp 259-264.
- [16] Anderson, D. B. and Badia, F. A., Journal of Engineering Power, Ser. A., Vol. 95, 1973, p. 132.
- [17] Wood, T. L. , Amos, A. L. and McNeil, M. B., Corrosion 92, Paper No. 180, Nashville, TN. 1992, NACE.
- [18] Smith, J. M., Chemical Engineering Kinetics, Third Edition, Ch. 7, McGraw Hill, 1981, Ch. 7.